ANKARA YILDIRIM BEYAZIT UNIVERSITY

GRADUATE SCHOOL OF NATURAL AND APPLIED SCIENCES

THE EFFECTS OF HARD TURNING AND DEEP ROLLING PROCESS ON SURFACE INTEGRITY AND FATIGUE LIFE OF DEEP GROOVE BALL BEARINGS

M.Sc. Thesis by

Gökhan SAĞIR

Department of Mechanical Engineering

December, 2021

ANKARA

THE EFFECTS OF HARD TURNING AND DEEP ROLLING PROCESS ON SURFACE INTEGRITY AND FATIGUE LIFE OF DEEP GROOVE BALL BEARINGS

A Thesis Submitted to

The Graduate School of Natural and Applied Sciences of

Ankara Yıldırım Beyazıt University

In Partial Fulfillment of the Requirements for the Degree of Master of Science in Mechanical Engineering, Department of Mechanical Engineering

by

Gökhan SAĞIR

December, 2021

ANKARA

M.Sc. THESIS EXAMINATION RESULT FORM

We have read the thesis entitled **"THE EFFECTS OF HARD TURNING AND DEEP ROLLING PROCESS ON SURFACE INTEGRITY AND FATIGUE LIFE OF DEEP GROOVE BALL BEARINGS"** completed by **GÖKHAN SAĞIR** under the supervision of **PROF. DR. ADEM ÇİÇEK** and we certify that in our opinion it is fully adequate, in scope and in quality, as a thesis for the degree of Master of Science.

Prof. Dr. Adem ÇİÇEK

Supervisor

Prof. Dr. Kubilay ASLANTAŞ

Jury Member

Assist. Prof. Dr. Yasin SARIKAVAK

Jury Member

Prof. Dr. Sadettin ORHAN

Director

Graduate School of Natural and Applied Sciences

ETHICAL DECLARATION

I hereby declare that, in this thesis which has been prepared in accordance with the Thesis Writing Manual of Graduate School of Natural and Applied Sciences,

- All data, information and documents are obtained in the framework of academic and ethical rules,
- All information, documents and assessments are presented in accordance with scientific ethics and morals,
- All the materials that have been utilized are fully cited and referenced,
- No change has been made on the utilized materials,
- All the works presented are original,

and in any contrary case of above statements, I accept to renounce all my legal rights.

Date: 20.12.2021 **Signature:**

Name & Surname: Gökhan SAĞIR

ACKNOWLEDGMENTS

First and foremost, I would like to express my sincere gratitude to my supervisor Prof. Dr. Adem ÇİÇEK for his guidance and encouragement throughout this study. At all stages of this research work I benefited from his immense knowledge and valuable advice. His positive outlook and confidence in my research inspired me and gave me confidence. Also, I am grateful to Necati UÇAK for technical assistance during evaluating results.

Besides, I would like to thank ORS Co. Inc. (Ortadoğu Rulman Sanayi A.Ş), which I am honored to work with and which is one of the most important bearing manufacturers in the world. I would like to thank Factory Manager Feridun Özhan and Manufacturing Manager Mehmet Kahraman for their financial and technical support. I am grateful to the director of R&D department Ozan Müştak and his team who contributed to the execution of all experiments.

I am also grateful to my esteemed supervisor Sezgin ŞİMŞEK for his understanding and guidance during my master education. I would also like to thank the qualified and devoted ORS technicians who supported me in the preparation and adjustment of the tools during the experiments. In addition, I would like to thank Ömer KAYKI for his help in making the measurements and supplying the cutting tools.

Finally, I would especially want to thank my wife Aysun and little son Mete for their endless love and understanding over the years. This accomplishment would not have been possible without them. Thank you.

2021, 20 December **Gökhan SAĞIR**

THE EFFECTS OF HARD TURNING AND DEEP ROLLING PROCESSES ON SURFACE INTEGRITY AND FATIGUE LIFE OF DEEP GROOVE BALL BEARINGS

ABSTRACT

It is well known that the raceways of ball bearings are often damaged due to the harsh operating conditions. The fatigue life of the bearings is directly related to the surface and sub-surface characteristics of their raceways. Currently, surface integrity of an inner ring raceway is ensured by grinding process in conventional bearing production. In this study, the effects of hard turning and deep rolling processes on surface integrity and fatigue life of inner ring raceway of deep groove ball bearings were investigated. The inner rings of the 6208-type deep groove ball bearings were employed as workparts during the tests. This study consists of two important steps. In the first step, the effects of cutting conditions and tool geometry on cutting forces, surface integrity, noise level of bearings were studied in hard turning of the inner ring raceways (62 HRC). In the second step, the performances of grinding (GR), hard turning (HT) and hard turning+deep rolling (DR) processes applied to raceways of inner rings are compared to each other in terms of surface integrity, noise level and fatigue life. Experimental results in the first step showed that the passive force was significantly affected by the effective rake angle and the magnitude of contact area at the tool-workpiece interface. Another finding of the study also is that minimal surface roughness, roundness error, compressive stresses substantially affecting the fatigue life of bearings are achieved by V-35 insert. Therefore, the bearings with inner rings hard turned by V-35 insert were employed for evaluations in the second step. A remarkable point in second step is that although DR process under excessive pressures produces higher compressive residual stresses in the deeper layers of the work surface, DR bearings have a lower fatigue life than HT and GR bearings. HT bearings present longer fatigue life due to their inner ring raceways having high compressive stresses, low roundness error and surface roughness.

Keywords: AISI 52100, hard turning, bearing, residual stresses, fatigue life, deep rolling

SABİT BİLYELİ RULMANLARIN YÜZEY BÜTÜNLÜĞÜ VE YORULMA ÖMRÜ ÜZERİNE SERT TORNALAMA VE DERİN HADDELEME İŞLEMLERİNİN ETKİLERİ

ÖZ

Zorlu çalışma koşulları nedeniyle rulmanların yuvarlanma yollarının sıklıkla hasar gördüğü iyi bilinmektedir. Rulmanların yorulma ömrü, yuvarlanma yollarının yüzey ve yüzey altı karakteristikleri ile doğrudan ilişkilidir. Halihazırda, iç bilezik yuvarlanma yolunun yüzey bütünlüğü, geleneksel rulman üretiminde taşlama işlemi ile belirlenmektedir. Bu çalışmada, sabit bilyeli rulmanların iç bilezik yuvarlanma yollarının yüzey bütünlüğüne ve yorulma ömrüne sert tornalama ve derin haddeleme işlemlerinin etkileri araştırılmıştır. Testler sırasında iş parçası olarak 6208 tipi sabit bilyeli rulmanların iç bilezikleri kullanıldı. Bu çalışma iki önemli adımdan oluşmaktadır. İlk aşamada, iç bilezik yuvarlanma yollarının sert tornalanmasında (62 HRC) kesme koşullarının ve takım geometrisinin kesme kuvvetleri, yüzey bütünlüğü ve rulmanların gürültü seviyesi üzerine etkileri incelenmiştir. İkinci adımda, iç bileziklerin yuvarlanma yollarına uygulanan taşlama (GR), sert tornalama (HT) ve sert tornalama+derin haddeleme (DR) işlemlerinin performansları, yüzey bütünlüğü, gürültü seviyesi ve yorulma ömrü açısından birbirleriyle karşılaştırılmıştır. İlk adımdaki deneysel sonuçlar pasif kuvvetin, efektif talaş açısı ve takım-iş parçası temas alanının büyüklüğünden önemli ölçüde etkilendiğini göstermiştir. Çalışmanın bir diğer bulgusu da rulmanların yorulma ömrünü önemli ölçüde etkileyen minimum yüzey pürüzlülüğü, dairesellik, basma gerilmelerinin V-35 uç ile elde edilmesidir. Bu nedenle, ikinci aşamadaki değerlendirmeler için V-35 uç ile sert tornalanmış iç bilezikli rulmanlar kullanılmıştır. İkinci adımdaki dikkat çekici nokta, yüksek basınç altındaki DR işleminin iş parçası yüzeyinin daha derin katmanlarında yüksek basma gerilmeleri oluşturmasına rağmen, DR rulmanların HT ve GR rulmanlardan daha düşük yorulma ömrüne sahip olmasıdır. HT rulmanlar, yüksek basınç gerilmelerine, düşük yuvarlaklık hatasına ve yüzey pürüzlülüğüne sahip iç bilezik yuvarlanma yolları nedeniyle daha uzun yorulma ömrü sunmaktadır.

Anahtar Kelimeler: AISI 52100, sert tornalama, rulman, kalıntı gerilmeler, yoruma ömrü, derin haddeleme

CONTENTS

NOMENCLATURE

Roman Letter Symbols

A_c	Chip cross-sectional area, mm^2
ap	Depth of cut, mm
β	Shape parameter
f	Feed, mm/rev
F_c	Tangential force, N
F_f	Feed force, N
F_p	Passive force, N
h	Uncut chip thickness, mm
l	Cutoff length, µm
η	Scale parameter
R_a	Average surface roughness, µm
R_e	Roundness error, µm
RON_p	Peak value of roundness, µm
RON_t	Total of roundness, µm
RON_v	Valley of roundness, µm
R_q	Square average value of roughness, µm
R_t	Maximum height of profile of roughness, µm
t_{WL}	White layer thickness, µm
Vc	Cutting speed, m/min
x_f	Rolling shift, mm

Greek Letter Symbols

γ°	Normal rake angle, °
γ°_{eff}	Effective rake angle, °
κ_{ref}	Cutting edge angle, °

Acronyms

AISI	American iron and steel institute
Al_2O_3	Aluminum oxide
BUE	Built-up edge
CBN	Computer Numerical Control

Co	Cobalt
CO_2	Carbon dioxide
Cryo	Cryogenic
CW	Cold work
HRB	Hardness Rockwell B
HRC	Hardness Rockwell C
HV	Hardness Vickers
ISO	International Organization for Standardization
JIS	Japanese Industrial Standards
LN_2	Liquid nitrogen
LSC	Least Square Circle
MCC	Minimum Circumscribed Circle
MIC	Maximum Inscribed Circle
MQL	Minimum Quantity Lubrication
MZC	Minimal Zone Circle
PCBN	Polycrystalline cubic boron nitride
PCD	Polycrystalline diamond
SiC	Silicium carbide
TiAlN	Titanium Aluminum Nitride
TiC	Titanium carbide
TiN	Titanium nitride
WC	Tungsten carbide
XRD	X-ray diffraction
SEM	Scanning Electron Microscope

LIST OF TABLES

LIST OF FIGURES

CHAPTER 1

INTRODUCTION

In recent years, there are many new developments in manufacturing field in order to produce cost-effective and high-quality products. A wide variety of materials and manufacturing methods are still developed by the researchers to meet the requirements of key sectors such as defense, automotive and bearing industries. Hardened steels have very common use in these sectors due to their superior properties such as wear resistance and fatigue strength. They are frequently machined by abrasive processes such as grinding and superfinishing to provide the desired performance criteria such as better surface integrity and dimensional accuracy. However, hard machining as a substitution for grinding becomes more popular research field due to shorter cycle time, lower production cost and higher flexibility during especially machining of complex geometries. Hard machining can be defined as a machining operation of a workpiece (mostly hardened steels) with hardness values in the range of 45-70 HRC using ceramic or CBN cutting tools. It plays an increasingly important role by replacing time-consuming and expensive grinding process [1]. As well as the advantages of hard machining over the grinding, there are some issues during machining of hardened steels. Rapid tool wear is an obstacle to the hard machining process being economically applicable due to the high cost of CBN cutting tools and frequent tool change based longer machine idle time. Another issue is related to surface integrity characteristics such as white and dark layer formations, residual stresses, and surface roughness. White layer is a few micron thick untempered martensite formation which is more brittle and harder than the bulk material [2]. A white layer forms on steel surfaces machined under harsh cutting conditions and appears in white color under an optical microscope after standard metallographic preparation and etching processes. Therefore, it is frequently called “white layer”. The white layer is followed by over-tempered dark layer which is softer than both white layer and bulk material due to slower cooling rate. The white and dark layers have different hardness values and microstructures since the work material is subjected to different heat treatment cycles during the hard machining process. Therefore, they can have different levels of residual stresses. These different distribution and magnitude of residual stresses in the microstructure directly influence the fatigue life of the material due to premature crack formations [3]. Therefore, phase transformations during hard machining have a vital importance on bearing fatigue life.

Residual stresses are the stresses that remain in a material after the main reasons of the applied stresses such as mechanical and thermal loads on the material are removed. They can considerably affect the fatigue life, tribological properties and plastic deformation of machinery components [3]. There are two types of residual stresses: compressive and tensile residual stresses. Compressive and/or tensile stresses can remain on surface and subsurface of the final product according to the type of finishing processes. It is well-known that the work surface is plastically, thermally, and chemically affected during the machining of hardened steel. The forces applied by the cutting tool with negative rake angle to the workpiece lead to plastic compressive shear deformation during the cutting process and thus, produce residual compressive stresses on the work surface [4]. In addition, the frictions between tool-chip and tool-workpiece interfaces generate excessive heat during the hard turning process and this also induce tensile residual stresses. Therefore, the controlled heat generation and plastic deformation on final work surface has a vital importance in successful machining of hardened steels. Compressive residual stresses have a positive effect on fatigue performance of machinery components. Since they act to resist the applied tensile stresses and thus, they retard crack propagation, they are requested their formations at surface and near-surface regions during machining operations. The compressive residual stresses can be generated by hard turning operations. It is known that hard turning processes in which cutting inserts with negative rake angle are employed produce them. Unlike compressive stresses, it also is a known fact that tensile residual stresses have a negative effect on fatigue life of machinery components. The tensile stresses are harmful to fatigue behavior of hardened parts as they lead to the crack formation on the work surface and rapid crack propagation [5]. The main problems in hard machining are tensile residual stresses caused by untempered martensite (white layer), over-tempered martensite (dark layer) and cracks during cutting operation [5–

7]. Furthermore, tensile residual stresses in the surface and near-surface regions negatively affecting the fatigue life of bearings can occur during the grinding processes. Even if proper operating conditions and lubrication are utilized, the bearings fail prematurely because of surface and subsurface defects such as gaps, cracks or inclusions. Tensile residual stresses can occur in aggressive grinding conditions due to thermal shocks. Therefore, hard turning process is a good alternative to grinding process to prolong service life of machinery components [7]. Today, as well as hard turning, other manufacturing methods such as shot peening, laser shock peening and deep rolling are also used to increase the compressive stresses on the work surface. Recently, the deep rolling process is commonly applied to especially hardened steels in order to increase the compressive stresses and improve surface quality in industrial area. It minimizes cracks and fractures originated stress and thus, increases fatigue life of components. However, both hard turning and deep rolling parameters should be properly selected to achieve longer fatigue life.

The deep groove ball bearing is one of important load carrying components commonly used in industrial area, so the selection of a bearing for a specific application is dependent on type and magnitude of a load to be carried and its ability to cope with the loading conditions. As well as phase transformations and residual stresses, surface roughness and roundness error of raceway of this type of the bearing are very important for longer fatigue life and lower noise level. Surface roughness refers to irregularities remaining from machining operations in the direction of the normal vector on a real surface. It is well-known that crack initiation on rougher surfaces is easier than that on smoother surfaces due to notch effect of deeper feed marks. In addition, the frictions on rougher surfaces are more dominant than those on smoother surfaces due to larger contact area between balls and inner and outer rings. Therefore, the surface roughness substantially affects the fatigue life of the bearings. Roundness error can be defined as a measure of the deviations of a real circle or arc from an ideal circle. Similarly, raceways with lower roundness error are a reason to achieve longer fatigue life for the bearings due to their ideal forms. In addition, corrosiveness, lubrication conditions, and dust are other factors affecting the fatigue life.

In this study, the effects of hard turning and deep rolling process on surface integrity and fatigue life of raceway of deep groove ball bearings were investigated. The inner rings of the 6208-type deep groove ball bearings were employed as the workparts during the tests. This study consists of two important steps. In the first step, the effects of cutting conditions and tool geometry on, cutting forces, raceway roundness error and surface integrity (surface roughness, residual stresses, subsurface phase transformations) were studied in hard turning of the inner ring raceways (62 HRC). In the second step, the performances of grinding, hard turning, deep rolling operations applied to raceway of inner rings are compared to each other in terms of surface integrity, noise level and fatigue life. Finally, ball bearings were tested on a fatigue life tester and noise level tester for better understanding the effects of grinding, hard turning, hard turning+deep rolling processes on their fatigue life and noise level.

The rest of this chapter presents general information about AISI 52100 bearing steel, hard machining, surface integrity, tool material and geometry and deep rolling. In addition, a review of some related works is given in this section. The rest of the thesis is organized as follows:

- Chapter two presents experimental setup and procedure of the study. The materials, instruments and experimental and assessment procedures used in this thesis study are also described.
- Chapter three discusses the test results in detail in terms of scientific perspective.
- Chapter four presents concluding remarks of the study and some recommendations for future works.

1.1 Hard Machining

Hard machining is machining of hardened steels with a hardness of above 45 HRC. However, it is mainly applied to materials with a hardness of 58-65 HRC. The work materials in the hard machining include different types of hardened tool steels, case-hardened steels, nitrided steels and heat-treated powder-metallurgical parts. Hardened steels are widely used in ball bearing industry as well as in the gear, mold and tool industries [8]. They are primarily employed in finishing or semi-finishing processes of machinery components desired higher dimensional accuracy and better surface finish [9]. Today, hardened steels are frequently finished using abrasive processes such as grinding operations. Owing to the recent developments in cutting tool materials, now, it is possible to cut the hardened steels at higher speeds using conventional turning, milling, and drilling tools rather than grinding wheels. So, advanced machining processes such as hard machining become increasingly more popular [4, 5] in machining of complex components [8] to provide lower machining costs, more efficient cutting performance and better part quality. Figure 1.1 shows a hard turning process.

Figure 1.1 A hard turning process [10]

Abrasive processes such as grinding, superfinishing, honing and lapping are finishing operations applied to hard engineering materials with a hardness value of over 60 HRC. The hard machining operations in which cutting tools with proper tool material and tool geometry are employed can provide comparable dimensional accuracy and surface finish to abrasive processes. So, hard machining processes increasingly become common in industrial area recently. For being a good alternative to the abrasive processes, hard machining should provide better surface integrity and longer tool life. Although the abrasive processes have some advantages in terms of surface integrity in comparison to hard machining, it is an important machining strategy due to its remarkable properties such as higher material removal rate, process flexibility and sustainable machining capabilities. Comparison of hard machining and grinding which is an abrasive process can be clearly seen in the Figure 1.2.

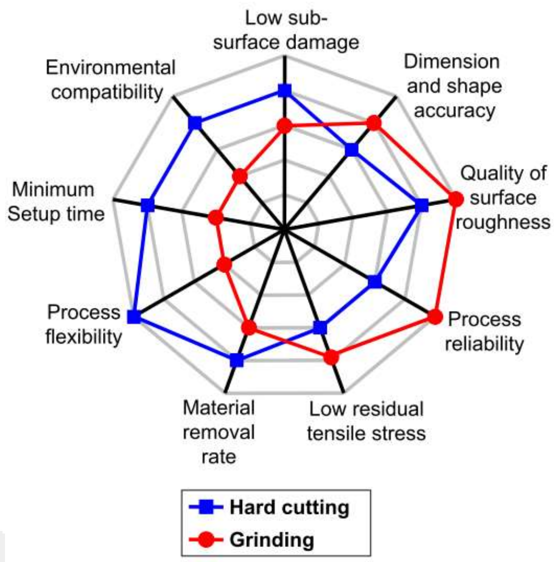

Figure 1.2 Comparison of grinding and hard machining operations [11]

Hard machining processes can be generally divided into two subclasses as hard milling and hard turning. Hard turning is commonly employed in the automotive industry to produce some cylindrical parts such as shafts, gears and bearings whereas hard milling is generally preferred in the mold industry to produce the prismatic parts such as dies and molds. Machinery components such as ball bearings in these sectors must be resistant to wear and fatigue since they are frequently operated under higher cyclic loads and vibrations. To satisfy these requirements, the components should have good fatigue and surface integrity properties. Ball bearings are machinery elements widely used to support radial and axial loads acting on rotating and reciprocating shafts. In general, the bearings are produced in nine steps. Firstly, bar raw materials are forged. Since the forging process is conducted at 1100 °C, the spheroidizing process which is one of the heat treatment methods is also performed at this temperature simultaneously. In this way, a ductile material with more spherical grains and hardness of 80-90 HRB are obtained prior to a turning operation. Cold rolling operation is carried out to enlarge the inner and outer diameter of the forged material. After the turning process, a heat treatment is applied to the turned components in order to increase their hardness and wear resistance. Thus, the hardness of the materials increases up to 60-65 HRC. Then, the grinding operation, one of the finish operations, is applied to inner and outer rings of the bearing to obtain close tolerances and better surface finish. Finally, the raceways of rings are also subjected to a superfinishing abrasive process to minimize friction between the ball and the raceway. Thus, the bearing parts now are ready for assembly. Conventional production line of the bearings can be clearly seen in the Figure 1.3.

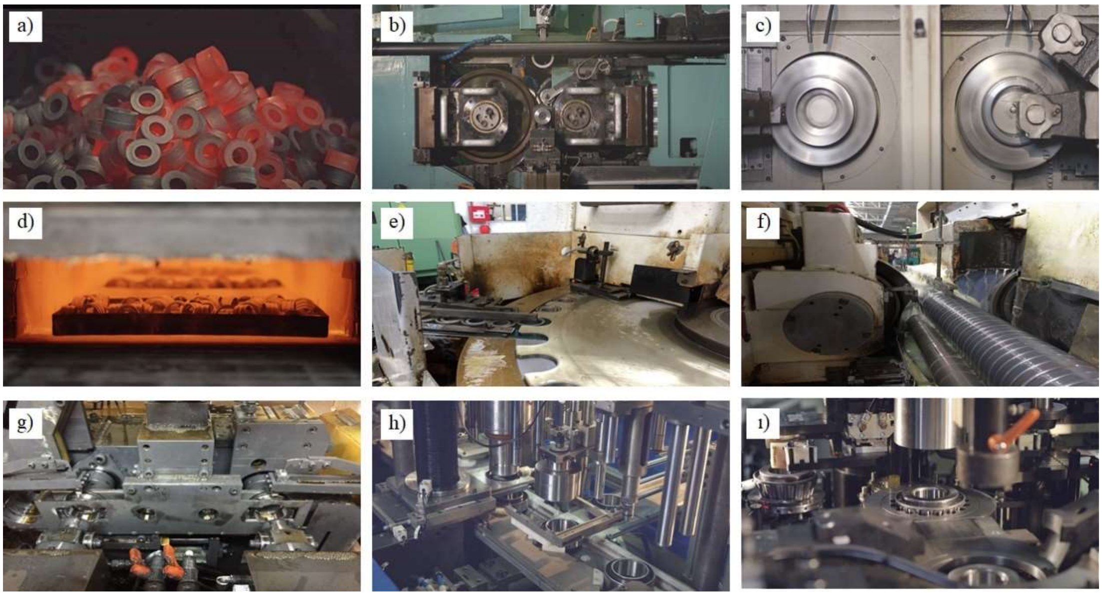

Figure 1.3 Conventional production line of the bearings, a) forging and spheroidizing, b) cold rolling, c) turning, d) heat treatment, e) face grinding, f) centerless grinding, g) superfinishing h) and ı) assembly

As mentioned earlier, hard turning has a great potential to become a good alternative to grinding operations in the bearing industry. Hard turning offers several advantages over grinding and these can be listed as follows:

- The comparable surface roughness values to grinding can be produced during hard turning [5, 9].
- Complicated geometries can be easily created in hard turning operations [12, 13].

- Higher cutting speeds can be achieved using a hard turning process [14]. Therefore, while increasing the metal removal rate, processing time can be reduced up to 60% [15, 16].
- Hard turning produces long chips that can be recycled, while grinding produces metal dust that is difficult to collect, throw away or recycle.

In addition to the advantages mentioned above, it is well-known that a hard turning process has some disadvantages. The elevated temperatures are generated during the hard cutting process due to higher hardness of the parts [17]. For this reason, rapid tool wear, undesired stresses and phase transformations can be frequently observed in hard turning operations. They negatively affect the machining costs (shorter tool life) and product quality (worse surface integrity). In order to improve the performance of a hard turning process, the mentioned disadvantages should be minimized using optimal cutting conditions and high-performance cutting tools.

1.2 Cutting Tools

1.2.1 Tool materials

The cutting tool material and geometry should be determined in accordance with cutting conditions, machine tool and work material employed during hard machining. Otherwise, premature tool failure that increases the machining costs can take place during/after hard cutting process [5,17]. It is a known fact that WC-Co (Tungsten Carbide-Cobalt), PCD (Polycrystalline Diamond), ceramics, cermets and CBN (Cubic Boron Nitride) are widely used as cutting tool materials in conventional machining processes in industrial area. WC cutting tools are one of the most preferred cutting tool materials in conventional machining operations. Owing to their low hot hardness and wear resistance, they do not often prefer in hard turning operations in which high cutting temperatures are generated. PCD is the hardest cutting tool material [19]. However, it is not suitable for the machining of ferrous metals due to its high chemical affinity with steels. This case also leads to rapid crater wear and thus, premature tool failure. As well as high hardness, the ceramics have higher thermal resistance, chemical inertness, and longer tool life than WC tools. However, they are very susceptible to fracture in case of the tension and bending stresses due to their lower toughness [20]. Considering the harsh cutting conditions of hard turning, ceramics can be a cheap and low-performance alternative to CBN tools. Their cutting performance is low at especially higher speeds due to rapid tool wear. CBN tools are the most suitable option for hard machining thanks to its higher wear resistance, hot hardness, chemical stability and corrosion resistance at higher speeds [21]. Therefore, polycrystalline cubic boron nitride (PCBN) tools are widely employed in hard machining operations due to their superior properties in industrial area although they are very expensive. The CBN inserts are frequently produced by brazing a layer of PCBN with about thickness of 0.5 mm on a tungsten carbide substrate as shown in Figure 1.4.

Figure 1.4 A PCBN insert

The CBN tools include different amounts of CBN particles with various grain sizes. The particle size and content, and binder type selected for CBN tool materials determine their mechanical and physical properties. In general, three different types of CBN tools are used in machining operations of hardened steels. They can be listed as follows:

- The straight CBN contains a high amount of CBN particles (about 90wt.%) and a metal binder (Al).
- High content CBN contains a medium amount of CBN particles (about or less than 80wt.%) and a metal/ceramic binder.
- Low content CBN contains a low amount of CBN particles (less than 70 wt.%) and ceramic (TiN or TiC) binder [22].

As the amount of CBN particles increases in the microstructure of a tool, its toughness increases. It is well-known that cutting tools with high toughness are generally preferred to be used for interrupted cutting processes such as milling [23]. As a continuous cutting process (turning) is conducted in the scope of this study, low content CBN inserts are chosen as tool materials for providing a more efficient cutting performance during hard turning.

1.2.2 Tool geometry

The primary goal of tool geometry is to provide the efficient separation of chips from the work material. Hence, the selection of proper tool geometry to cutting conditions and work materials has a critical importance in terms of a high-performance cutting process in machining operations. During turning operations, indexable inserts are commonly used to reduce their costs and to enhance efficiency. Several types of the insert shapes are shown in Figure 1.5 [24].

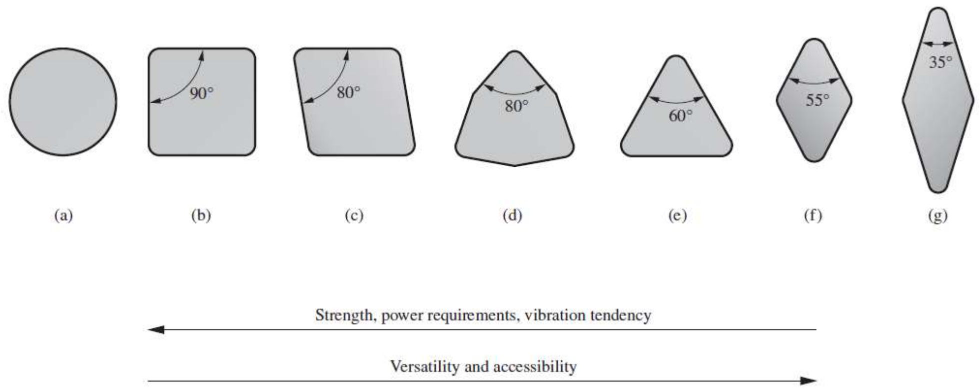

Figure 1.5 The insert shapes: (a) round, (b) square, (c) rhombus with 80°-point angle, (d) hexagon with three 80°-point angles, (e) triangle, (f) rhombus with 55°-point angle, (g) rhombus with 35°-point angle [24]

The inserts shapes should be selected according to machining needs such as strength, power requirements, and vibration tendency or versatility and accessibility for maximum tool performance and product quality. For example, since the round inserts has larger nose radius, they are stronger and more resistant to chipping and/or fracture. However, they need more cutting power and produce more vibration during machining operations. There is an economic advantage of round inserts because they can be indexed multiple times for more machining operations per insert. The rhombus shapes with acute point angles are suitable because of their versatility and accessibility for machining operations such as turning in tight spaces, facing and finishing cuts. As the rhombus inserts have only two cutting edges, they are not a cost-effective insert type.

In addition to shapes of cutting inserts, there are some angles on each of them such as rake angle, clearance or relief angle and cutting-edge angle to provide an efficient cutting process. The rake angle plays an important role in providing the insert strength and forming compressive residual stresses in hard turning operations. In general, rake angles have two configurations; positive and negative angles as shown in Figure 1.6 [25].

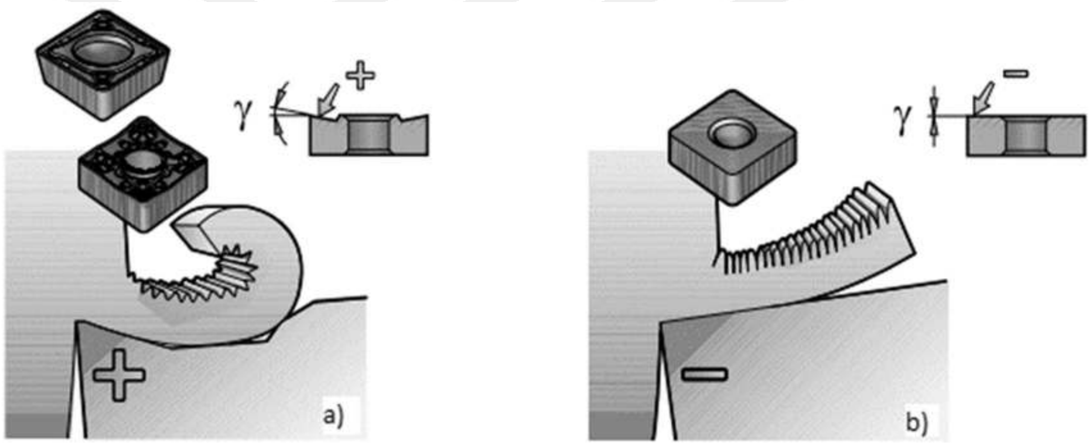

Figure 1.6 The rake angle types, a) positive rake angle and b) negative rake angle [25]

A positive rake angle (γ°) forms a sharp cutting edge as illustrated in Figure 1.6.a. In a cutting process where inserts with a positive rake angle are employed, cutting forces and surface roughness reduces due to becoming chip separation easy from work material by means of their sharper cutting edges. However, the inserts with this geometry have less cutting-edge strength. For this reason, it is not frequently preferred in machining of hard-to-cut materials such as hardened steels. The negative rake angles assure longer tool life, and they provide an opportunity to roughing cuts of ductile steels or semi-finishing and finishing operations of hard-to-cut materials such as hardened steels due to their higher cutting-edge strengths than positive rake angles.

The ceramic tools such as CBN, Al_2O_3 and SiC are ground with negative rake angles due to their higher hardness and lower toughness. In addition, their bending and tensile strengths are very low in comparison to their compressive strength. This also is another reason for negative rake angles of ceramic tools. Unlike grinding operation, in hard finish turning operations, cutting inserts with negative rake angles also produce larger compressive residual stresses on work surface and subsurface, which improve fatigue life of machinery elements [26].

As mentioned earlier, under harsh conditions such as hard turning, a better tool performance can be achieved using tool geometries with negative rake angles. However, the cutting-edge configurations of cutting inserts such as chamfer honing, round honing and so on also plays a dominant role in a machining success [27]. Cutting-edge preparations in industrial use are shown in Figure 1.7.

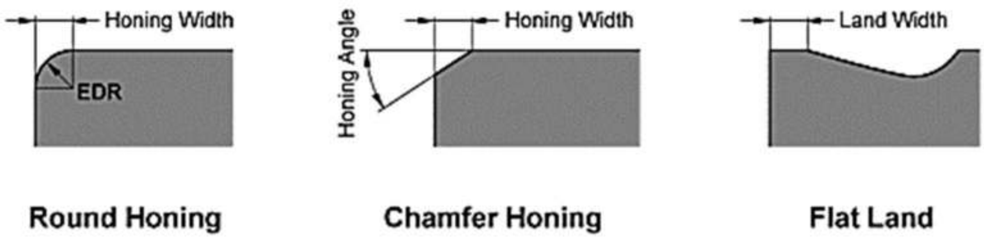

Figure 1.7 Cutting edge preparations [28]

Cutting-edge preparations significantly prolong tool life by minimizing micro-chippings and fractures on especially hard and brittle cutting tools such as CBN, diamond and ceramics [29]. In addition, chamfered or honed inserts can lead to rake angles (effective rake angle) to enlarge at some cutting conditions during machining operations such as hard turning and micro-milling [30]. The effective rake angle is defined as an angle between normal direction to the finished work surface to chip-flow direction. The effective rake angle (γ_{eff}), the nominal rake angle (γ), and the uncut chip thickness (h) are illustrated in Figure 1.8. As shown in Figure 1.8, in case uncut chip thickness is less than chamfer distance of cutting edge, effective rake angle is equal to the sum of the nominal rake angle and chamfer angle. This case leads to an increase in compressive zone (CZ) and thus, a reduction in tensile zone (TZ) (Figure 1.8). This also means that larger effective rake angles produce more compressive residual stresses instead of tensile stresses on surface and subsurface of work material. In addition, the chamfered cutting edges can create better surface integrity than the honed cutting edges [31]. Therefore, chamfered cutting edges are widely used in hard turning operations.

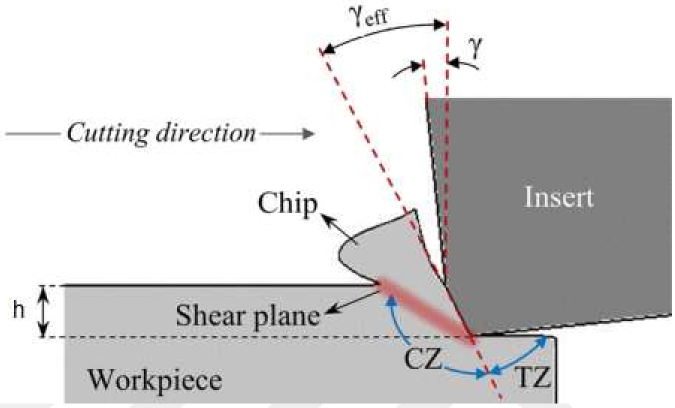

Figure 1.8 Effective rake angle (γeff) and nominal rake angle (γ) [32]

In finishing cuts of hardened steels, lower surface roughness values less than 0.8 μm (Ra) is usually achieved by grinding operations. This requirement can be also provided at low feed values in hard turning operations. Moreover, wiper inserts are employed to further improve the surface roughness values in machining operations recently. A wiper insert has a larger main radius or a rectilinear edge defined by several smaller radii. The geometries of conventional and wiper inserts are shown in Figure 1.9.

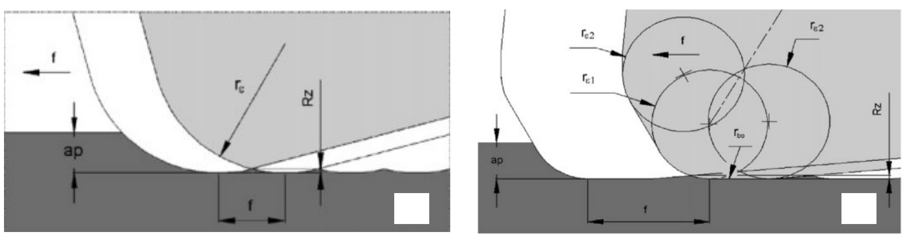

Figure 1.9 Inserts with (a) wiper and (b) conventional geometries [33]

Since the contact distance at tool-workpiece interface increases thanks to the larger radius or rectilinear edge of the wiper inserts, they produce better surface roughness than conventional inserts in hard turning operations. The increasing contact distance also means that higher cutting temperatures are generated owing to increasing frictions at tool-chip and tool-workpiece interfaces. Therefore, the tool life of the wiper inserts is shorter than that of conventional inserts [33].

During hard turning operations in which the wiper inserts are employed, various cooling and/or lubrication methods can be needed to minimize excessive frictions and heat generation in the cutting zone. Conventional fluids, MQL and cryogenic cooling are some of these cooling and/or lubrication methods. In recent, new hybrid CryoMQL (MQL+CO2 and MQL+LN2) techniques have been introduced to machining sector. In case of the use of wiper inserts, it is reported that hybrid techniques generally are successful in providing of better tool life and surface integrity [32].

1.3 Cutting Forces

Cutting forces can be simply defined as a measure of resistance of the material against cutting tool. Force directions and magnitudes may differ in different cutting processes such as turning, milling, drilling and so on. In general, there are three force components acting on a cutting tool used to separate the chip from the work material during a turning operation. These are feed force (Ff), radial force (Fp), and tangential force (Fc). The feed force acts on the tool in the axial direction (feed direction) and tends to push the tool away from the chuck. The radial force acts on the tool in the radial direction (depth of cut direction) and tends to push the tool away from the workpiece. Tangential force acts on the tool in the normal direction to its rake face (speed direction) and tends to resist to rotation of work part. Of the three force components in a conventional turning operation, the tangential force is the greatest, the feed force is less in magnitude and the radial force also is the least. Tangential (Fc), feed (Ff) and radial force (Fp) components are shown in Figure 1.10. The magnitudes of the force components generally depend on workpiece material, tool geometry, and cutting conditions [34].

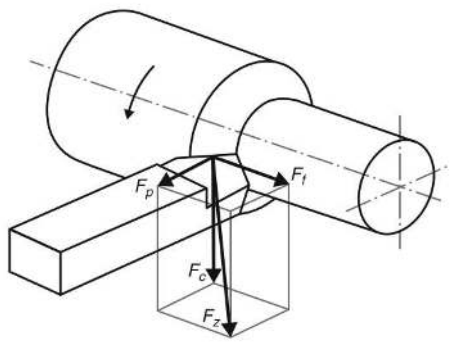

Figure 1.10 Force components in a turning process [34]

Figures 1.11 illustrates the variation of the cutting forces with cutting conditions. As shown in Figure 1.11, cutting forces are drastically affected by cutting conditions. They increase with increasing feed and depth of cut owing to an increase in chip cross-section while they generally decrease with increasing cutting speed due to thermal softening of work material and a reduction in built-up edge tendency at elevated cutting temperatures.

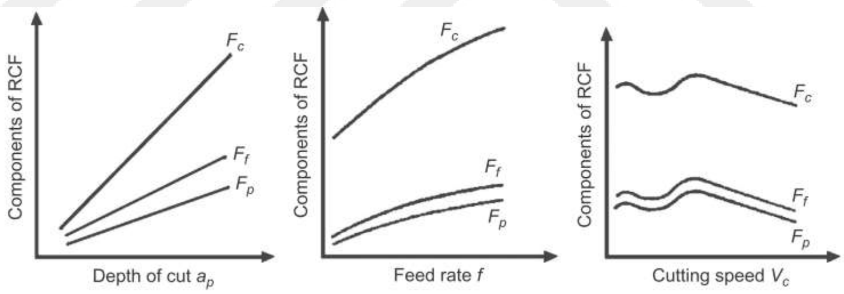

Figure 1.11 Variation of cutting forces with cutting conditions [35]

In addition to cutting conditions, the rake angle of a cutting insert is one of the most important factors affecting the cutting forces during turning operations. An increase in the rake angle (from negative rake angle to positive one) reduces the force values due to increasing cutting-edge sharpness but also lowers cutting-edge the strength (Figure 1.12). This case may cause to fractures and/or chippings on cutting edge with the effect of excessive forces. For this reason, the positive rake angles are applied to tough tool materials such as high-speed steels, cast cobalt alloys and tungsten carbide. As mentioned earlier, since brittle tool materials such as the ceramic, PCD and CBN inserts have high hardness and low toughness [22], they cannot exhibit higher strength to bending and tensile stresses. Therefore, they should be ground with negative rake angles. The negative rake angles produce higher cutting forces and present an excellent cutting-edge strength. So, they are very suitable for brittle cutting tool materials and harsh cutting conditions such as roughing cuts, hard turning and so on.

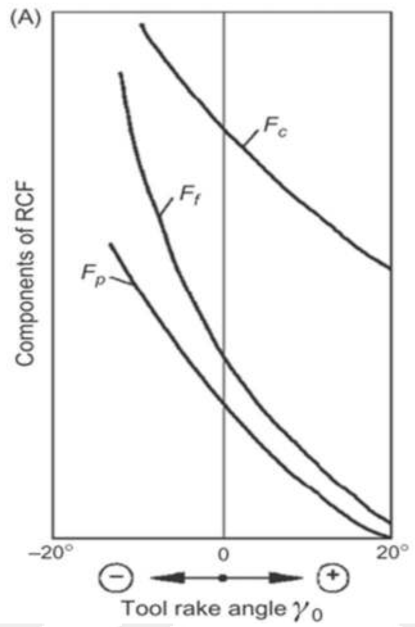

Figure 1.12 Variation of cutting forces with rake angle [35]

It is a known fact that the cutting forces during a hard turning operation can vary in accordance with the hardness of the work material. The relationship between the force components and hardness of work material (AISI 5115 steel) is given in Figure 1.13. As shown in Figure 1.13, first, the forces from cutting of highly ductile work material are relatively high due to high BUE tendency and as the hardness value increases up to 45 HRC, they decrease thanks to a reduction in BUE tendency along with increasing cutting temperature. Along with the steel hardness higher than 45 HRC, the cutting forces dramatically increase owing to higher yield strength of work material and rapid tool wear originated excessive cutting temperatures during the cutting. This hardness value is also accepted as the limit of the hard machining [36].

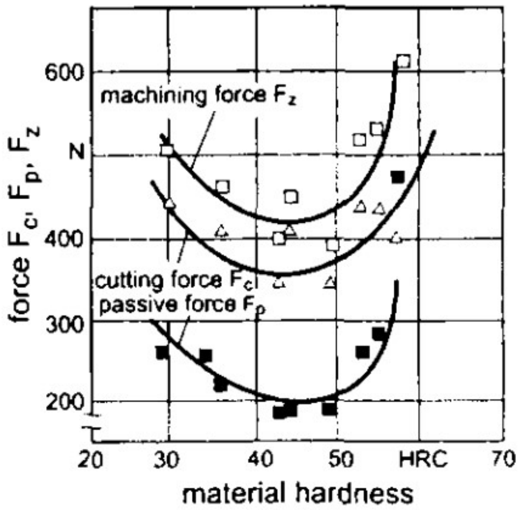

Figure 1.13 Variation of cutting forces with work material hardness [13]

It is well-known that a hard turning process generally is a finishing process. Therefore, as smaller depths of cut (0.05-0.3 mm) and feeds (0.05-0.2 mm/rev) are frequently used during finishing cuts, both the ratio of depth of cut to tool nose radius and the ratio of uncut chip thickness to cutting-edge radius are less than 1 [22]. Unlike a conventional cutting operation, this case provides to be the largest force component of the radial force among others during the hard turning (Figure 1.14). This case also leads to more rigid and stable cutting process. As shown in Figure 1.14, medium level and lowest ones of force components are tangential and feed forces, respectively.

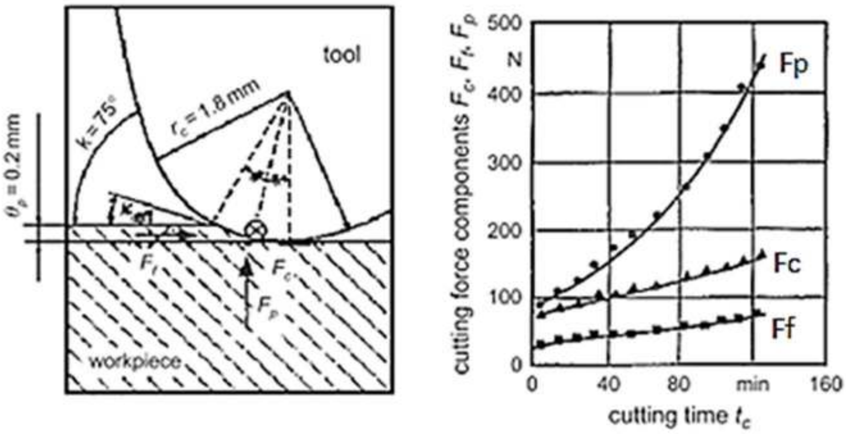

Figure 1.14 a) A schematic view of the cutting forces during hard turning, b) variation of cutting forces with cutting time [35]

1.4 Surface Integrity

Surface integrity is defined as surface and subsurface conditions of a work part plastically deformed by machining operations. It is considered as one of the most important indicators showing final product quality [31, 32]. The surface integrity involves surface finish, microstructure, phase transformations, and residual stresses. It is generally affected by thermo-mechanical loads generated during machining operations. They depend on many parameters such as the work material, cutting conditions, tool material and geometry, machine tool characteristics and so on.

1.4.1 Surface Roughness

The surface roughness is an important indicator for the product quality, which significantly affects fatigue strength, wear rate, friction coefficient, and corrosion resistance of the machinery components. In practice, there are many factors affecting the surface roughness such as cutting tool (tool material and geometry), work material (mechanical and physical properties, and heat treatment condition), cutting conditions (cutting speed, feed, depth of cut and cutting fluid) and machine tool (rigidity and vibration) [37]. Figure 1.15 shows a schematic view of tool-workpiece interaction and formation of surface roughness in an orthogonal plane [38].

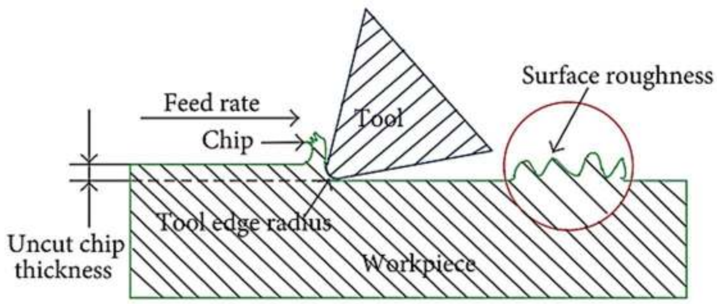

Figure 1.15 A schematic view of tool-workpiece interaction in orthogonal plane [38]

To prolong fatigue life of machinery elements such as bearings and gears operated at higher rotational speeds better surface quality is desirable. Because of their higher friction coefficients, the rougher surfaces are exposed to rapid wear and plastic deformation under harsh working conditions. The surface roughness is positive and/or negative finely spaced micro-irregularities in normal direction to a definite surface newly created during machining operations (Figure 1.16) [39].

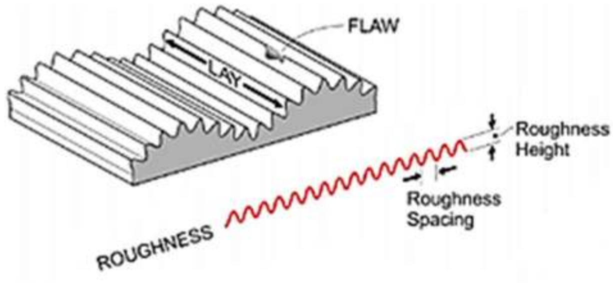

Figure 1.16 A surface roughness profile [39]

In terms of the surface roughness, a defined area is characterized using several linear measurement methods. These methods are Ra (average roughness), Rt (maximum height of the profile) and Rz (average maximum height of the profile). The vertical distance between the highest and lowest points on the sampling length is defined by Rt. On the other hand, Rz is the mean value of five maximum consecutive peak-to-valley distance on the sampling length. According to ISO 4287, Ra is characterized by the arithmetic average value of the profile heights and depths on the measured range. Finally, Rq is defined as the root mean square average value of the roughness profile heights and depths. Ra and Rz roughness parameters quantified in this study are shown in Figure 1.17.

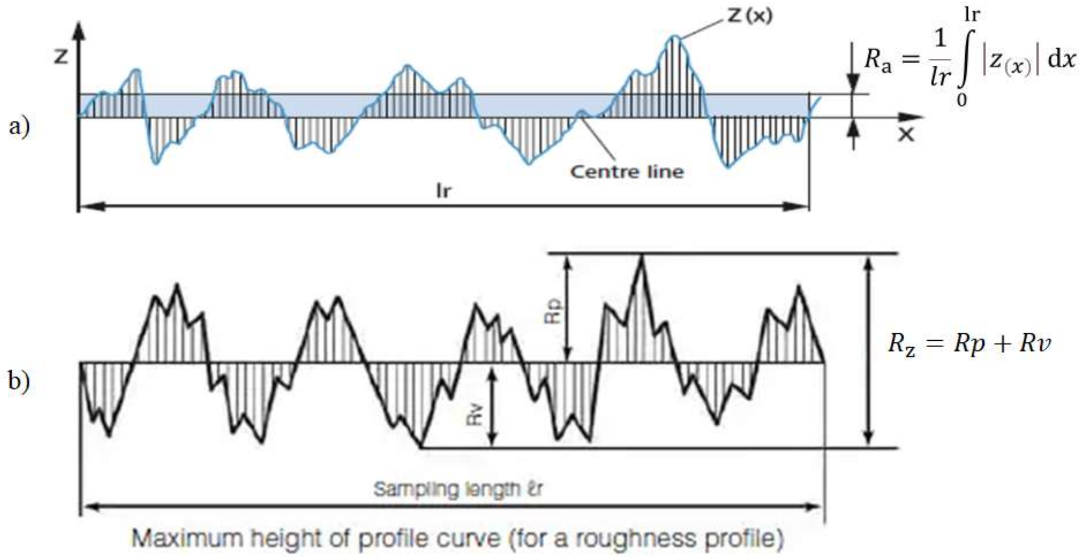

Figure 1. 17 a) Ra and b) Rz roughness parameters

It is a known fact that the cutting conditions employed in a turning process substantially affect the surface roughness. Figure 1.18 shows variation of the roughness parameters (Ra, Rt and Rz) with cutting speed (Vc), feed (f) and depth of cut (a_p) [40]. As shown in Figure 1.18, the surface roughness increases with increasing feed. This case can be attributed to the increases in vibrations with increasing cutting forces and in scallop heights between feed marks created by cutting tools during metal cutting. Although the cutting speed has not a theoretical effect on the surface roughness, many researches works in the literature report that surface roughness improves with the increasing cutting speed. This case can be also explained with decreasing cutting forces and BUE tendency at higher cutting speeds. Although the depth of cut has a negative effect on the surface roughness due to increasing vibrations during the cutting, this effect generally is at a negligible level [41].

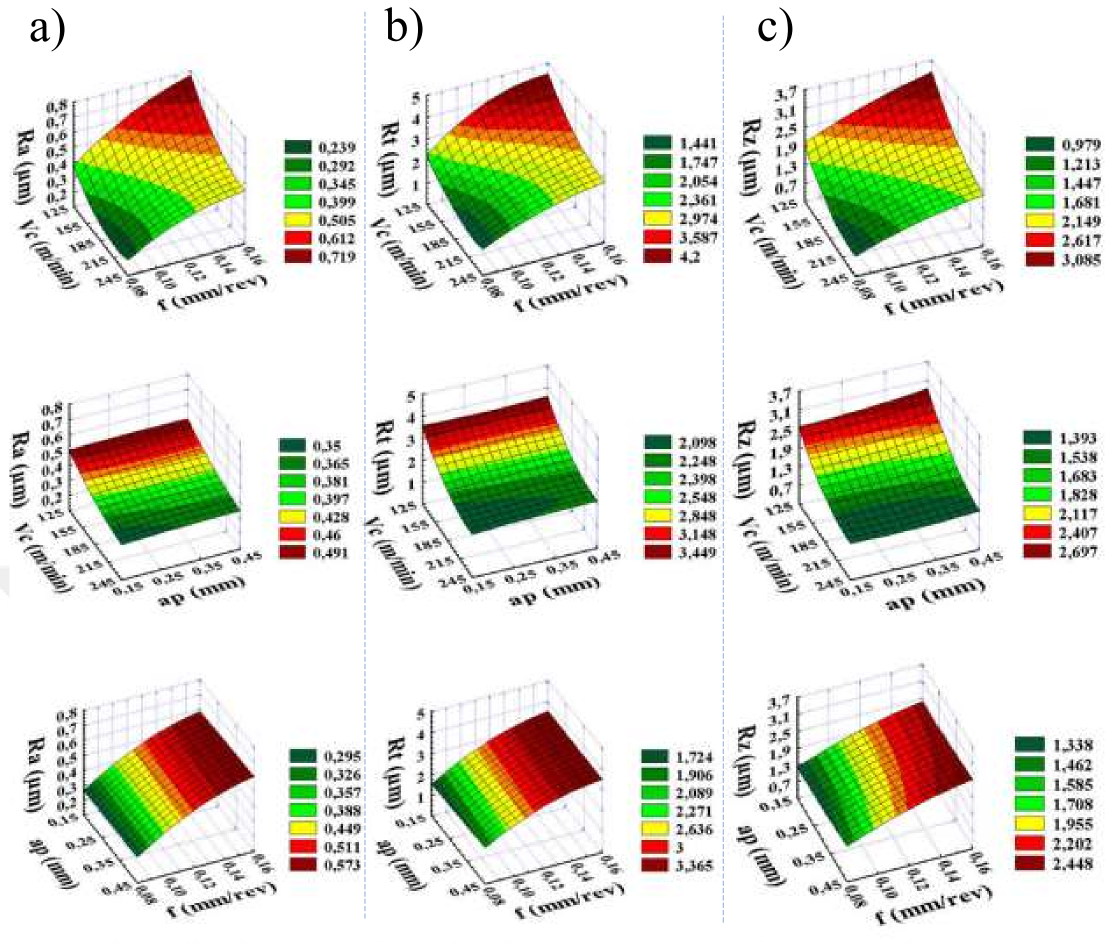

Figure 1.18 The effects of cutting conditions on roughness parameters, a) Ra, b) Rt and c) Rz [40]

Another alternative to conventional inserts for producing better roughness values is wiper inserts. As mentioned earlier, the wiper inserts have a larger main radius, or a rectilinear edge defined by several smaller radii (Figure 1.9). Thanks to their larger nose radius or rectilinear edge, the wiper inserts can produce better surface roughness values than the conventional inserts and even similar values to those of grinding operations. With the use of the wiper inserts, the surface roughness values obtained at low feeds become possible at higher feeds [8]. For that reason, the use of wiper inserts has become increasingly more common in industrial area in order to provide significant improvements in the surface roughness and machining time. However, the rapid tool wear formed during turning of hard-to-cut materials such as hardened steels has limited the common use of the wiper inserts. They also are not suitable for tight machining spaces such as raceway of a bearing because it is not possible to obtain the desired roundness error values.

It is a known fact that owing to a need to higher surface quality, the accurate components such as the bearings employed at higher rotational speeds are subjected to abrasive processes (generally grinding) after conventional turning and heat treatment procedures. Ra values in the range of 6.3-0.4 µm are generally produced during conventional turning operations while they can lower down to a value between 1.6-0.1 µm during grinding operations. However, using hard turning operations that are an alternative to grinding operations, it is possible to lower Ra values below 0.4 µm at low feeds and depths of cut [42]. Another way to improve the surface quality is implementation of a deep rolling process to the surface after machining operations. Thanks to deep rolling, the feed marks formed during machining operations are crushed with the effect of applied high working pressures to the machined surface. For that reason, after the deep rolling process, the surface roughness can improve more than twice. The Ra values can be even less than 0.3 µm (Figure 1.19) [43].

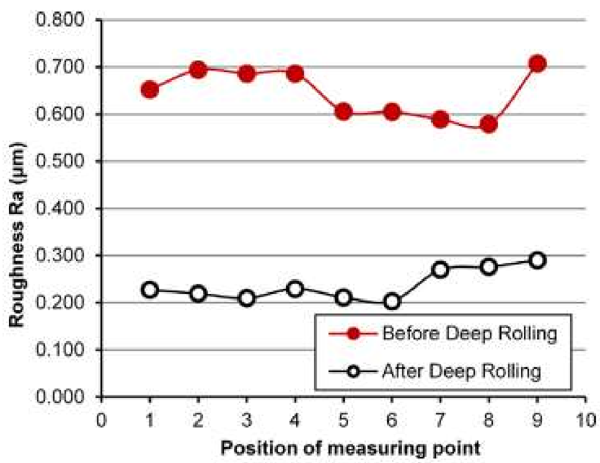

Figure 1.19 Ra values before and after deep rolling process [43]

1.4.2 Roundness error

The roundness error can be defined as a measure of deviation between maximal and minimal radii on a real circular profile projected from cylindrical surfaces (Figure

1.20.a). It is one of the important geometric tolerances for cylindrical surfaces and substantially affects the performance of rotational parts [44, 45].

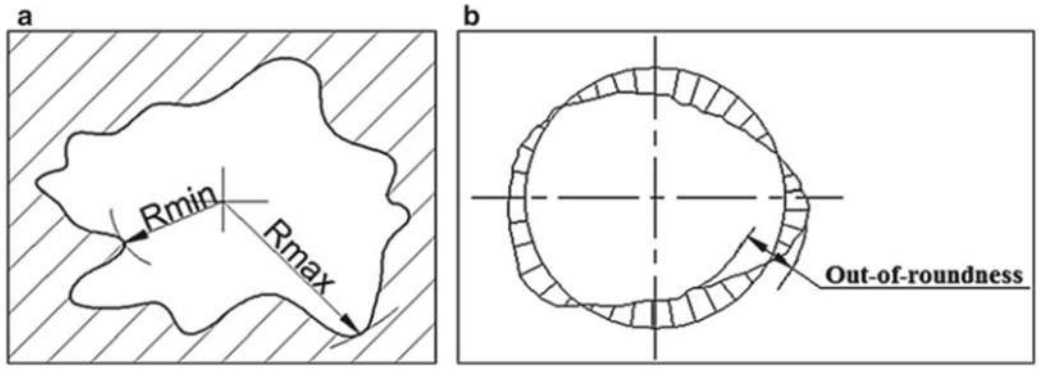

Figure 1.20 a) Minimal and maximal radii and b) out-of-roundness [46]

In the literature, there are several methods for roundness error measurements. These are the minimum circumscribed circle (MCC), the maximum inscribed circle (MIC), the minimum zone circles (MZC) and the least squares circle (LSC). In this thesis study, the LSC method is employed in order to determine roundness error of raceways of ball bearings.

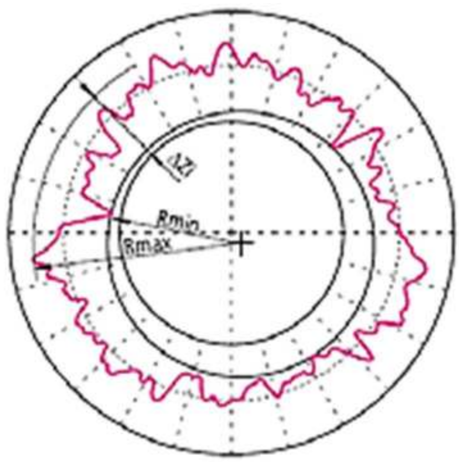

Figure 1.21 The least squares circle method [47]

The least squares circle is fitted inside the profile such that the sum of the squares of radial ordinates between the circle and profile are minimized as shown in Figure 1.21. The center of the LSC is then used to draw a circumscribed and an inscribed circle on the polar profile and the out-of-roundness value (Figure 1.20.b) is the radial separation of these two circles. The least squares circle and its center are unique because there is only one that meets the definition, and its accuracy depends on the number of points taken [47]. The measurement of roundness error (usually referred to simply as roundness) is very important in terms of product quality. For instance, a ball bearing with faulty raceway tends to be noisy and to fail prematurely [48]. The cutting conditions (cutting speed, feed, and depth of cut) dramatically affect the roundness error of cylindrical surfaces. That is, thermo-mechanical loads during hard turning determine its magnitude.

Roundness total (RONt) is defined in ISO 1101 as the separation of two concentric circles that enclose the circular section of interest. RONt results determined for four different geometries with diameter of 25 mm are shown in Figure 1.22. The roundness error values created by concentric circles which inscribe and circumscribe the real geometries are quite different from each other even if their diameters are the same. These shapes are extreme cases. In hard turned materials, the roundness should be as low as 1-5 µm.

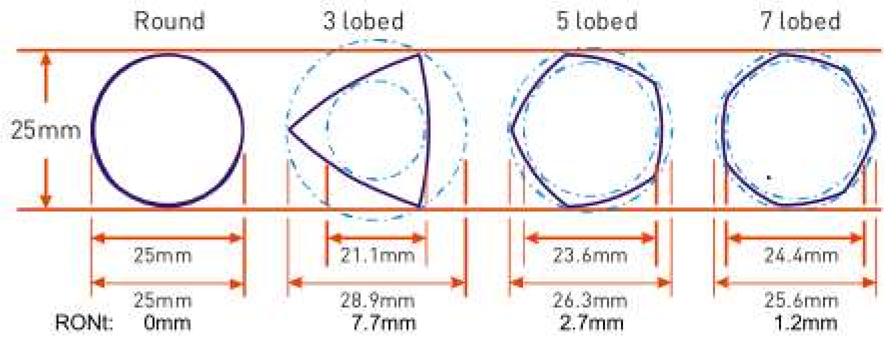

Figure 1.22 Some roundness error form of cylindrical parts [44]

In addition, an example for roundness error measurement of a hard turned part is shown in Figure 1.23. RONt (sum of roundness) is the most common parameter. RONt was previously defined as “peak-to-valley”. It is the sum of RONp (roundness peak) and RONv (roundness valley). In this study, RONt is considered as roundness error value.

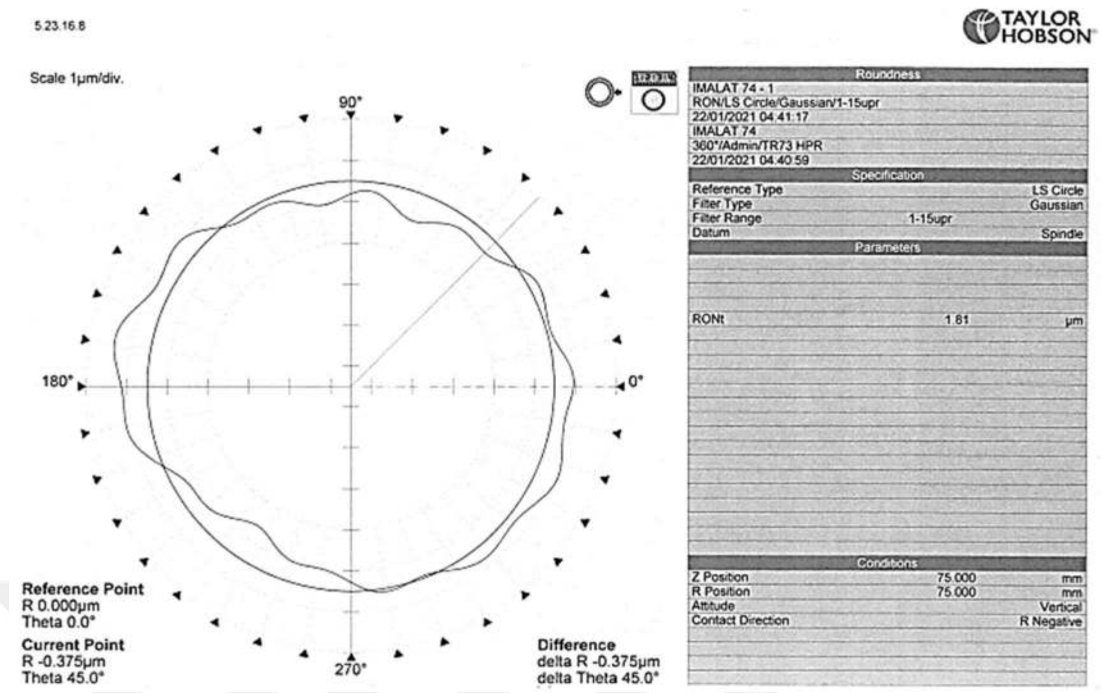

Figure 1.23 An example for roundness error measurement of a hard turned part

1.4.3 Phase transformations

Thermal cycles (higher temperatures and subsequent rapid cooling) generated during some manufacturing processes such as hard machining and grinding can lead to some microstructural changes on the work material. They can negatively affect its surface and subsurface conditions and thus, fatigue life. In the literature, there are two types of the phase transformations frequently encountered during grinding and hard machining operations. They are white and dark layers. The white layer is generally at a few microns thick and is hard and brittle due to its untempered martensitic structure. On the other hand, the dark layer has higher thicknesses (20-40 μm) than the white layer and a softer and more ductile structure owing to the presence of overtempered martensite [49]. It is reported that the white layer is undesirable due to its negative effect on fatigue life of the machinery parts. It produces a network of micro-cracks and tensile residual stresses on the work surfaces. For this reason, it should be removed from surface prior to final product or prevented its formation with the selection of proper cutting conditions. Besides, it is clear that the dark layer has also a significant influence on the magnitudes and inhomogeneous distribution of residual stresses [3, 38].

As mentioned earlier, the excessive cutting temperatures generated during machining of the hardened steels cause to some microstructure changes on their surface and subsurface. Under harsh cutting conditions, the workpiece temperatures can exceed their austenitization temperature with the effect of friction and plastic deformation. If the cutting temperatures exceed the austenitization temperature of the steel, the ferrite phase in its microstructure transforms into the austenite phase and after quenching, a white layer (a harder phase than bulk material) with a high-stressed and crack-prone martensitic structure forms on work surface. Besides, if the cutting temperatures exceed its tempering temperatures and but do not reach to its austenitization temperature, then an overtempered zone called dark layer (a softer phase than bulk material) takes place [27]. White layer and dark layer formations are shown in Figure 1.24.

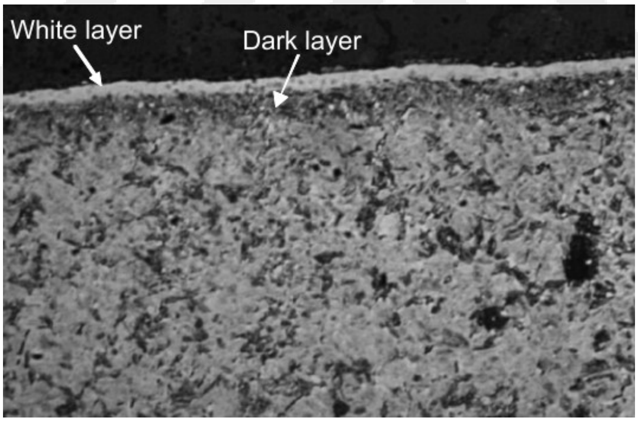

Figure 1.24 White and dark layer formations [50]

As a result of typical characteristics of the phases created by different thermal cycles, different types and magnitudes of the residual stresses occur in the white and dark layers and their interface [33]. In addition, it is a known fact that fatigue life significantly decreases with an increase in thickness of white layer containing tensile residual stresses. Moreover, at a certain period, white layer can partially delaminate and thus, cause to a premature failure under high contact pressures [5].The negative effects of these residual stresses on fatigue life are discussed in the Section 1.4.3.

It is clear that as the cutting speed increases, the temperatures in the cutting zone increase due to the increasing strain rate of the work material. Therefore, white and dark layer formations and their magnitudes is closely related to the cutting conditions (especially cutting speed) employed during a cutting process. The effects of cutting speed on cutting temperatures and white layer thicknesses are shown in Figure 1.25 [51].

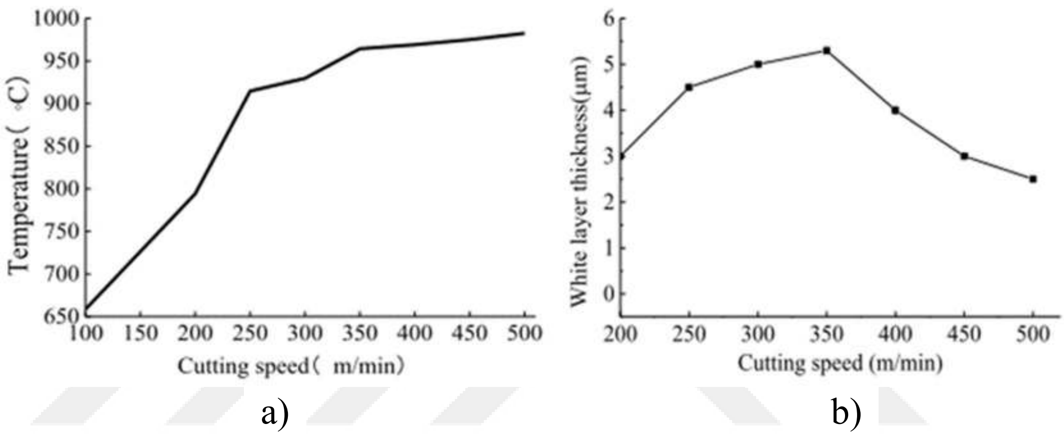

Figure 1.25 The effects of cutting speed on a) cutting temperatures and b) white layer thicknesses on AISI 52100 bearing steel [51]

As shown in Figure 1.25.b, the increased cutting temperatures lead to an increase in the white layer thickness due to heat intensity effect at relatively lower speeds. Another remarkable point in Figure 1.25.b is that it decreases as cutting speed increases after cutting speed of 350 m/min. This case can also be explained with temperature gradient effect [52]. As contact time between the tool and the workpiece becomes shorter with an increase in cutting speed, the heat cannot be transferred into deeper subsurface regions. This case leads to a decrease in subsurface temperatures at higher speeds and thus, a reduction in white layer thicknesses.

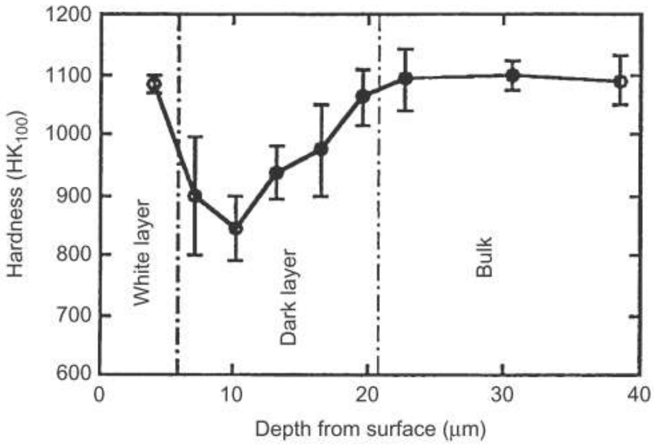

Figure 1.26 Hardness values of different phases after hard turning [22]

Figure 1.26 illustrates microhardness variations in different phases (white layer, dark layer and bulk material) from machined surface to a certain depth (40 μm) after a hard turning operation. It is observed from Figure 1.26 that the hardness value of white layer with untempered martensitic structure is similar to that of the bulk material. On the other hand, the dark layer with overtempered martensitic structure is more ductile than both bulk material and white layer. It is reported that thickness of heat affected zone has become about 20 μm which is one-tenth of the depth of cut (a_p = 200 μm) [22].

1.4.4 Residual stresses

Residual stresses substantially affect fatigue life of mechanical components. Thermo-mechanical effects during cutting process are main reasons of the residual stresses. For instance, the pressure applied by a cutting insert with negative rake angle to the workpiece surface leads compressive residual stresses at newly created surface. In addition, it is well-known that thermal effects (heating and rapid cooling) generated during grinding process in which cutting temperatures are very high induce to tensile residual stresses. The resultant residual stresses existing on the machined surface depends on relative importance of each factor [53].

The type and magnitude of the residual stresses are determined using the XRD (X-ray diffraction) method to assess the surface conditions of work material. This approach essentially tests the angle at which the highest diffracted pressure occurs in irradiated crystalline particles [54]. Since there are two principal motions (cutting speed and feed motions) in turning operations, measurements are conducted in hoop (cutting speed direction) and axial directions (feed direction) for evaluating of the residual stresses. Both axial and hoop (circumferential) directions identified for residual stress measurements on an inner ring of a ball bearing are shown in Figure 1.27.

Figure 1.27 The measurement directions of residual stresses for an inner ring

It is well-known that characteristics of depth profiles of residual stresses are important in providing of longer service life for a mechanical part [55]. The residual stresses produced on surface and subsurface of work material during hard turning are affected by many parameters. Some of them can be listed as tool and work materials, nose radius and cutting-edge preparations (chamfer, honed and land), cutting parameters (speed, feed and depth of cut), tool wear, cutting fluid, tool geometry and so on.

As mentioned earlier, the residual stresses can be originated from a combination of mechanical and thermal effects during a cutting action. The mechanical action usually requires a plastic deformation process and leads to compressive residual stresses. Besides, thermal effect (temperature increases due to friction and plastic strain, and subsequent rapid cooling) produces tensile and/or compressive residual stresses (mostly tensile stresses) depending on the type of phase transformations. During transformation of austenite phase to martensite phase with the effect of rapid cooling, a volume expansion takes place owing to a transition from a face-centered cubic structure to a more open tetragonal structure. This case also results in compressive stresses at work surface layers. However, the deeper layers of work surface are subjected to lower temperatures and cool at slower speeds, so the higher pressure of the top layers restrains their contraction. Thus, tensile residual stresses can be produced at deeper layers of the work surface. The residual stresses formed during a cutting process depends on the magnitudes of the mechanical and thermal effects [45].

A main factor that controls distribution of elastic stresses in subsurface layer is rake angle. As indicated in Fig 1.28, when a cutting operation is performed using the inserts with larger negative rake angles or rounded cutting edges, the compressive zone noticeably enlarges while tensile zone decreases (Fig 1.28c and Fig 1.28d) [22].

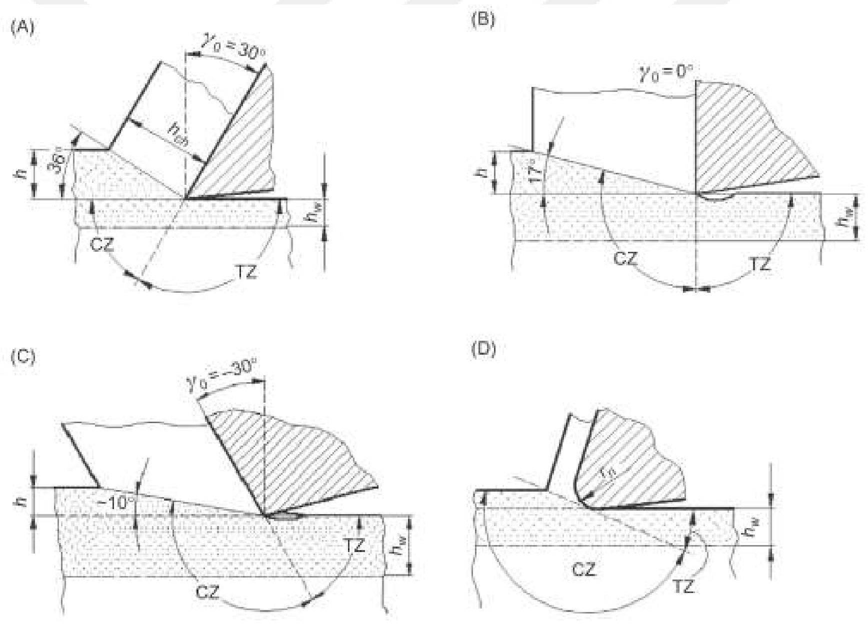

Figure 1.28 Variation of compressive and tensile zones with a) positive, b) zero, c) negative rake angles and d) rounded cutting edge

Higher compressive stresses on subsurface layers of work material can be induced by larger negative rake angles (or effective rake angles). The maximum stress position is pushed into deeper layers of the work surface with an increase in negative rake angles [26]. In machining operations, the cutting-edge strength of the inserts is always ensured with the edge preparations such as chamfer, honed and land. If not, the insert cutting edge can prematurely fails with the effect of fractures and micro-chippings induced by fluctuations in cutting forces in earlier periods of the cutting process. A cutting-edge preparation profile is shown in Figure 1.29. In CBN inserts widely used in hard turning operations, either chamfered or chamfered-honed cutting-edge profiles are preferred to increase edge strength and cutting efficiency.

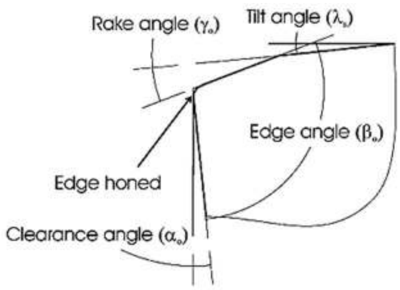

Figure 1.29 A cutting-edge profile

In some cases, the cutting-edge chamfer angle may have important effects on magnitudes of the compressive residual stresses. For example, if uncut chip thickness is less than chamfer distance in a hard turning process, the cutting-edge chamfer angle leads to a negative rake angle to increase. In this case, effective rake angle is equal to the sum of chamfer angle and nominal rake angle (Figure 1.30). This case also induces higher compressive stresses due to a larger effective rake angle.

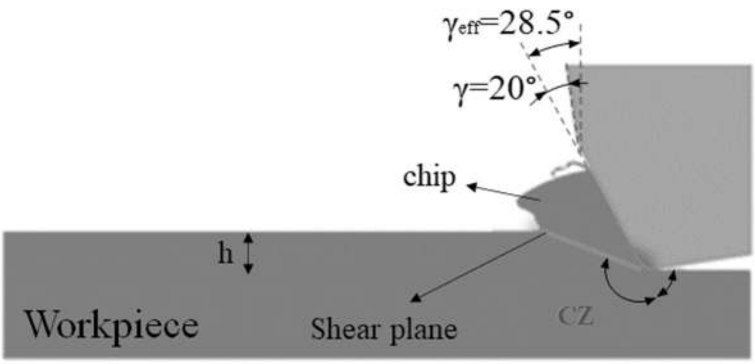

Figure 1.30 Schematic representation of nominal rake angle (γ), effective rake angle (γ_{eff}) and uncut chip thickness (h)

Another important factor affecting residual stresses is the feed. More compressive residual stresses can be obtained by preferring a higher feed values in both the axial and circumferential directions [56]. The main reason for this is that as the feed increases, the cutting forces increase. The effects of feed on compressive stresses are shown in Figure 1.31. As shown in Figure 1.31, there is an increase in residual stresses (especially hoop stresses) with increasing feed values.

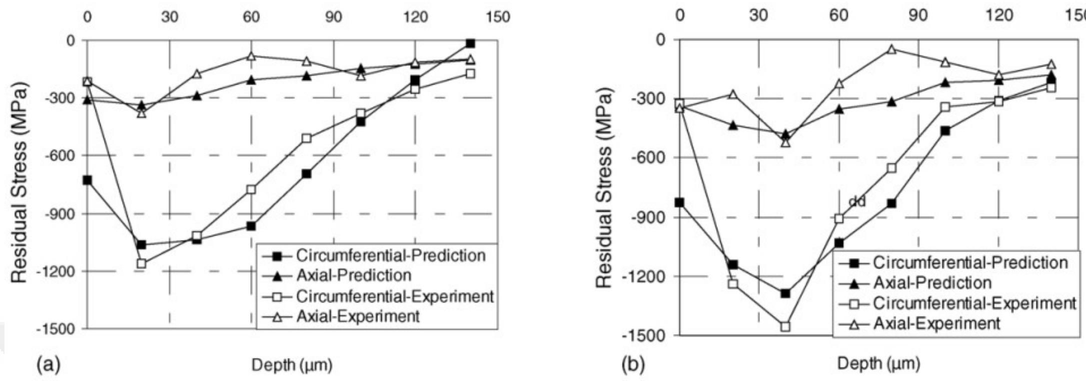

Figure 1.31 The effect of feed on compressive stresses a) 0.28 mm/rev and b) 0.56 mm/rev [56]

1.5 Deep Rolling

The performance of mechanical components commonly employed in sectors such as the aerospace, power generation and automotive is very significant because cyclic mechanical loads significantly shortens their useful life. [51, 57]. Surface treatments are a series of processes applied to metallic materials in order to produce compressive residual stresses on work surface and subsurface against cyclic loading conditions and thus, to improve their service life. Shot peening, laser shock peening and the deep dolling are some of the most widely used surface treatment methods [58].

The deep rolling is a method by which a mechanically or hydraulically driven a ball or roller element applies an aggressive pressure onto a workpiece to plastically deform its surface and subsurface regions. This method produces a layer (1-2 mm) of compressive residual stresses which is helpful to extend fatigue life of mechanical components. In addition to the formation of compressive stresses, it also offers two advantageous mechanisms: strain hardening and better surface finish [53, 54, 59]. The rolling pressure on the work surface induces to a slight amount of plastic deformation and thus, a deeper layer of compressive residual stresses. Although deep rolling is a more cost-effective method in comparison to traditional shot peening and laser shock peening, it is not possible to apply the method to especially mechanical components with thin and intricate geometries (small radii and fillet) due to its rolling tool with low accessibility [60].The schematic view of a deep rolling process is shown in Figure 1.32.

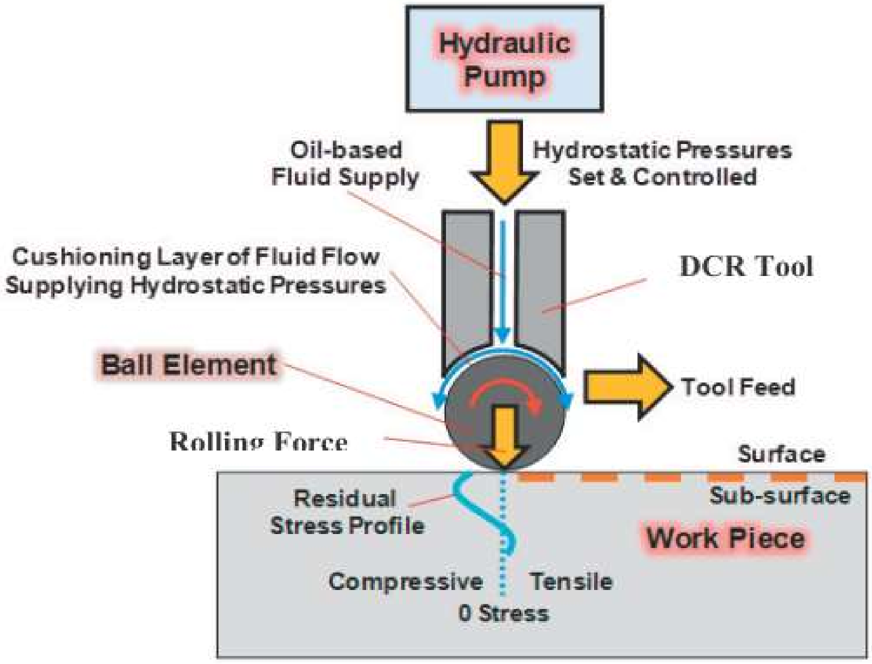

Figure 1.32 A deep rolling process [60]

In the deep rolling, the tool moves along a direction determined by rolling speed and feed when a load greater than its yield strength is applied to the work material. The effects of the deep rolling on residual stresses and hardness distributions in steels are shown in Figure 1.33. As a consequence, along with an increase in hardness and in strength due to strain hardening effect after deep rolling process, axial and hoop compressive residual stresses also increase [61–63].

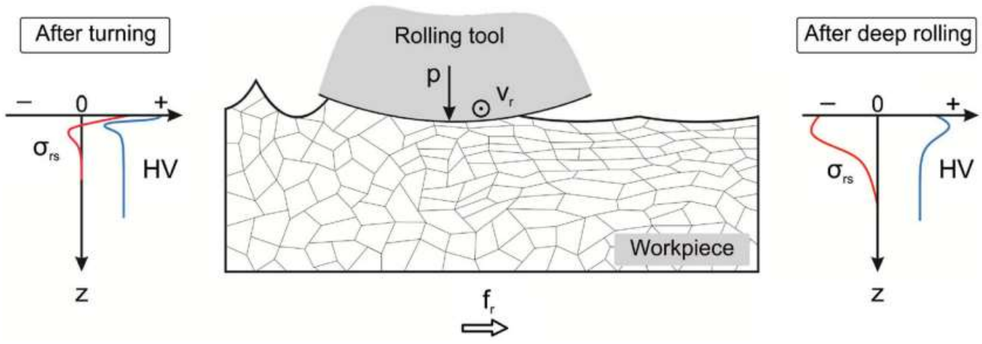

Figure 1.33 The effects of deep rolling on residual stresses and hardness distributions [61]

Although the main goal of the deep rolling is to produce the compressive residual stresses, its positive impact on the surface quality of the mechanical components should not be neglected. For example, hard turning and the subsequent deep rolling can result in better surface integrity characteristics than grinding processes. Grzesik and Zak investigated the surface quality of hard turned alloy steel (59-61 HRC) subjected to superfinishing and deep rolling. They reported that both hard cutting-abrasive processes and hard cutting-deep rolling processes can be an alternative to conventional turning and grinding operations to produce high-quality hard parts [64, 65].

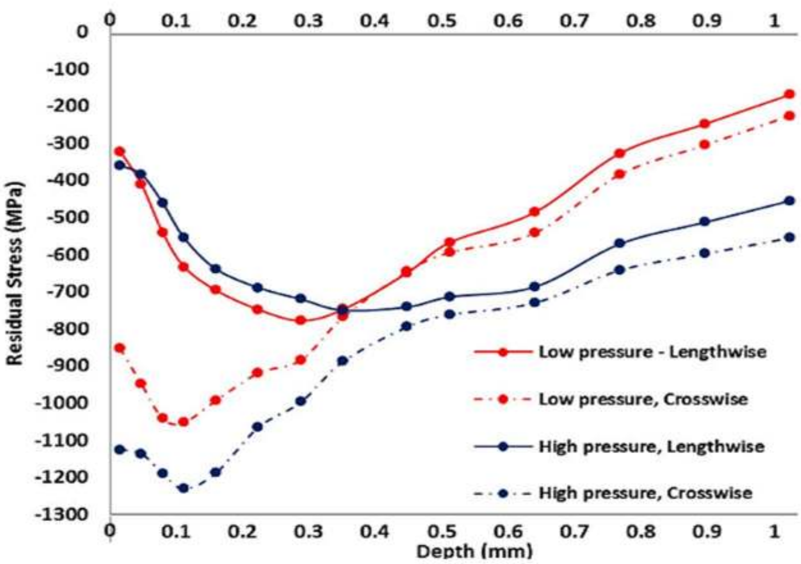

Figure 1.34 The effects of high- and low-pressure deep rolling on residual stress profiles [65]

The residual stress depth profiles obtained after deep rolling processes at two different pressures (i.e., high, and low) are shown in Figure 1.34. It can be observed from Figure 1.34 that the crosswise path exhibits higher compressive residual stress in the subsurface zone down to a depth of around 0.4 mm. After 0.4 mm, a significant decrease in stresses takes place towards the tensile direction. When a comparison is made between the applied rolling pressures, it can be said that the deep rolling process with high pressure is more effective in producing of higher compressive stresses in deeper subsurface zones (between 0.4-1mm).

1.6 Literature Review

The bearings are one of machinery elements required a long service life due to its common use in industrial area. The tensile residual stresses play an important role in the premature initiation of fatigue cracks which directly affects the service life of any machinery element [66]. On the other hand, to ensure a longer fatigue life, the formation of compressive residual stresses on surface and subsurface of the work material are desired. It is well-known from earlier explanations that hard turning produces compressive residual stresses that ensure longer fatigue life unlike grinding. To produce additional compressive stresses in deeper zones and to increase stress density, a combination of hard turning and deep rolling processes is implemented to hardened steels. This combination is employed as an alternative to conventional turning and grinding operations for finishing of hardened steels.

This literature review investigates the effects of the process parameters of the hard turning and the deep rolling processes on surface integrity and fatigue life of the mechanical components.

1.6.1 Surface Integrity in Hard Turning

Recently, because of its high application potential, the turning of hardened steels is an important research topic in industrial and academical fields. In the literature, the researchers have aimed to investigate the effects of different tool geometries, tool materials, cutting conditions on cutting performance and product quality in hard turning processes generally. In addition, they have carried out many experiments and/or modelling studies for better understanding the effects of process parameters on surface integrity that is the most important indicator of the product quality.

Since cutting-edge geometry and cutting conditions have important effects on the residual stresses, many researchers have focused on a relationship between them [17, 29, 64, 67]. Thiele et al. [30] performed a study the effects of different cutting-edge geometries (honed and chamfered) on residual stresses of hardened AISI 52100 steel with two different hardness values (41 HRC and 57 HRC) at a certain cutting condition. They reported that honed-edge produces more compressive residual stresses than chamfered-edge in machining of work materials with hardness values of both 41 HRC and 57 HRC. However, when machined harder work material (51 HRC), they observed that higher compressive residual stress was produced in the subsurface. That is, as hardness of the workpiece increases from 41 HRC to 57 HRC under the same cutting conditions, maximum compressive hoop residual stress increases from 700 MPa to 1800 MPa (Figure 1.35).

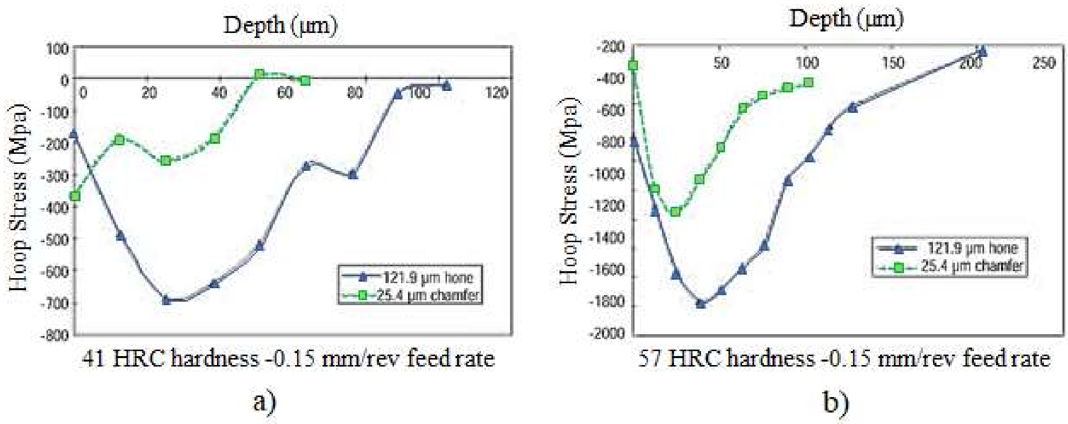

Figure 1.35 Variation of hoop compressive stresses with hardness a) 41 HRC and b) 57 HRC [30]

Hua et al. [7] investigated residual stresses in hard turning of bearing steel (62 HRC) using different cutting edge geometries. They reported that larger honed-edge and chamfered+honed-edge produce larger compressive stresses than other edge geometries (sharp, chamfered and small honed) as shown in Figure 1.36. However, the cutting tool with larger hone radius achieves larger penetration depth as well as higher compressive residual stresses. This case is associated with increasing contact area at the tool-workpiece interface. An increase in contact area produces the higher cutting forces and this case also leads to the increases in residual stresses and their penetration depth.

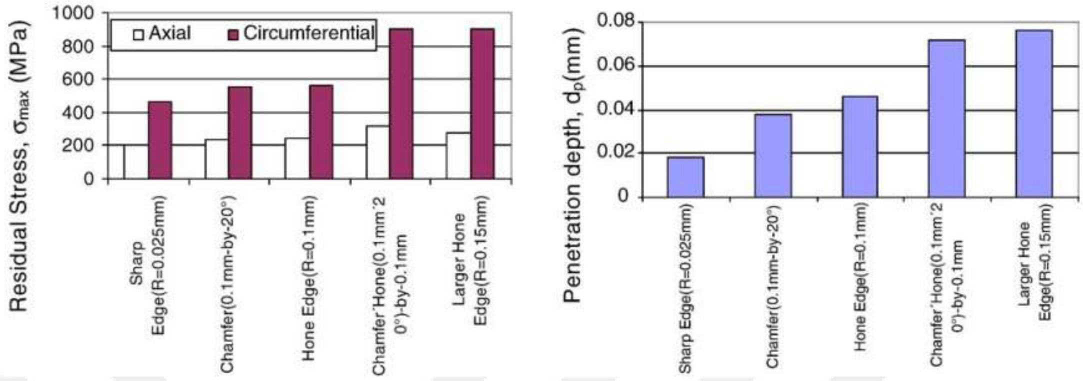

Figure 1.36 The effects of cutting-edge geometry on a)maximum stresses and b)penetration depth [7]

Dahlman et al. [26] performed a number of hard turning tests on AISI 52100 steel (62 HRC) using cutting inserts with rake angles of -6°, -21°, -41°, -61°. They reported that cutting inserts with a greater negative rake angle produce higher compressive stresses. Another result of the study is that the maximum stress position is pushed into deeper layers of work surface with increasing negative rake angles. The effects of rake angle on stresses are shown Figure 1.37.

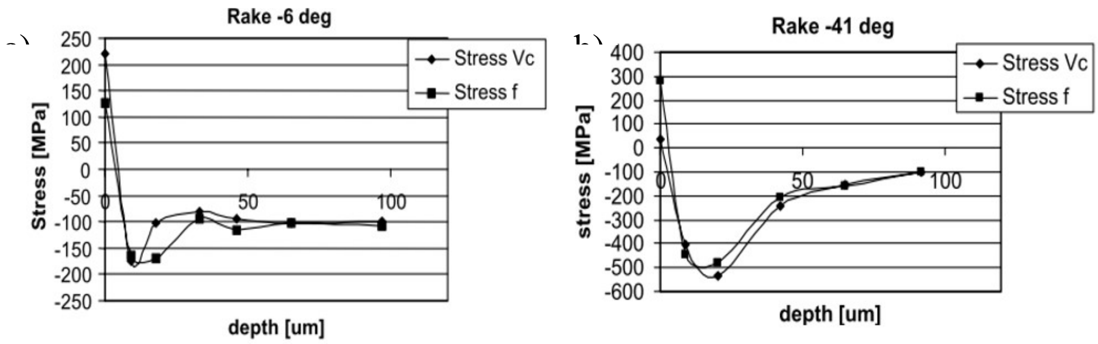

Figure 1.37 The effects of rake angle on stresses; a) -6º and b) -41º [26]

They also investigated the effects of feed and depth of cut on residual stresses at a fixed cutting speed value. They found that depth of cut does not have any significant effect on residual stresses, however, the stresses increase as the feed increases (Figure 1.38).

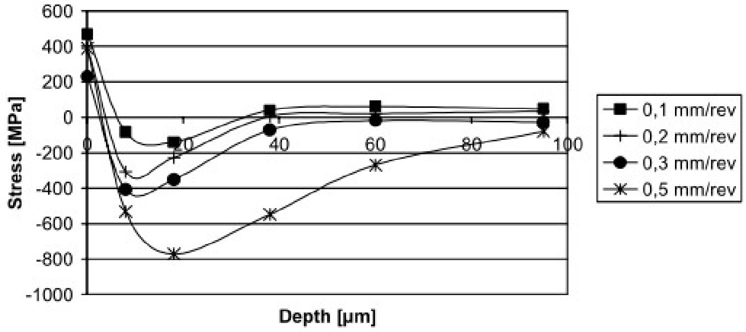

Figure 1.38 The effects of feed on hoop stresses [26]

Caruso et al. [68] studied the influences of the cutting-edge geometry, workpiece hardness, cutting speed, and white and dark layers formations on the residual stresses in dry orthogonal hard machining of AISI 52100 steel. They claimed that tool geometry, workpiece hardness and cutting parameters dramatically affect the surface and subsurface stress conditions. In addition, they reported that the compressive residual stresses in both axial and hoop directions increase with increasing cutting speeds in case of the use of chamfered inserts as shown in Figure 1.39. Another finding of this study is that phase transformations have a major influence on the magnitude and position of maximum compressive residual stress peaks. They also found that at white-dark layer interface, the highest residual stress value is produced.

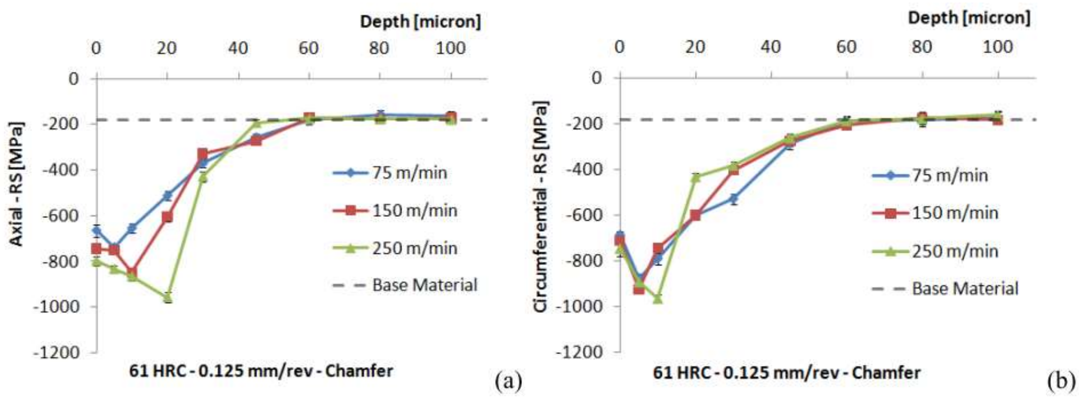

Figure 1.39 Variation of residual stresses with cutting speed in a) axial and b) hoop directions [68]

In another study, Revel et al. [55] claimed that precision hard turning is convenient for the finishing of AISI 52100 bearing components. They used hydrostatic slideways to ensure high stability and stiffness in the machine tool during machining. They indicated that precision hard turning induces compressive residual stresses at the surface and subsurface, which corresponds to the transition zone. Moreover, increasing cutting speed leads to increase the level of compressive residual stresses. They reported that the cutting speed (thus, cutting temperature) has a significant effect on the formation and distribution of residual stresses in the hard turning of the AISI 52100 bearing steel (61 HRC).

Zhou et al. [69] found that cutting forces increase with an increase in the cutting-edge chamfer angle in turning of hardened AISI 52100 steel (60-62 HRC). Another finding of this study is that the passive force (Fp) in the radial direction is higher than the main cutting force (Fc) in tangential direction unlike conventional turning operations. The passive forces increase more dramatically than other force components do with increasing chamfer angle as shown in Figure 1.40. In addition, an increase in the chamfer angle (thus, an increase in forces) also leads to higher compressive residual stresses on deeper layer of the work material.

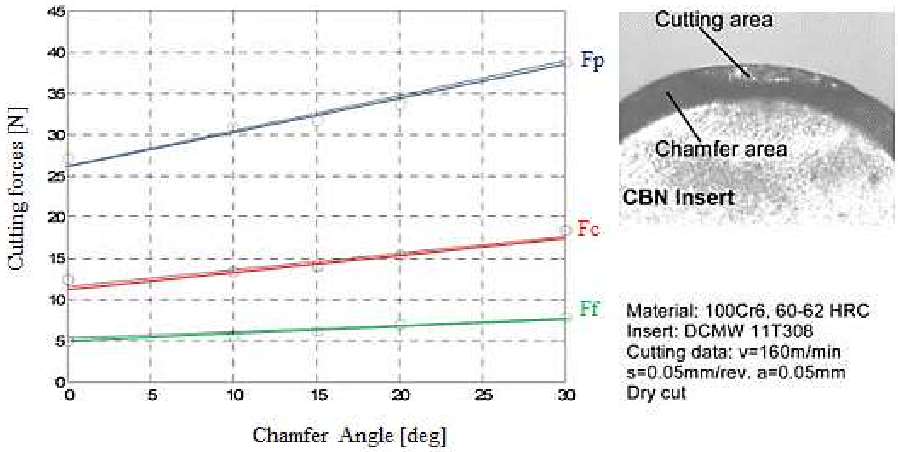

Figure 1.40 Variation of cutting forces with increasing chamfer angle [69]

The researchers still study on several aspects of hard turning and present their own suggestions to improve future studies. Commonly held method is the use of high speed, low feed, and low depth of cut due to nature of a finishing process. When the literature studies are examined, it is observed that cutting speed values employed in machining of different hard materials varies in range of 100 and 250 m/min [22, 27, 29, 64, 70]. Some researchers have worked at higher speed values than this range, but most of them prefer to keep this range due to the negative effects of stability problems on the part quality, cutting tool and machine tool [71]. Ozel et al. [72] studied the effects of different cutting-edge geometry (chamfered and honed), workpiece hardness (51.3 HRC and 54.7 HRC), feed (0.05, 0.1 and 0.2 mm/rev) and cutting speed (100 and 200 m/min) on surface roughness and cutting forces in hard turning of AISI H13 steel. Experimental results showed that honed edge geometry and lower work hardness produce better surface roughness (Figure 1.41). Another finding of the study is that the cutting-edge geometry, workpiece hardness and cutting speed are effective on force components. In addition, it was found that the lower workpiece hardness and small cutting-edge radius lead to lower tangential and radial forces.

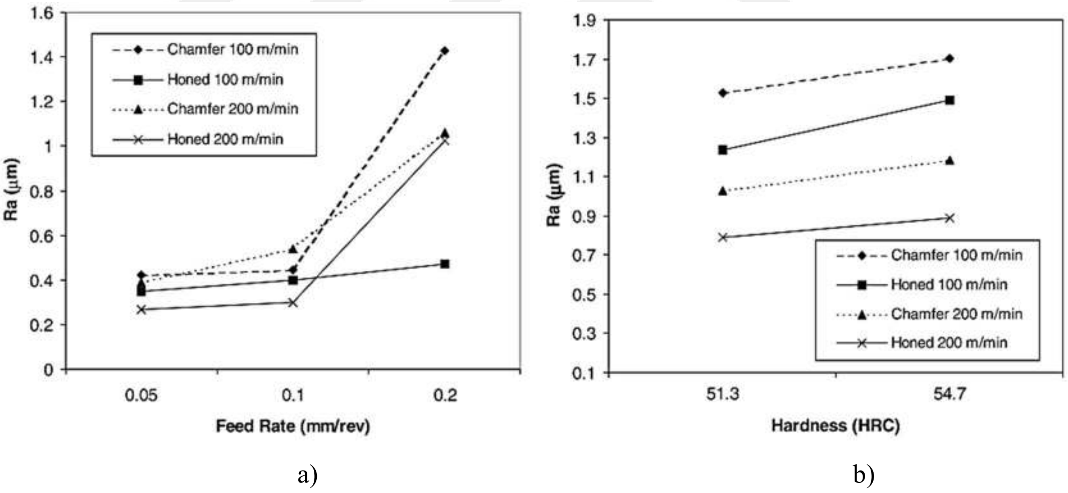

Figure 1.41 The effects of process parameters on surface roughness [72]

Bouacha et al. [40] conducted some hard turning tests on AISI 52100 steel to establish a between among cutting forces and process parameters such as work material hardness and cutting speed. As illustrated in Figure 1.42.a, the cutting forces decrease with increasing cutting speed due to thermal softening of work material at elevated temperatures. Another finding of this study is that as the material hardness increases, the cutting forces increase. This case is attributed to higher yield strength of harder work materials. In addition, the authors have carried out some tests to determine the effects of cutting conditions on surface quality. The test results showed that surface roughness values decrease with increasing cutting speed while they increase with an increase in feed values. In addition, it is reported that material hardness, negative rake angle, tool wear are the most effective parameters on the passive forces.

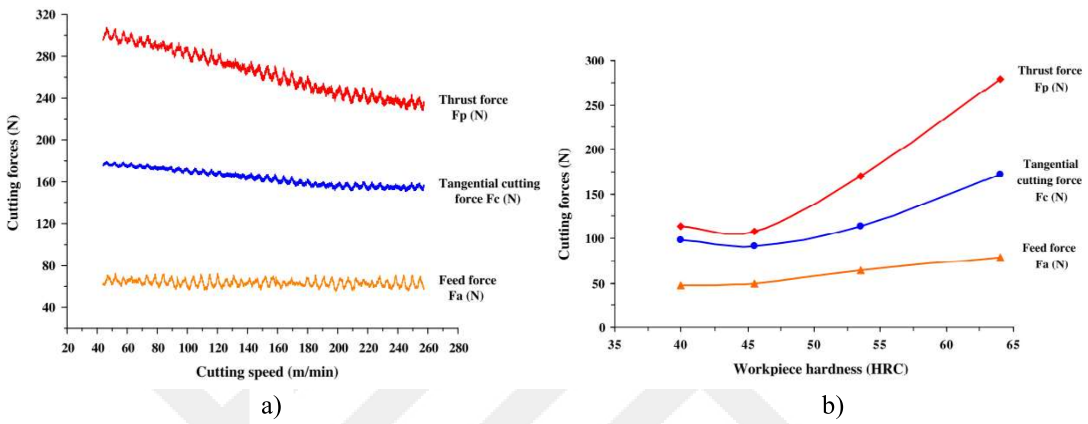

Figure 1.42 Variation of cutting forces with a) cutting speed and b) work material hardness [40]

Singh et al. [73] carried out a number of tests to determine the effects of cutting conditions and tool geometry on the surface roughness in the finish hard turning of the bearing steel (AISI 52100). Mixed ceramic inserts with different nose radii and effective rake angles were used as the cutting tools during the tests. Experimental results indicated that feed rate is major factor determining the surface roughness. In addition, it was reported that the nose radius and cutting speed significantly affect the surface quality. On the other hand, it was found that the effect of effective rake angle on the surface finish is less. They reported that feed and nose radius are two of the most important factors affecting surface quality of work material (Figure 1.43).

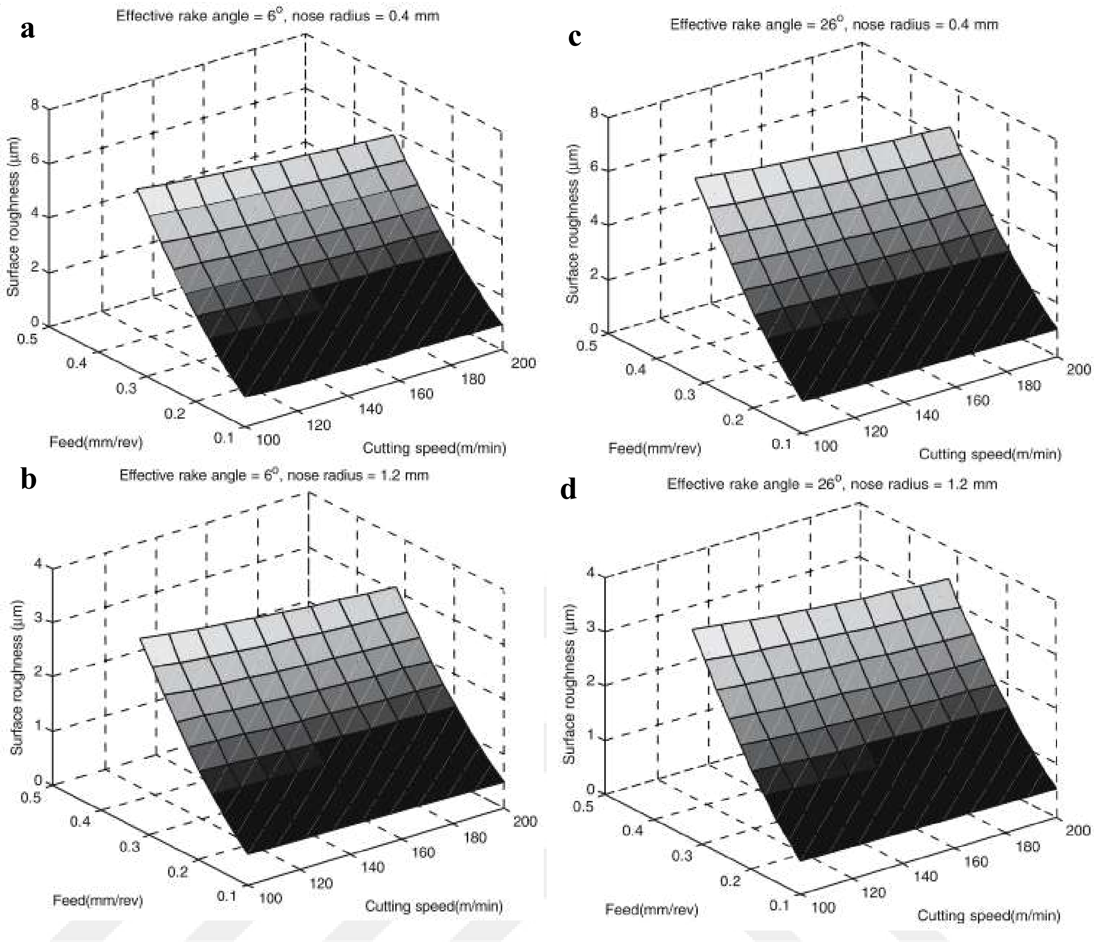

Figure 1.43 Variation of surface roughness with cutting conditions and tool geometry [73]

Liu et al. [74] investigated influence of tool nose radius and tool wear on residual stress distribution in hard turning of JIS SUJ2 bearing steel. They employed three types of CBN tools with different nose radii (0.4, 0.8 and 1.2 mm) during tests. They found that passive (thrust) forces (Fp) are more critical than the tangential (cutting) forces (Fc) in hard turning tests. In case of an increase in the nose radius of the CBN inserts, they observed that passive forces increase drastically. However, feed force (Ff) slightly decreases with increasing nose radius. Both cases are attributed to a decrease in cutting-edge angle due to an increase in nose radius. The variation of cutting forces with nose radius is shown in Figure 1.44. They also proved that as the tool nose radius increases, compressive stresses tend to shift to tensile stresses. The thermal effect caused by an increase in contact area at tool-workpiece interface is main reason for this transformation.

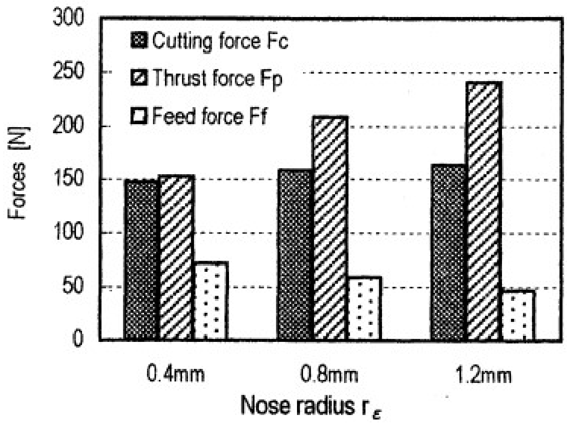

Figure 1.44 Variation of cutting forces with nose radius [74]

The presence of compressive stresses at the surface and subsurface of work material positively affects its fatigue life [8, 40, 71, 72]. For longer fatigue life, it is expected that compressive stresses reach to the maximum depth. Hua et al. [7] reported that as feed increases, penetration depth of residual stresses increases due to increasing cutting forces in turning of hardened bearing steel. Another finding of the study is that when work material hardness increases from 52 HRC to 66 HRC, penetration depth also increases (Figure 1.45).

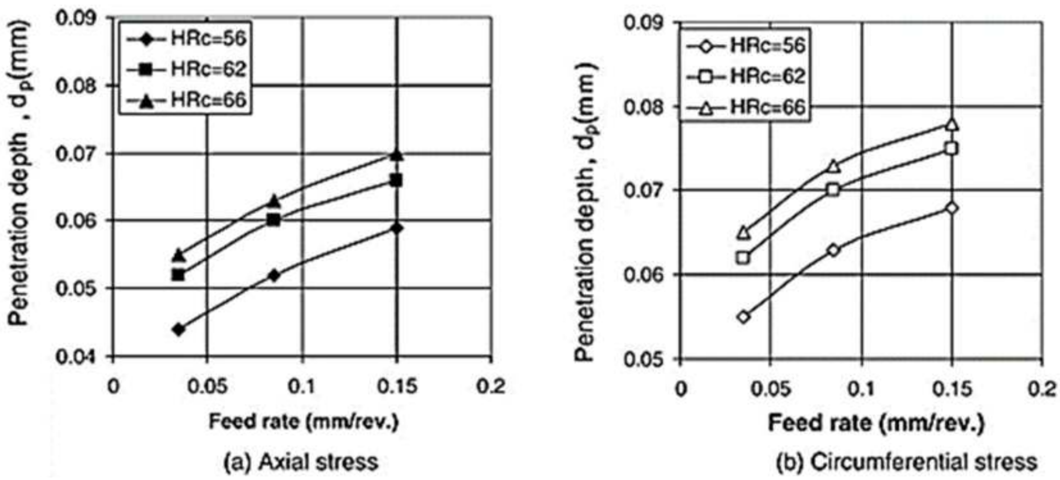

Figure 1.45 The effects of feed and work hardness on penetration depth of residual stresses in a) axial direction b) circumferential direction [7]

Javidi et al. [75] investigated the effects of feed and nose radius on residual stresses and the fatigue life in the hard turning of AISI 4340 steel. The test results showed that the residual stresses tend to become more compressive with increasing feed value. On the other hand, it was found that increasing nose radius leads to a decrease in compressive residual stresses. Another finding of the study is that compressive residual stresses improve the fatigue life of the work material. Variation of fatigue life with nose radius is shown in Figure 1.46.

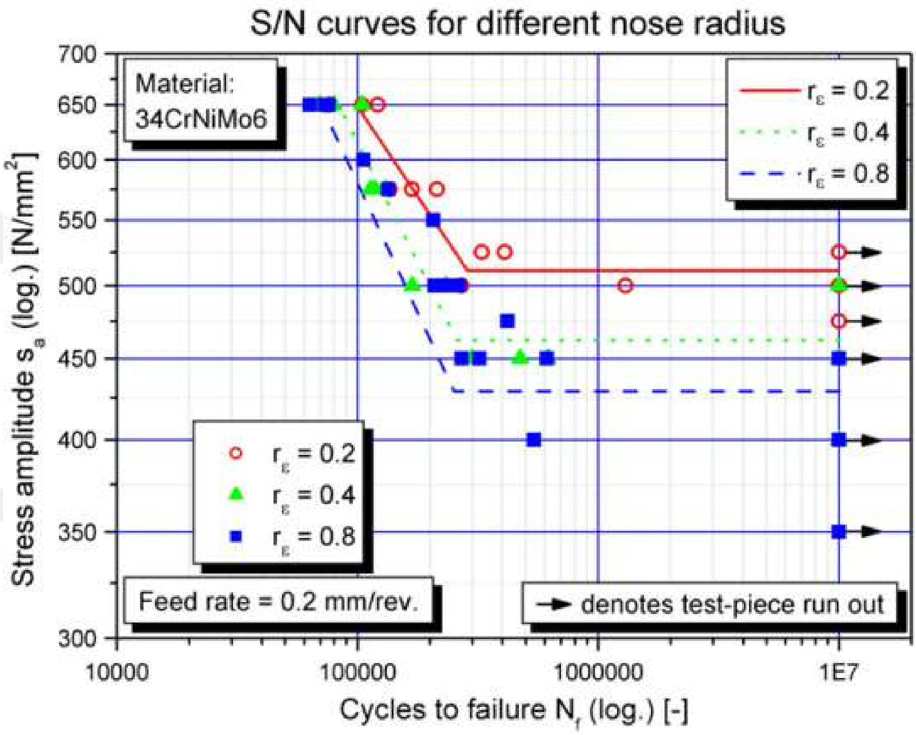

Figure 1.46 Variation of fatigue life with nose radius [75]

Matsumoto et al. [57] investigated the effects of precision hard turning on rolling contact fatigue life. Taper roller bearings with hardness values in range of 52-58 HRc were employed during the tests. The tests showed that hard turning provides a comparable fatigue performance to grinding. It was observed that hard turning pushes compressive stresses to a deeper layer of work surface. Finally, it was found that cutting-edge geometry is a major factor on stress profile.

Jouini et al. [76] studied the effects of precision hard turning of AISI 52100 steel on rolling contact fatigue life. Life tests are performed on a twin-disc test rig. It was found that there is a close correlation between fatigue life and surface roughness. Fatigue life increases with an improvement in surface quality (5.2 million cycles at Ra=0.11 µm and 0.32 million cycles at Ra=0.25 µm). In addition, it was found that with precision hard turning, fatigue life reaches 5.2 million cycles at Ra=0.11 µm while with grinding+honing it reaches 3.2 million cycles at Ra=0.05 µm. This case shows a positive impact of hard turning on fatigue life. The variation of fatigue life with surface roughness and machining method is shown in Figure 1.47.

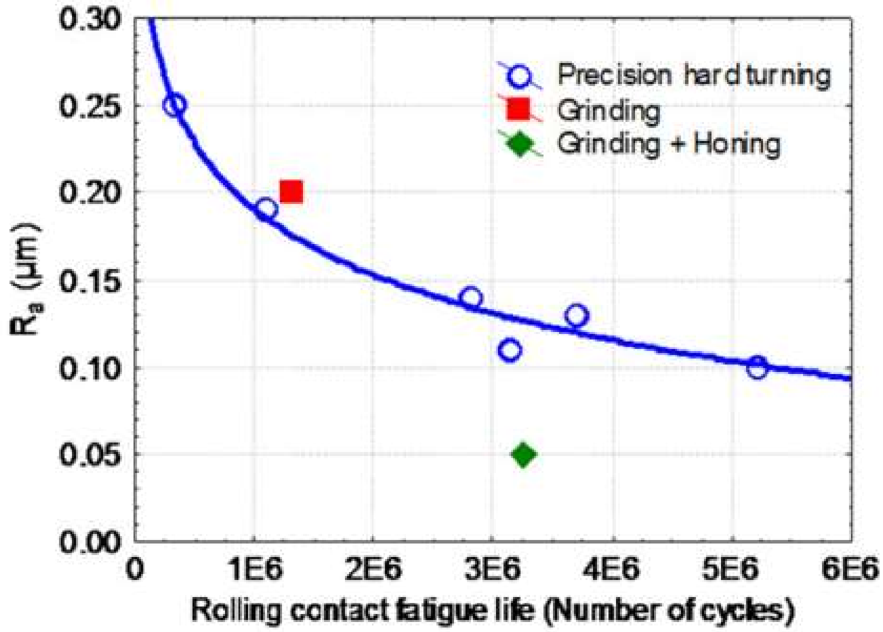

Figure 1.47 The variation of fatigue life with surface roughness and machining method [76]

Zhang et al. [51] studied the effects of tool wear and cuttting speed on white layer and they observed a significant increase in white layer ticknesses with increasing tool wear (flank wear). Microstructures and thicknesses of phase formations (white and dark layers) are clearly shown in SEM pictures (Figure 1.48). As shown in Figure 1.48, the inserts with larger flank wear produce thicker white and dark layers. This is because increasing frictions due to a more worn tool cause to higher cutting temperatures at the tool-workpiece interface.

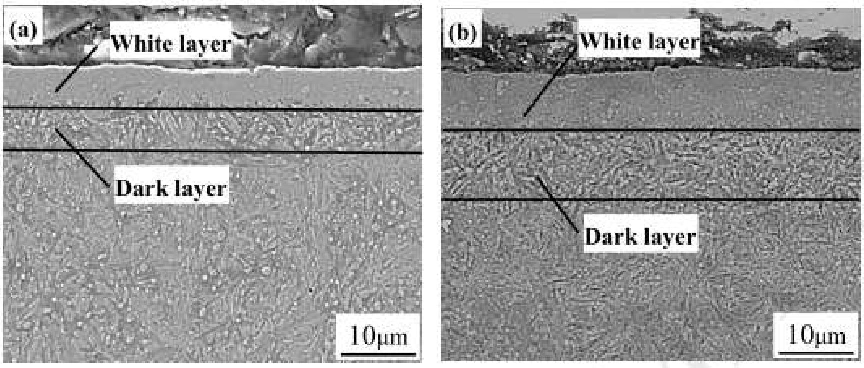

Figure 1.48 SEM pictures of phase transformations in case of a) flank wears of 0.1 mm and b) 0.2 mm [51]

1.6.2 Surface Integrity in Deep Rolling

Deep rolling is a mechanical surface treatment procedure that a roller or ball tool is rolled on the work surface under sufficient pressure to produce the compressive residual stress and thus, to improve strength to fatigue failure of a mechanical component. It enhances fatigue life of work material by providing work-hardening and by producing compressive residual stresses in its surface and near-surface layers. It is a known fact that the residual stresses are induced by the external loads that exceed the yield strength of a material. Thus, deep rolling process in which extreme pressures (for example, 300 bars) are applied is available for producing smoother surfaces as well as compressive stresses. In this context, Perenda et al. [43] conducted a number of deep rolling tests on AISI 4340 steel with hardness of 54 HRC at different working pressures and feed values in order to investigate the effect of deep rolling on material hardness and surface roughness. The test results showed that deep rolling process produces smoother work surfaces due to suppression of feed marks, micro-notches and burrs and leads to an increase in material hardness due to strain-hardening effect (Figure 1.49).

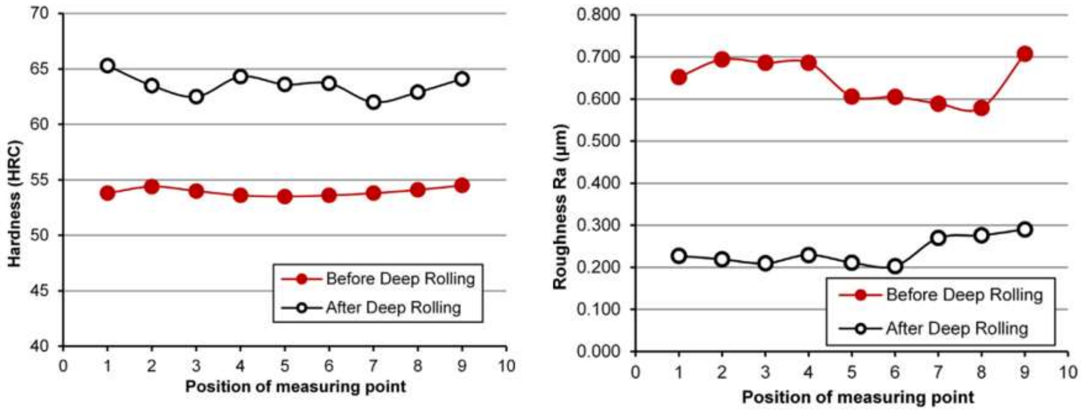

Figure 1.49 The effects of deep rolling on a) material hardness and b) roughness [43]

Abrão et al. [64] reported surface and subsurface alterations induced by deep rolling at different pressures (200 and 300 bars) and at number of rolling passes (1, 2 and 3 passes) for hardened AISI 1060 steel. As shown in Figure 1.50, they observed that there is a significant improvement in surface quality and that the feed marks decrease after deep rolling.

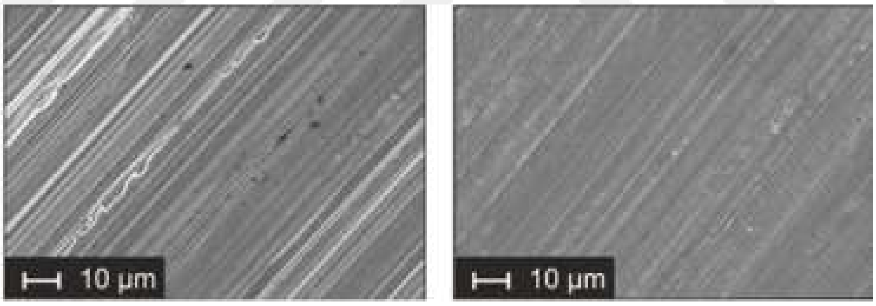

Figure 1.50 a) Hard turned and b) deep rolled surface textures [64]

Low level of tensile axial residual stresses measured near the machined surface after a turning operation shifts to maximum compressive stress value (-1730 MPa) after a deep rolling process at a rolling pressure of 300 bar and three rolling passes. They found that as rolling pressure and number of passes increase, compressive stresses increase. The residual stress values measured after deep rolling process are shown in Figure 1.51.

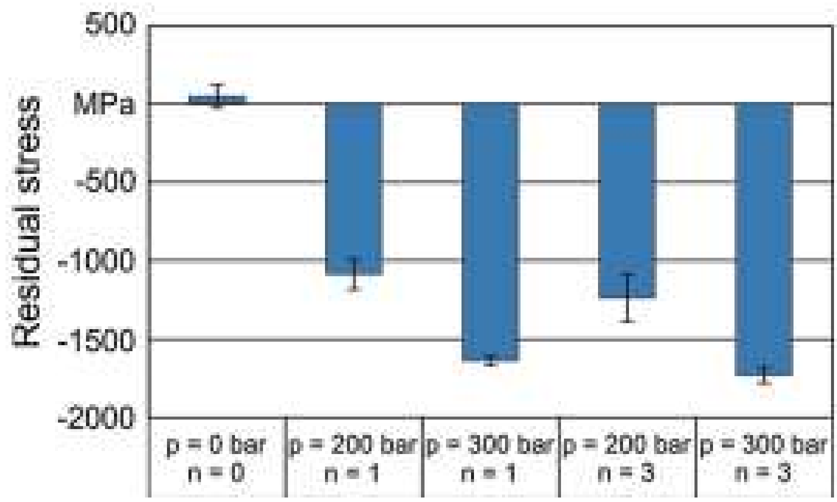

Figure 1.51 The effects of rolling pressure and number of passes on the axial residual stresses [64]

Maiß et al. [77] performed a study on a hybrid process of inner rings of roller bearings using hard turning and subsequent deep rolling operations. In recent years, hybrid manufacturing processes called hard turn-rolling is a combination of deep rolling and hard turning operations. Figure 1.51 illustrates a hard turn-rolling tool and schematic representation of a hard turn-rolling process.

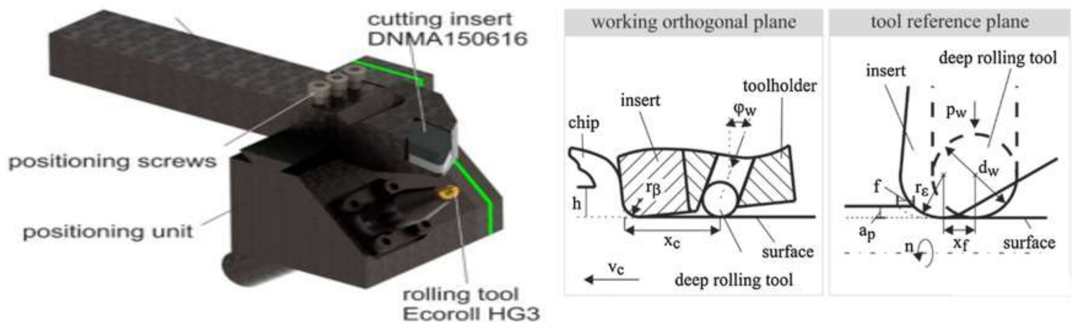

Figure 1.52 A hard turn-rolling tool and schematic representation of a hard turn-rolling process [77]

As shown in the Figure 1.53, if a distance between nose radius of CBN insert and ball radius of deep rolling tool is determined properly, feed marks on machined surface shorten under high pressures and thus, a better surface quality is obtained. This distance is defined as rolling shift (x_f), and it should be half the feed value (f).

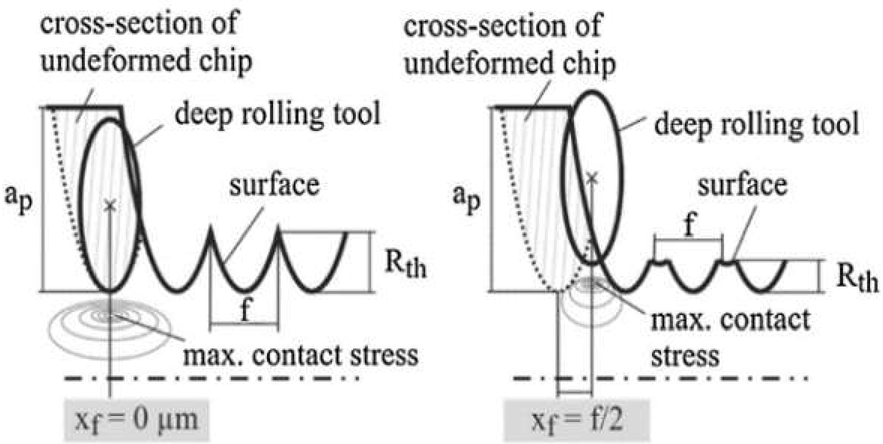

Figure 1.53 Effects of rolling shift on surface roughness [77]

Pape et al. [78] studied the effects of residual stresses produced in different manufacturing processes (honing, hard turning and deep rolling) on endurance time of NU206 type of roller bearing. They reported that maximum compressive stresses take place in deep rolling process and it is followed by hard turning (Figure 1.54) [79].

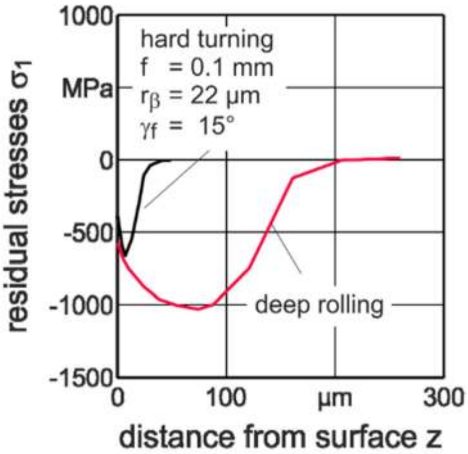

Figure 1.54 The effects of different manufacturing processes on residual stresses [79]

For bearings, the estimated curves suit very well with experimentally determined probability of surviving as shown in Figure 1.55. Although the probabilities of surviving for honed and hard-turned bearings are similar to each other, those of hard-turned and subsequently deep rolled bearings increase dramatically. An improvement in fatigue life is attributed to more intensive compressive residual stresses induced during hard turning and subsequent deep rolling processes.

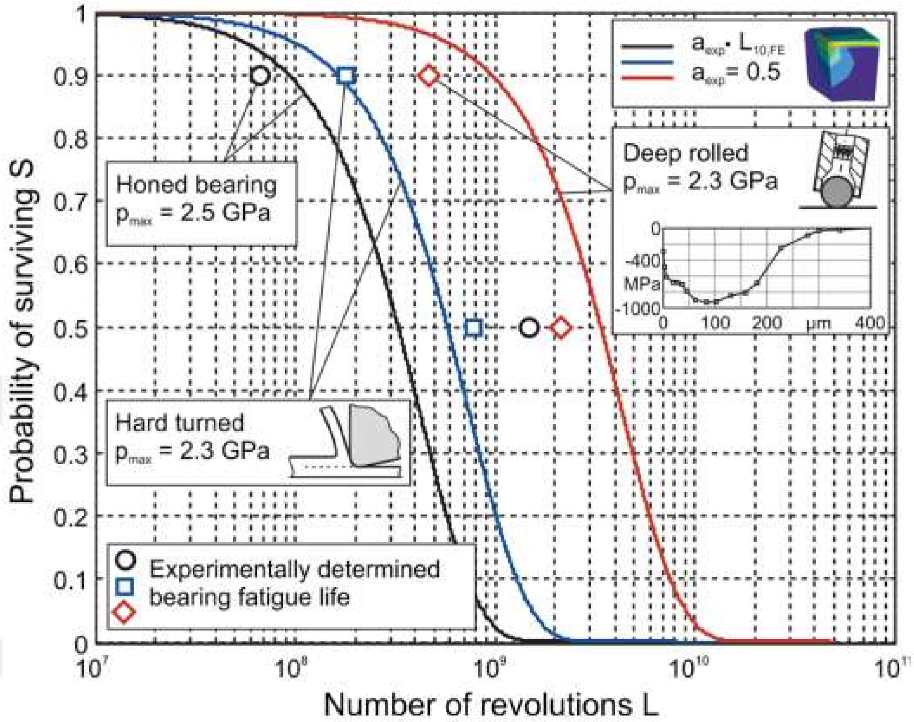

Figure 1.55 Assessment of computational model by analysis of probabilities of surviving and experimental results [79]

1.7 Aim of This Study

In this study, the effects of hard turning and deep rolling process on surface integrity and fatigue life of raceway of deep groove ball bearings were investigated. The inner rings of the 6208-type deep groove ball bearings were employed during the tests. This study consists of two important steps. In the first step, the effects of cutting parameters and tool geometry on cutting forces, raceway roundness error and surface integrity (surface roughness, residual stresses, subsurface phase transformations) were studied in hard turning of the bearing steel (62 HRC). In the second step, the performances of grinding, hard turning, deep rolling operations applied to raceway of inner rings are compared to each other in terms of surface integrity, noise level and fatigue life. Finally, ball bearings were tested on a fatigue life tester and noise level tester for better understanding the effects of grinding, hard turning, hard turning + deep rolling processes on their fatigue life and noise level.

Novel aspects of this study can be listed as follows.

- For the first time in the literature, both hard turning and deep rolling processes are applied to the inner ring raceway of a deep groove ball bearing.
- For the first time in the literature, the roundness error is examined in detail by applying a hard turning operation to the inner ring raceway of the deep groove ball bearing.
- The performance of CBN inserts with different geometries (insert shape and cutting-edge configuration) using different cutting parameters are discussed in terms of surface integrity (surface roughness, residual stresses, white/dark layer formations) in detail.
- In case of use of CBN inserts with different tool shapes and effective rake angles, changes in surface integrity are analyzed in detail.

CHAPTER 2

EXPERIMENTAL SETUP AND PROCEDURE

In this chapter, an experimental setup employed for tests at different cutting condition, and measurement and evaluation methods used for the performance criteria such as cutting forces, surface roughness, roundness error, residual stresses, phase transformations (white and dark layers), noise level and fatigue life are discussed in detail. All tests were carried out on raceway of the inner rings of the 6208-type deep groove ball bearings. This study consists of two important steps. Schematic illustration of test steps is shown in Figure 2.1.

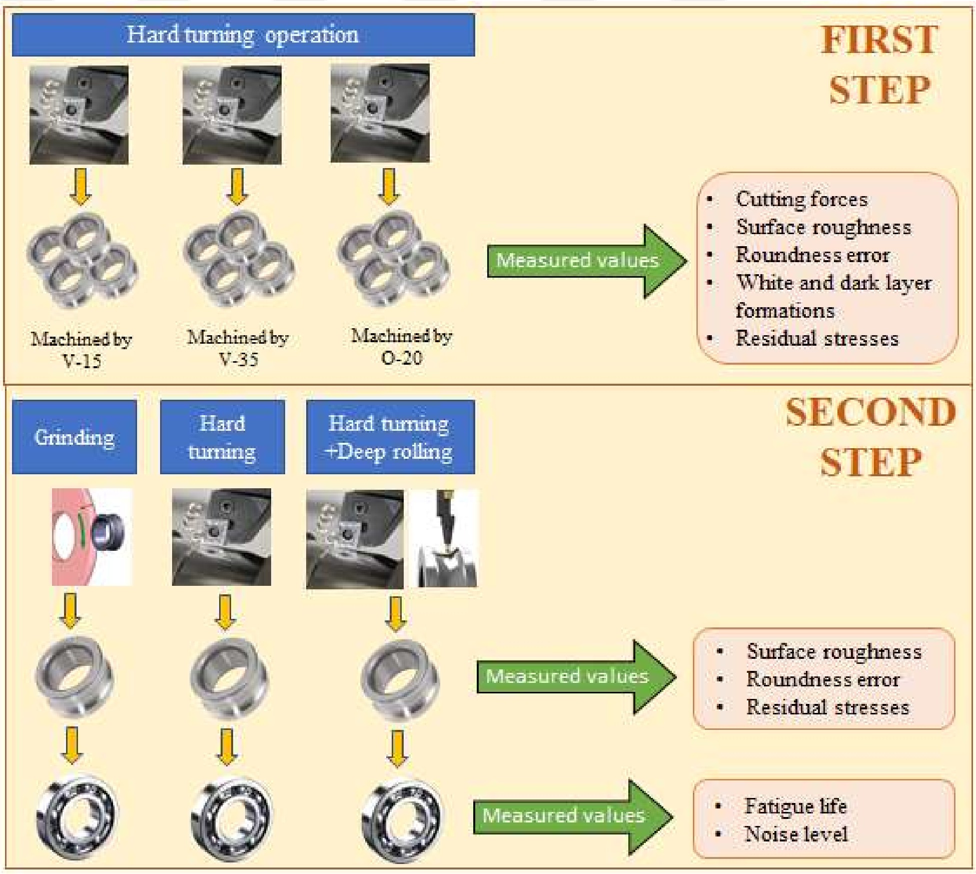

Figure 2.1 Schematic illustration of test steps

In the first step, the effects of cutting conditions and tool geometry on, cutting forces, raceway roundness error and surface integrity (surface roughness, residual stresses, subsurface phase transformations) were studied using three different cubic boron nitride (CBN) inserts in hard turning of the bearing steel (62 HRC). Twelve samples were prepared for hard cutting tests (two cutting speeds, two feeds and three inserts with different geometries). In the second step, the performances of grinding, hard turning, hard turning+deep rolling operations applied to raceway of inner rings are compared to each other in terms of surface integrity, noise level and fatigue life. For each process, 4 inner rings were prepared and total 12 samples were assembled with outer rings and balls into final ball bearing products.

2.1 Work Material

AISI 52100 steel is commonly used as work material in bearing industry. AISI 52100 (DIN 100Cr6) steel is a high-carbon (0.98-1.10%) and low-alloy eutectoid steel with chromium content of 1.3-1.6%. Thanks to the chromium content in the bearing steel, its corrosion and oxidation resistances are high. In addition, it has higher hardening ability and wear resistance due to its high carbon content (~1%). The bearing steel can be hardened up to 64 HRC using a proper heat treatment procedure. These hardness values are very suitable for grinding and hard turning processes which are finish machining methods in bearing steels. The chemical composition, and some physical and mechanical properties of AISI 52100 steel are given in Table 2.1 and Table 2.2 respectively.

Table 2.1 The chemical composition of AISI 52100 steel [80]

Element	**Weight %**
Iron, Fe	96.5- 97.32
Chromium, Cr	1.30- 1.60
Carbon, C	0.980- 1.10
Manganese, Mn	0.250- 0.450
Silicon, Si	0.150- 0.300
Sulfur, S	≤ 0.0250
Phosphorous, P	≤ 0.0250

Table 2.2 Some physical and mechanical properties of AISI 52100 steel [81, 82]

Density	Melting point	Elastic modulus	Poisson's ratio	Hardness	Thermal conductivity	Yield strength (200°C)	Tensile strength (200°C)	Fracture strength (200°C)
7.81 g/cm^3	1424 °C	190-210 GPa	0.27-0.30	60-67 HRC	46.6 W/mK	1672 Mpa	2482 Mpa	2731 Mpa

In this study, a number of tests is conducted on raceways of ball bearings made of bearing steel in order to clarify the effects manufacturing methods (hard turning, grinding and deep rolling), cutting conditions (feed and speed) and tool geometry (insert shape and cutting-edge configuration) on their roundness error, surface integrity, fatigue life and noise level. The technical drawing of the inner ring employed during the tests is shown in detail in Figure 2.2.

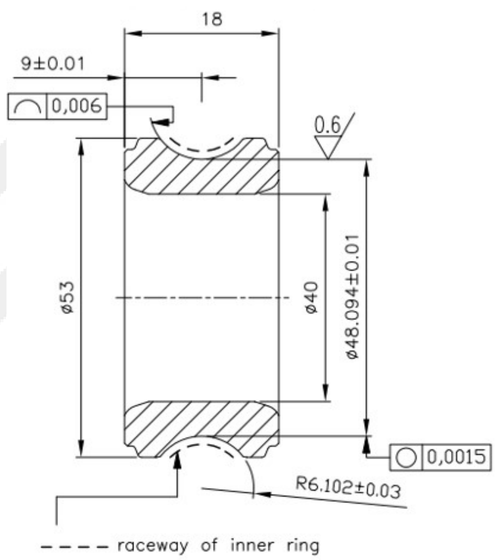

Figure 2.2 Technical drawing of an inner ring

2.2 Experimental Setup and Cutting Conditions

In this study, the tests were carried out on the inner rings of the 6208 deep groove ball bearing samples. The hot forging, spheroidizing, cold rolling and turning processes are applied to raw material in order to manufacture semi-product of inner rings. Then, the inner ring specimens were hardened to 62 HRC using a proper heat treatment procedure. In the heat treatment procedure, firstly, specimens were austenitized at 857 °C for 35 minutes and then, they were quenched within a water/salt bath. As a final process, specimens were tempered at 200 °C for 90 minutes in order to reduce internal stresses and martensite brittleness. After heat treatment operation, face grinding, hole grinding operations were carried out on semi-product samples, respectively. Then, all samples that will be employed during the tests were organized into three categories. The raceways of inner rings in the first category were machined by grinding and superfinishing processes (called GR). In second category, the raceways were machined by hard turning superfinishing processes (called HT). In final category, they were machined by hard turning, deep rolling and superfinishing processes (called DR). Finally, each inner ring was matched with a proper outer ring, nine balls and cage and all of them were assembled into a deep groove ball bearing. Manufacturing processes of three categories are illustrated in Figure 2.3.

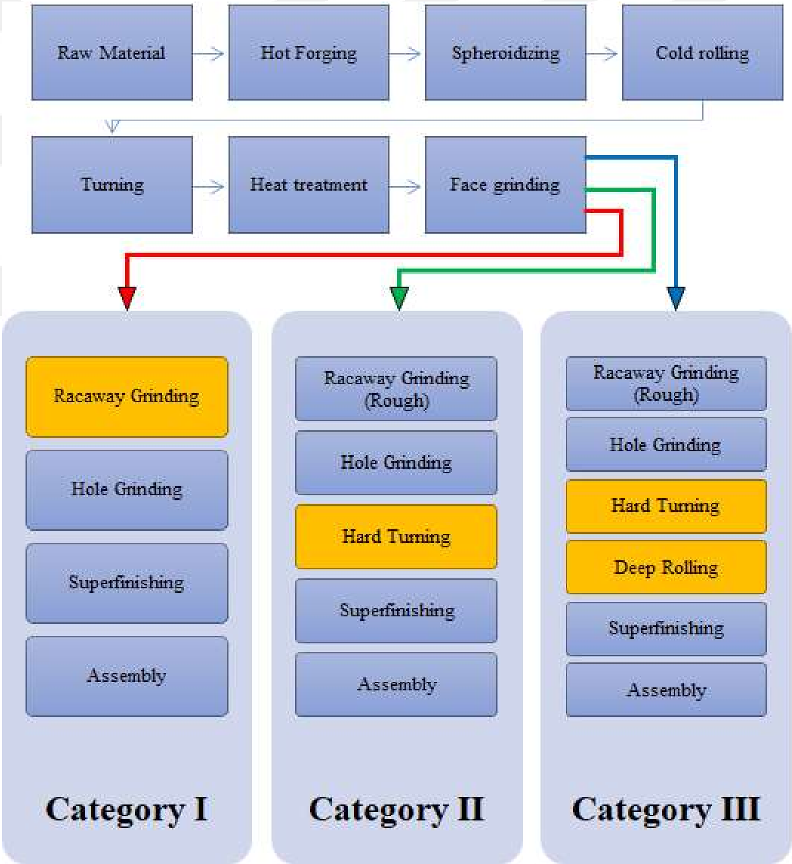

Figure 2.3 Manufacturing processes of sample categories

Hard turning operations were conducted on MURATEC MD120 CNC lathe (Figure 2.4) with maximum speed of 4500 rpm and machine power of 7.5 kW. No coolant was used during hard turning operations.

Figure 2.4 Test set-up for hard turning process

GILDEMEISTER NEF520 CNC lathe (Figure 2.5) with maximum spindle speed of 3050 rpm and machine power of 17 kW was used for deep rolling process due to its higher rigidity.

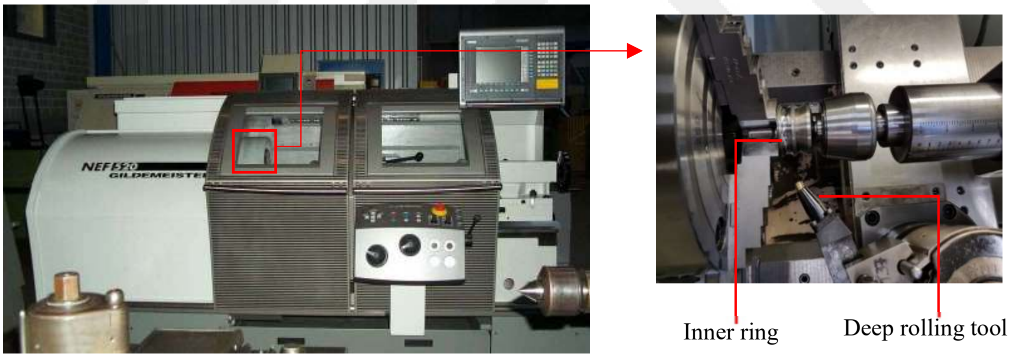

Figure 2.5 Test set-up for deep rolling process

TOYO T-235CNC external grinder with a rigid mechanical construction, and an anti-heat displacement system (Figure 2.6) was used in raceway grinding process to obtain consistent roundness form and dimensional accuracy.

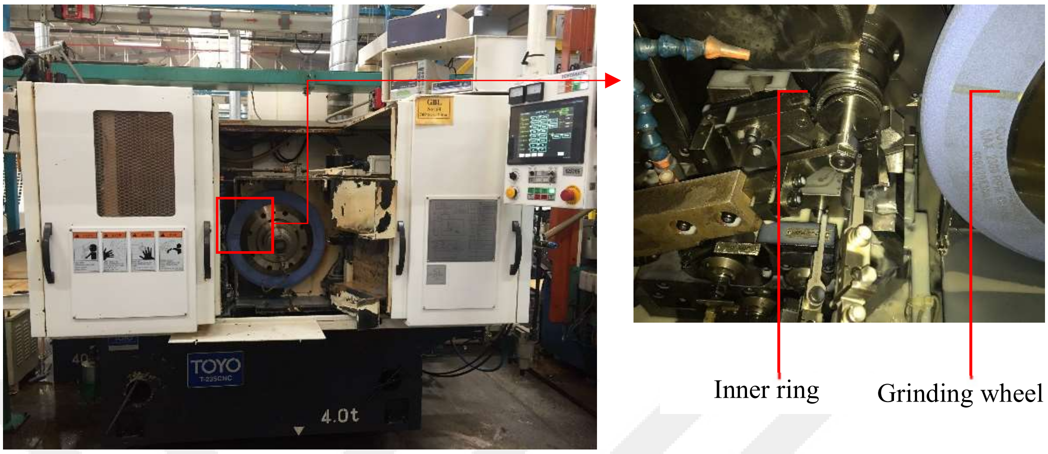

Figure 2.6 Test set-up for raceway grinding

DAISEI SF-R-21-SB superfinishing machine (Figure 2.7) was employed during superfinishing process. It has rough and finish machining units to ensure smoother surfaces.

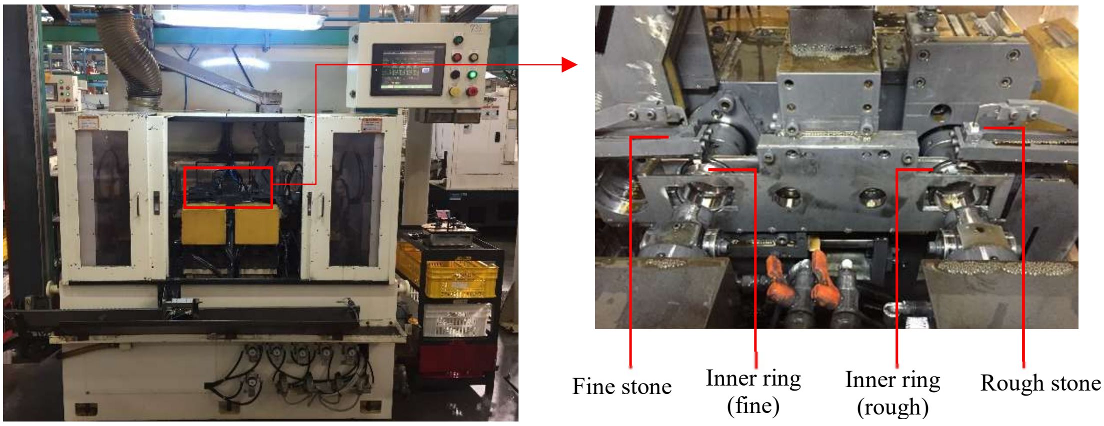

Figure 2.7 Test set-up for superfinishing

As mentioned earlier, the effects of deep rolling process on surface integrity and fatigue life in hard turning of raceway of deep groove ball bearings are investigated in this study. It was reported in the literature that cutting conditions significantly affect surface integrity of bearing steels. Therefore, two different cutting speeds and feeds were employed during hard turning tests. On the other hand, depth of cut values were kept constant. Besides, chuck clamping pressure also substantially affect roundness error the raceways of inner rings. In consequence of preliminary tests, optimal chuck clamping pressure was determined to both minimize the roundness error of inner rings and firmly hold them during hard turning process. Cutting parameters of hard turning process are shown in Table 2.3.

Table 2.3 Hard turning parameters

Cutting speed (m/min)	Feed (mm/rev)	Depth of cut (mm)	Chuck clamping pressure (bar)
175	0.05	0.06	4
350	0.05	0.06	4
175	0.1	0.06	4
350	0.1	0.06	4

The process parameters for deep rolling process were kept constant in order to compare the deep rolling with hard turning and grinding processes in terms of surface integrity and fatigue life. Deep rolling parameters are represented in Table 2.4.

Table 2.4 The process parameters for deep rolling

Spindle speed (rpm)	Feed (mm/rev)	Pressure (bar)	Ball diameter (mm)
240	0.04	300	Ø 6

The process parameters for raceway grinding and superfinishing were kept constant for all inner rings. These values are given in the Table 2.5 and Table 2.6, respectively.

Table 2.5 The process parameters for raceway grinding

Depth of cut (µm)	Work speed (rpm)	Grinding wheel speed (rpm)	Feed rate for rough grinding (mm/s)	Feed rate for finish grinding (mm/s)
110	750	2250	0.100	0.050

Table 2.6 The process parameters for superfinishing

Depth of cut (µm)	Work spindle speed (rpm)	Oscillation speed (rpm)	Oscillation angle (°)	Tool pressure (kgf/cm^2)
3	3000	300	18	3

2.3 Test tools

Four different machine tools were employed during the tests and each of them has its special tools (grain size, tool material and geometry). For example, CBN inserts, hydrostatic tool, grinding wheel, superfinishing tool are employed in hard turning, deep rolling, raceway grinding, superfinishing operations respectively.

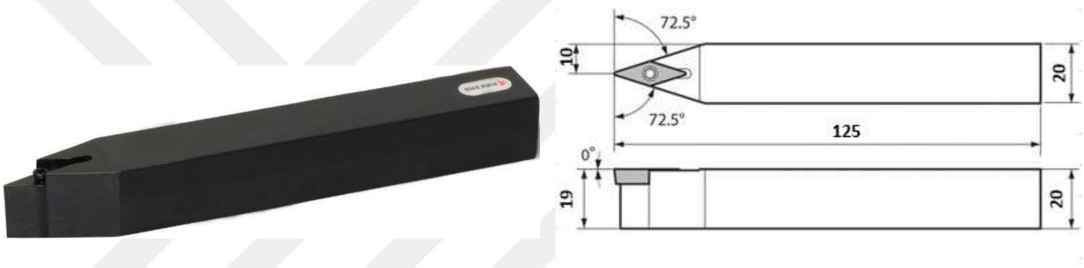

Figure 2.8 SVVBN 2020 K11 tool holder and its dimensions

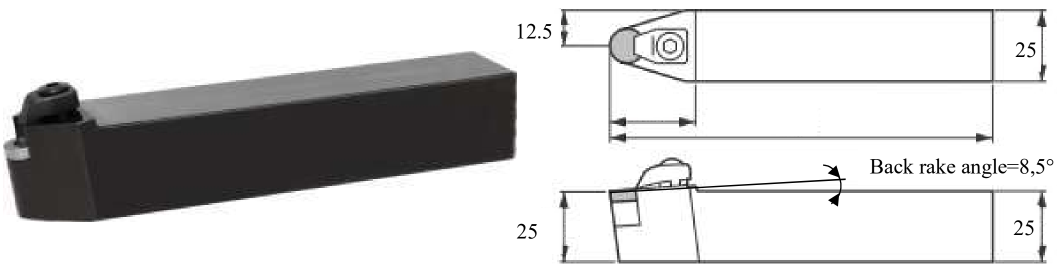

Figure 2.9 CRDNN 2525 M09-A tool holder and its dimensions

CUW120K5V type grinding wheel with high abrasive grain number and hardness grade was used. Some properties of grinding wheel are shown in Table 2.7.

Table 2.7 Properties of raceway grinding wheel

CUW120K5V	
Dimensions	508x20x304,8
Abrasive type	Silicon carbide
Grain size number	120
Hardness	K grade
Structure	5
Binder	Vitrified

In the first step tests, three CBN inserts with different forms (rhombus and round) and effective rake angles (-15°, -35° and -28.5°) and corresponding tool holders to them were used. The toolholders and inserts are manufactured by KYOCERA. SVVBN 2020 K11 toolholder was used for rhombus inserts while CRDNN 2525 M09-A toolholder was employed for round inserts. SVVBN and CRDNN toolholders and their dimensions are illustrated in Figure 2.8 and Figure 2.9, respectively. In this step, VBGW160408 T00815, VBGW160408 S01035 and RNMN090300 S02020 inserts were chosen as CBN inserts, and they are coded for ease of use as V-15, V-35, O-20, respectively. The rhombus inserts (V-15 and V-35) have zero normal rake angle (γ = 0°) whereas the round ones (O-20) have negative normal rake angle (γ = -8.5°). Since the cutting edges of all CBN inserts are chamfered in different angles (15° and 35° for rhombus inserts and 20° for round inserts) and uncut chip thickness (feed in orthogonal plane) is equal to or smaller than cutting edge chamfer distance, effective rake angle of the inserts (γ_{eff}) differs from each other and becomes equal to the sum of normal rake angle and chamfer angle. In this case, the effective rake angles of V-15, V-35, O-20 are -15° and -35° and -28.5°. In addition, for smoother surface finishes, fine grained CBN tools should be selected [83]. Therefore, KBN525 grade (grain size under 1 µm) was preferred for all CBN inserts. The dimensions and some properties of CBN insert are shown in Table 2.8.

Table 2.8 The dimensions and some properties of CBN inserts

	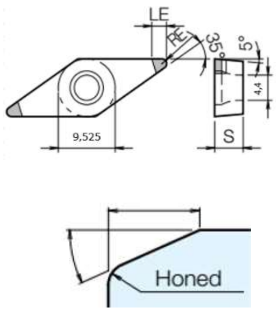	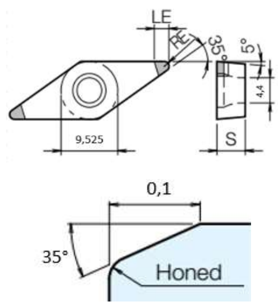	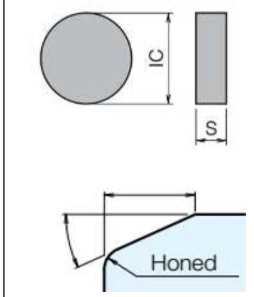
	VBGW160408 T00815	VBGW160408 S01035	RNMN090300 S02020
Code	V-15	V-35	O-20
Toolholder	SVVBN 2020 K11	SVVBN 2020 K11	CRDNN 2525 M09-A
Normal rake angle	0°	0°	-8.5°
Number of cutting edge	2	2	Depends on a_p
Insert included angle	35°	35°	Round
Relief angle	5°	5°	0°
Chamfer angle	15°	35°	20°
Effective rake angle	-15°	-35°	-28.5°
Cutting edge effective length (LE)	1.7 mm	1.7 mm	-
Nose radius (RE) (IC)	0.8 mm	0.8 mm	4.7625
Insert thickness (S)	4.76 mm	4.76 mm	3.18
Cutting edge R-honed and chamfer	0.08 mm x 15°	0.1 mm x 35°	0.2 mm x 20°
Grade	KBN525	KBN525	KBN525
Average grain size	≤ 1 µm	≤ 1 µm	≤ 1 µm

HG6-9 hydrostatic tools produced by ECOROLL company were used during deep rolling process. Hydrostatic tool and its dimensions are shown in Figure 2.10. Hydrostatic tool has a ceramic ball which is a hard and brittle material hydrostatically mounted into tool holder. The ball is pressed with a certain rolling pressure against work surface in order to shape it. The process induces to compressive residual stresses into work surface and subsurface, increases the strength of the material and provides a smoother surfaces [84].

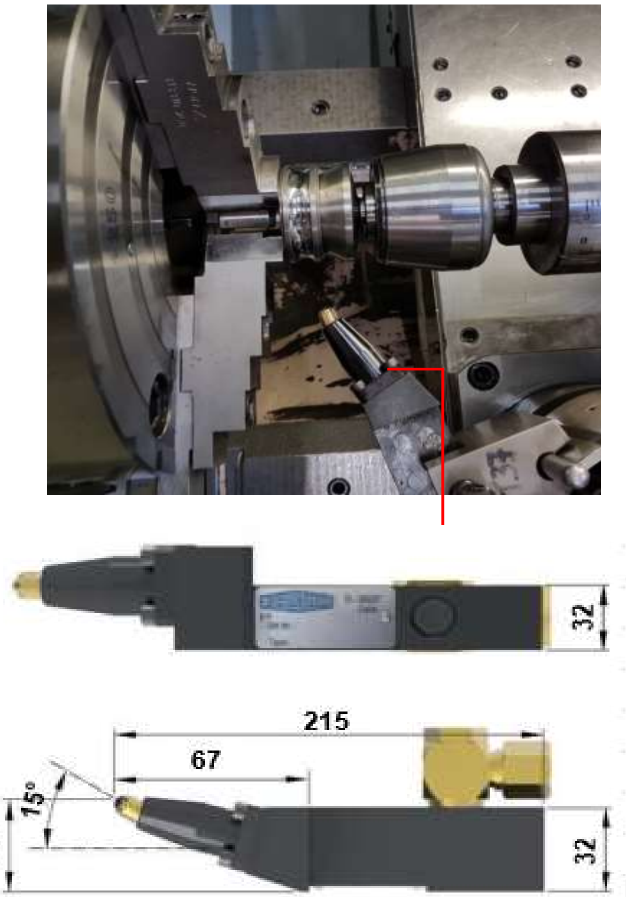

Figure 2.10 HG6-9 deep rolling tool and its dimensions

2.4 Measurement Techniques

At the end of the tests, a number of measurement techniques were employed to evaluate all specimens in terms of cutting forces, roundness error, surface integrity noise level and fatigue life in this study. This section clarifies the techniques in detail.

2.4.1 Cutting Forces

In machining operations, cutting forces are one of the important indicators for the machinability characteristics of engineering materials. Therefore, three components of cutting forces (tangential force, feed force and radial force) were measured during hard turning operations under dry conditions. The measurement of cutting forces were carried out using a Kistler 9121 dynamometer as shown in Figure 2.11.

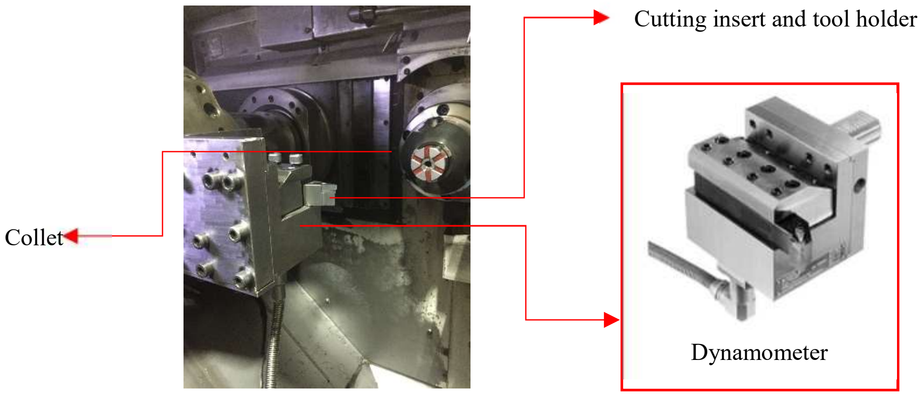

Figure 2.11 Cutting force measurements

The dynamometer was connected to the Kistler Type 5070A multichannel charge amplifier and the measurement results were evaluated using a Dynoware software. Technical specifications of dynamometer and amplifier are given in the Table 2.9.

Table 2.9 Technical specifications of dynamometer and amplifier

 **Kistler 9121 Dynamometer**			
Range	Fx, Fy	kN	-3…3
	Fz	kN	-6…6
Threshold		N	<0.01
Sensitivity	Fx, Fy	pC/N	~-7,9
	Fz	pC/N	~-3.8
Natural Frequency clamped, with toolholder	(x,y,z)	Hz	~1000
Weight		Kg	5

 **Kistler Type 5070A Multichannel charge amplifier**		
Number of channels		8
Measuring range	pC	200…200000
Frequency range	kHz	~0…>45
Output voltage	V	± 10
Voltage	V AC	100…240
Interface		RS 232C

2.4.2 Surface Roughness

The roughness values of the machined surfaces were quantified using a Taylor Hobson Talysurf PGI 1230 profilometer in the Ortadoğu Rulman Sanayi Inc. (Figure 2.12).

Figure 2.12 Taylor Hobson Talysurf PGI 1230 profilometer

As the surface roughness values, Ra (average roughness) and Rz (average maximum height of the profile) values were measured by scanning along full length (approximately 15 mm) of a machined surface.

2.4.3 Roundness error

The roundness error measurements of raceway profile of the inner ring were carried out on Taylor-Hobson Talyrond 73 device with radial accuracy of ±0.01 µm in the Ortadoğu Rulman Sanayi Inc. (Figure 2.13). Least squares circle method (LSC) is employed to evaluate the roundness error (Re).

Figure 2.13 Taylor-Hobson Talyrond 73 device

Re measurements for three different points on raceway (entry, middle and exit) of an inner ring were performed as shown in Figure 2.14. Their mean value is accepted as a roundness error value.

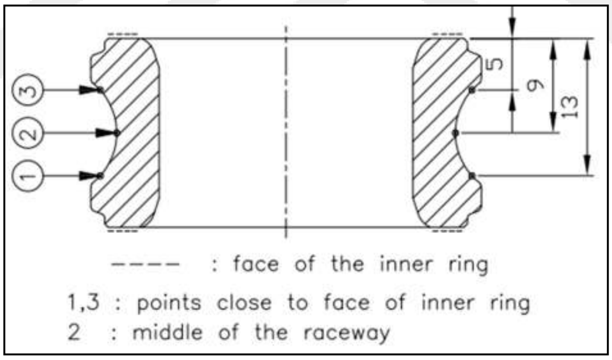

Figure 2.14 Measurement points for roundness error

2.4.4 Residual Stresses

Residual stresses are the one of the most important subtitles of the surface integrity and strongly related to cutting conditions and tool geometry. The residual stresses may change according to directions and magnitudes of forces and may significantly affect the fatigue life of the machinery elements. Therefore, both hoop (in cutting speed direction) and axial (in feed direction) residual stresses were measured by depending on depth. The residual stress measurements were performed using the parameters in Table 2.10 on a Seifert XRD 3003 PTS device (Figure 2.15) in the Ortadoğu Rulman Sanayi Inc.

Table 2.10 X-Ray diffraction parameters

X-ray radiation	Cr-K α
Bragg angle (2θ)	~ 156°
Lattice plane	{2 1 1}
Number of Ψ angles (±40°)	5
Collimator diameter	1,5 mm
Filter type at the detector	Vanadium
Measurement type	continuous
Detection methods	Parabolic and C.O.G. (Center of gravity)

Figure 2.15 Seifert XRD 3003 PTS

2.4.5 White and Dark Layer Formations

The specimens must be properly cut, ground, polished and etched before microscopic examinations to clearly observe the white and dark layer formations. In this context, proper small pieces were cut from the machined parts using metal cut-off grinder and they were embedded into the bakalite. Then, every piece was ground by means of sandpapers with grit sizes of 320, 400, 600, 800 and 1000. After grinding process, specimens were subjected to a final polishing process by using a suspension containing diamond abrasive particles with a grit size of 3 µm. This process was repeated until scratches disappeared on work surface. As final process, prior to microscopic examinations, specimens were etched within a solution of 5% nitric acid and 95%

alcohol for 6 seconds. After these processes, the microstructure of bearing steel (white and dark layer formations) was observed under an OLYMPUS BX51M microscope as shown in Figure 2.16.

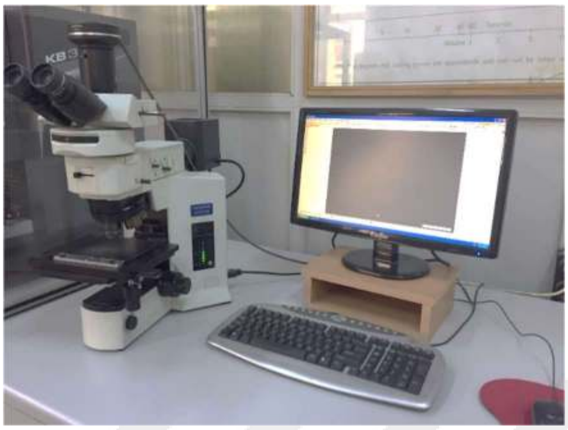

Figure 2.16 White and dark layer observations

2.4.6 Fatigue Life Test

The fatigue life of bearings depends on many factors and variables such as the magnitude and direction of loadings, geometry and roughness of the contact surfaces, material type, operating temperature, applied lubricant, lubrication conditions, rotational speed. Fatigue life tests were carried out using some measurement conditions in Table 2.11 on a custom-designed fatigue life tester (Figure 2.17) in the Ortadoğu Rulman Sanayi Inc. Both radial and axial loads are applied to the bearings while rotating them during tests.

Table 2.11 Fatigue life test conditions

Fr-Radial load	10000 N
Fa- Axial load	4000 N
Rotational speed	3000 rpm
Lubrication	Oil Lubrication
Oil kinematic viscosity (40°)	22 mm^2/s
Oil kinematic viscosity (100°)	4 mm^2/s
Oil temperature	30°C
Oil density	860 kg/m^3
Max. Temperature Outer Ring	67 °C
Max. Temperature Inner Ring	90 °C

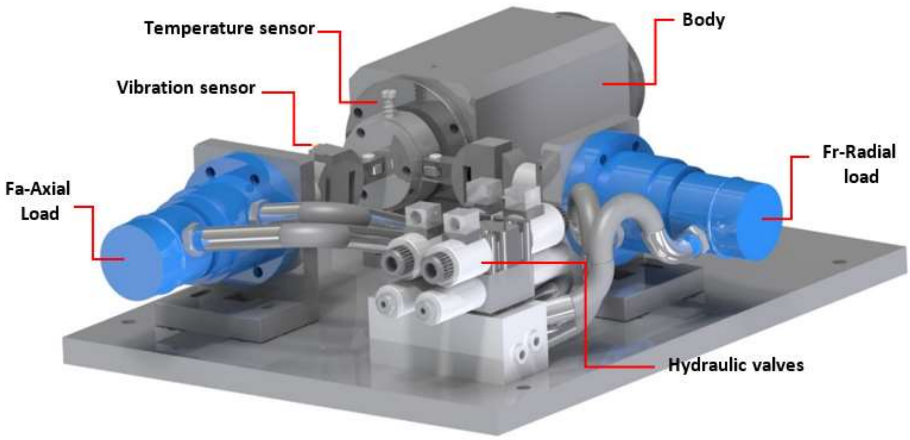

Figure 2.17 Fatigue life tester

2.4.7 Noise Level

Noise level of bearings is a very important criterion to determine product quality. The roundness error, surface roughness, impurity level of grease influence noise level of bearings. Noise levels for inner rings were checked in DALIAN S07907V bearing vibration tester as shown in Figure 2.18.

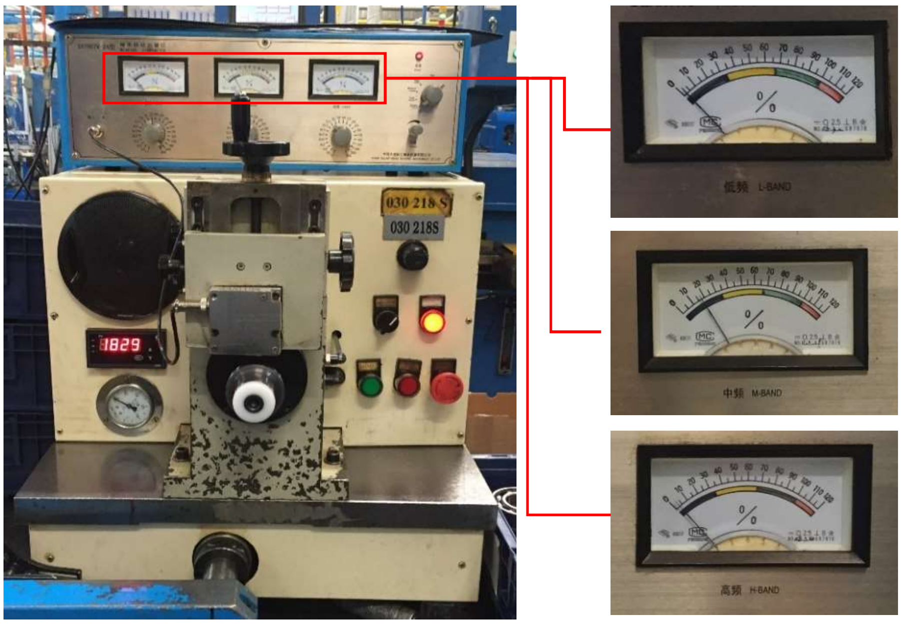

Figure 2.18 Bearing vibration tester

The inner ring is rotated at 1800 rpm (±2%) during the tests. Measurement is made with the help of a sensor that contacts the fixed outer ring. Noise level tester receives vibrations from the bearing during test and evaluate them in 3 frequency channels (Table 2.12).

Table 2.12 Frequency ranges of noise channels

A channel	B channel	C channel
Low frequency	**Medium frequency**	**High frequency**
50- 300 1/s	300- 1800 1/s	1800- 10000 1/s

The tester converts these frequency values into percentage values. Each percentage value corresponds to a level of noise in bearings. These levels are shown in Table 2.13.

Table 2.13 Noise levels for deep groove ball bearings

Noise level	L-band	M-band	H-band
	%	%	%
QQ6 (Very quiet)	<50	<50	<50
Q6 (Quiet)	<66	<66	<66
N (Standard noise quality)	<100	<100	<100
G (Noisy)	<130	<130	<130

CHAPTER 3

RESULTS AND DISCUSSION

In this chapter, the test results of thesis study are presented and discussed in detail. As mentioned earlier, experimental studies were applied to the inner ring of the 6208-type deep groove ball bearing made of 52100 bearing steel with hardness of 62 HRC. The performance evaluations are conducted in terms of some performance criteria such as, cutting forces, surface roughness, roundness error, residual stresses, subsurface phase transformations, noise level and fatigue life. The test results are evaluated in two steps. In the first step, the effects of cutting conditions and tool geometry on performance criteria in hard turning of the inner ring are discussed. HT process was performed using three CBN inserts with different effective negative rake angles (-15°, -28.5°, -35°). During HT experiments, two cutting speeds (175 and 350 m/min) and two feeds (0.05 and 0.1 mm/rev) were employed for each insert. Thus, twelve samples, four samples for each different insert, were prepared in the first step. In the second step, surface integrity, noise level and fatigue life results from GR, HT, DR operations are compared to one another. For each process, four inner rings were processed, and twelve inner rings were assembled with outer rings and nine balls into twelve deep groove ball bearings.

3.1 Test Results of the First Step

3.1.1 Cutting Forces

Cutting forces are one of the most indicators that dramatically influence tool wear and surface integrity. Therefore, feed force (Ff), tangential force (Fc) and passive force (Fp) were measured during hard turning of deep groove ball bearings using CBN inserts to observe the effects of cutting conditions and tool geometry on cutting forces. Tool geometries and the tool paths followed on the raceway of the ball bearing are shown in Figure 3.1.

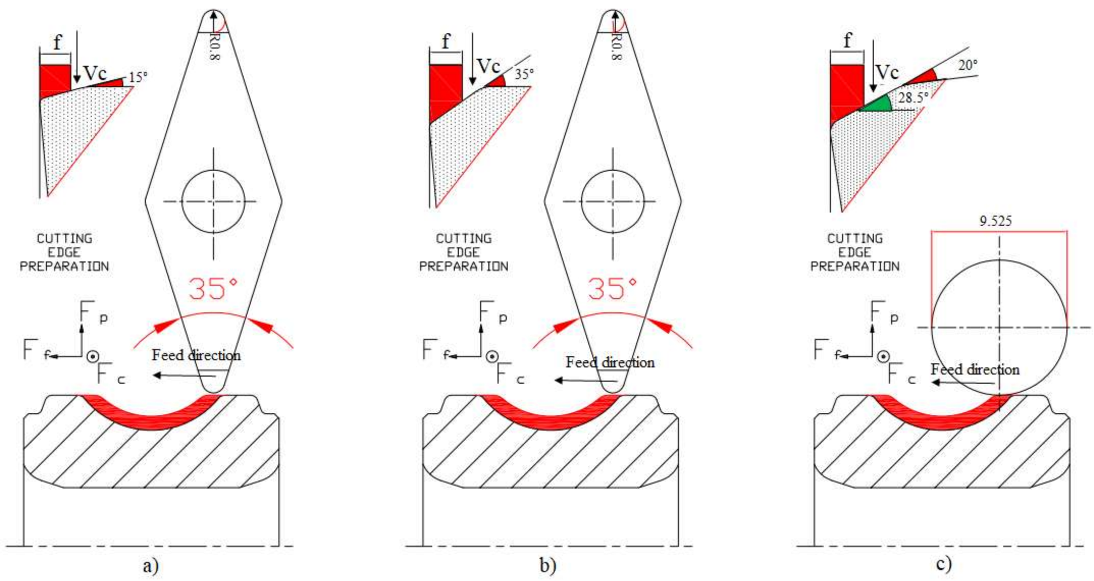

Figure 3.1 The geometries and tool paths of CBN inserts a) V-15, b) V-35 and c) O-20

Figure 3.2 shows the variation of Fc, Fp and Ff values with cutting time during hard turning of raceways of ball bearings using V-15, V-35 and O-20 inserts (V_c=175 m/min, f=0.1 mm/rev and a_p=0.06 mm). There are two remarkable points in these graphs. The first is that trend lines of Ff start in the negative direction and then end in the positive direction. This is because force acting on the insert in the feed direction changes its direction after passing the middle of the raceway. The second is that Fc and Fp values gradually become maximal in the middle of the raceway. Since the raceway surface of the inner ring has a semi-circular cross-section (the first diameter of raceway decreases and then increases during turning), the passive force (Fp) and the main cutting force (Fc) do not follow to a straight line in both graphs. During the evaluations, the maximum values of the cutting forces were taken into account. This case can be attributed to maximal tool-workpiece interaction in the middle of the raceway. Before and after middle of the raceway, force trendlines gradually increase from zero to maximal value and then gradually decrease from maximal value to zero.

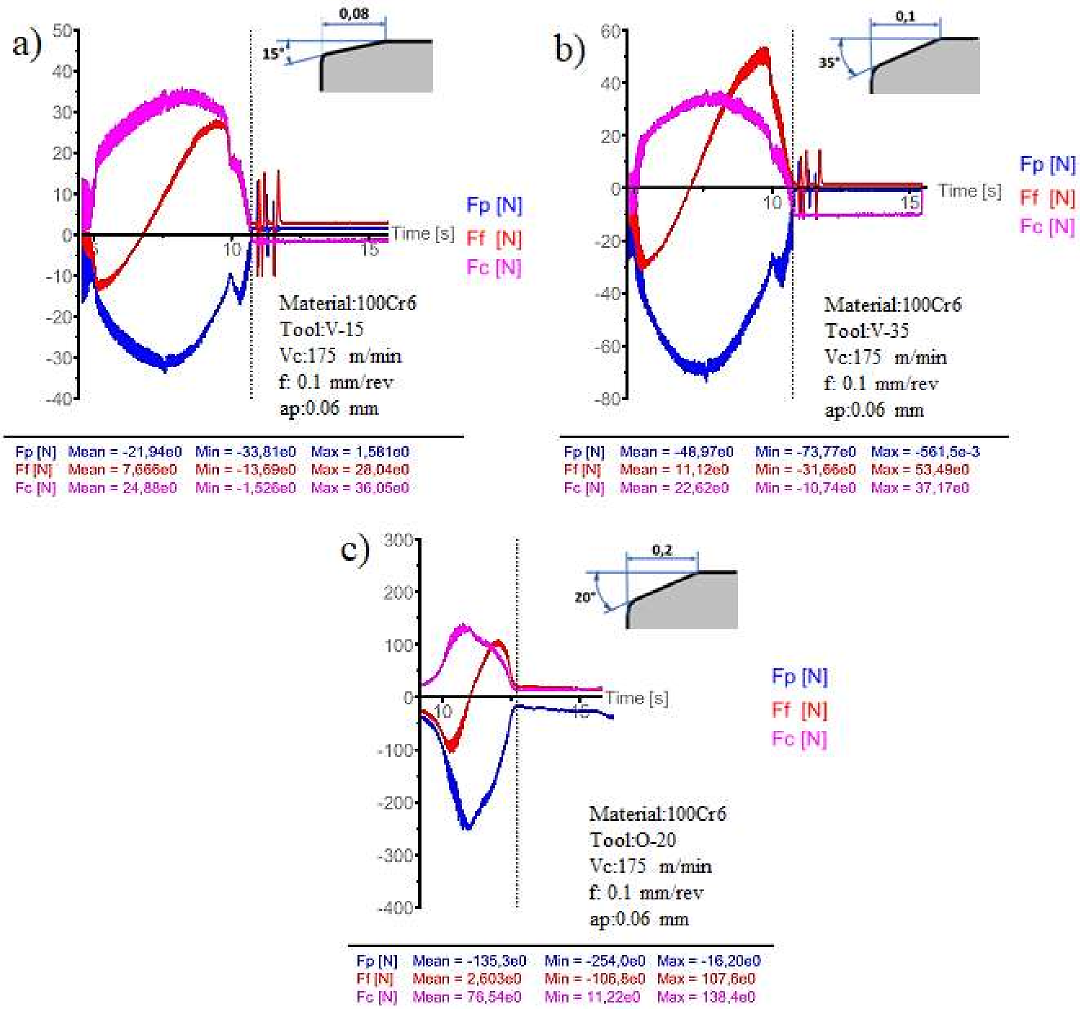

Figure 3.2 Cutting forces produced by a) V-15, b) V-35 and c) O-20 inserts (Vc=175 m/min, f=0.1 mm/rev and ap=0.06 mm)

Figure 3.3 shows the variation of Fc, Fp and Ff values with tool geometry, cutting speed and feed. As shown in Figure 3.3, Fp values are higher than Fc and Ff values under all cutting conditions. In conventional turning operations of ductile steels (unhardened state), as the depth of cut mostly is greater than nose radius, the tangential force always is the highest force component. On the other hand, since many hard turning operations contains finishing cuts, the depth of cut mostly is generally smaller than the nose radius. This case also leads to be larger the passive force than other force components. In addition, it is a known fact that the inserts with larger negative rake angles produce larger passive forces. It is possible to say that the cutting force results support the findings in the literature [22, 74, 85].

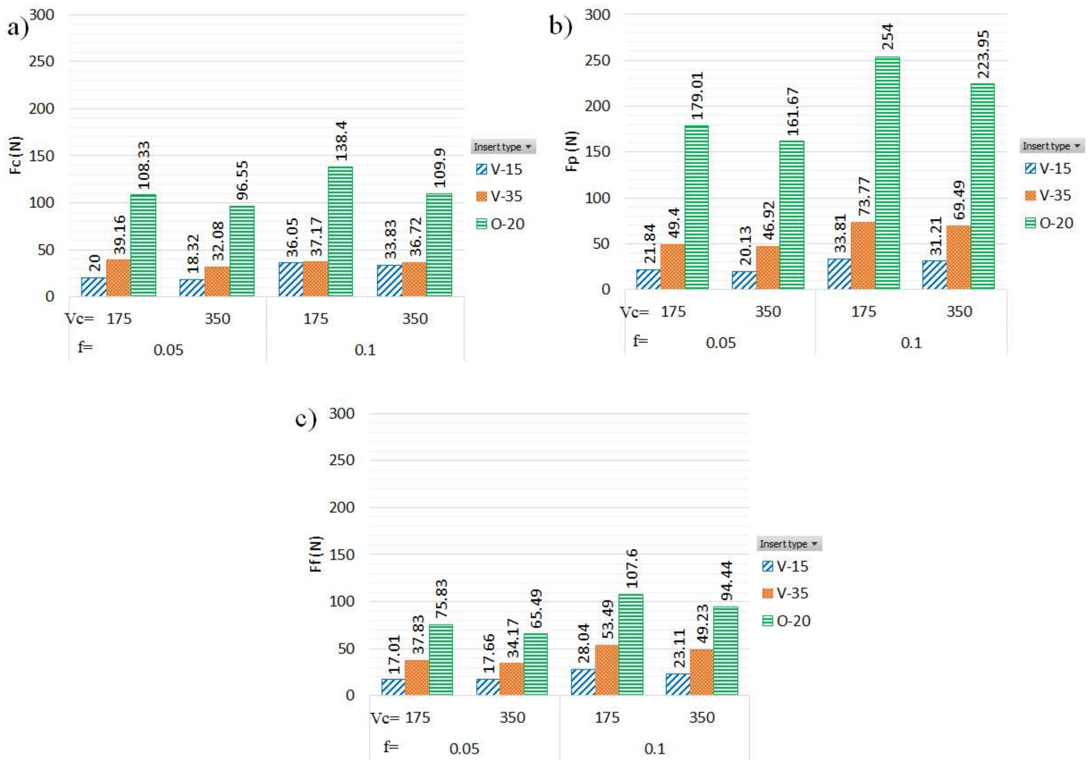

Figure 3.3 The variation of a) Fc, b) Fp and c) Ff values with tool geometry, cutting speed and feed

As shown in Figure 3.3, O-20 inserts produced much higher force values under all cutting conditions than V-15 and V-35 inserts. This can be mainly attributed to larger nose radius in O-20 insert. While nose radii of the rhombus shaped V-15 and V-35 inserts are 0.8 mm, O-20 inserts have nose radii of 4.7625 mm due to its round geometry. Larger nose radii ensure larger tool-workpiece contact area and thus, the forces increase due to increasing frictions at tool-workpiece interface. The high effective rake angle of O-20 inserts (normal rake angle + chamfer angle = -28.5°) has a secondary importance in measuring of the higher force values. As mentioned earlier, effective rake angles of the V-15 and V-35 inserts are -15° and -35°, respectively and both shapes are rhombus. V-35 inserts with larger negative effective rake angle produced higher force values in comparison to V-15 inserts under all cutting conditions. This case can be explained with larger tool-workpiece contact areas of V-35 inserts due to their larger effective rake angles. It is well-known that larger negative rake angles make chip formation difficult during machining operations. Therefore, the force values increase with an increase in negative rake angle during cutting operations.

To determine the tool-workpiece contact areas of all inserts, 3D turning simulations were performed using a DEFORM 3D software program. Analysis results are shown in Figure 3.4.

Figure 3.4 Contact areas at tool-workpiece interfaces for a) V-15, b) V-35 and c) O-20 inserts

As shown in Figure 3.4, after analysis, it was found that tool-workpiece contact areas of V-15, V-35 and O-20 inserts are 11.131×10^{-3} mm^2, 16.460×10^{-3} mm^2 and 47.531×10^{-3} mm^2 respectively. These results confirm the order-of-magnitude of cutting forces. In addition, larger contact area at the tool-workpiece interface leads to larger cutting-edge angle (κ_{ref}) [86]. Thus, the contact length increases and chip width in cutting zone decreases. Therefore, the cross-section area machined during the hard turning is thinner and wider. As the cross-sectional area of undeformed chip increases, cutting forces increase during hard machining [87, 88]. The passive force (thrust force) increases more when compared to tangential and feed forces.

It is well-known that cutting speed and feed may significantly affect cutting forces. In this study, two different speeds and feeds are used to clarify the effects of cutting conditions on cutting forces. As illustrated in Figure 3.3, the force values reduce with increasing cutting speeds (from 175 m/min to 350 m/min). This can be attributed to temperatures in the cutting zone increase due to increasing strain rate at higher cutting speed. The elevated temperatures decrease the yield strength of the work material (thermal softening) and thus, it can be plastically deformed with effect of less force [14, 89–91]. Contrary to the cutting speed, the force values substantially increase with increasing feed values (from 0.05 mm/rev to 0.1 mm/rev). This case can be explained with increasing chip cross-section. It is well-known that feed and depth of cut values determine the magnitude of chip cross-section during the cutting operations.

3.1.2 Surface Roughness

Surface roughness is considered as one of the most important indicators of product quality and is significantly affected by cutting tool geometry and cutting conditions. In this study, both Ra and Rz values were measured to make a detailed assessment of surface quality in hard turning of inner rings using CBN inserts with three different geometries at two speeds and feeds. Figure 3.6 illustrates the variation of Ra and Rz values with tool geometry and cutting conditions. As shown in Figure 3.6, Ra and Rz values produced by V-15 and V-35 inserts with the same nose radii (0.8 mm) are quite similar to one another. However, the roughness values of V-35 inserts are slightly lower than those of V-15 ones. It is thought that longer chips produced during hard turning operations performed using V-15 inserts with smaller negative effective rake angle form deeper micro-scratches on raceway of inner ring. This effect is less in hard turning operations in which V-35 inserts are employed because they produce shorter chips due to their larger negative effective rake angle. It is thought that this case leads to a slight amount of improvement in roughness values. The images of chip types produced by V-15 and V-35 inserts in Figure 3.5 support this claim.

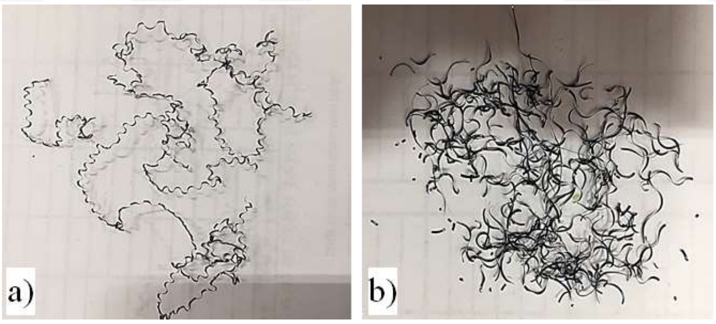

Figure 3.5 Chip types produced by a) V-15 and b) V-35 insert

It is a known fact that one of the important factors affecting the surface quality is the tool nose radius. In Figure 3.6, there are two different cases regarding O-20 inserts with larger nose radius (4.7625 mm) than those of V-15 and V-35 inserts (0.8 mm). The first is that Ra and Rz values of raceways machined by O-20 tool are lower than those of V-15 and V-35 inserts in tests performed at a higher feed value (0.1 mm/rev). Second also is that the roughness values O-20 tool is higher than those of V-15 and V-

35 inserts at feed of 0.05 mm/rev. It is well-known that cutting inserts with larger nose radii such as round and wiper inserts more effective on surface finish of work material at especially larger feed values. This effect is observed at the feed value of 0.1 mm/rev. This case can be attributed to shallower scallop heights between feed marks on work surface due to larger nose radii of O-20 inserts. At lower feed value (0.05 mm/rev), higher cutting forces and larger BUE are produced owing to larger tool-workpiece contact area. This case leads to an increase in roughness values of O-20 inserts in comparison to those of V-15 and V-35 inserts. It is a known fact that higher forces lead to higher vibrations during the cutting process and thus, they deteriorate surface finish of work material. The cutting force results confirm this claim. Similarly, it is another fact that BUE formation negatively affects roughness values owing to ploughing effect [92, 93].

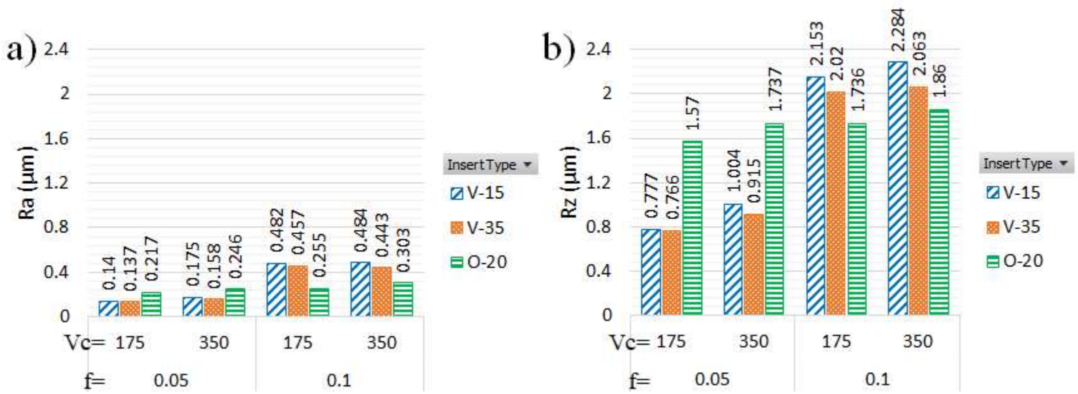

Figure 3.6 The variation of a) Ra and c) Rz values with tool geometry, cutting speed and feed

As well as tool nose radius, feed is one of the most important factors affecting surface roughness. As shown in Figure 3.6, Ra and Rz values of V-15 and V-35 inserts dramatically increase with increasing feed values. This case can be attributed to increasing cutting forces and larger scallop heights between feed marks with increasing feed. There are slight increases in roughness values of O-20 inserts with increasing feed from 0.05 mm/rev to 0.1 mm/rev. This case can be explained with larger nose radii of O-20 inserts (4.7625 mm) than V-15 and V-35 inserts (0.8 mm). The cutting speed has a slighter effect on surface roughness in comparison to feed. As shown in Figure 3.6, Ra and Rz values of V-15 and V-35 inserts generally increase with increasing speed values. This case can be attributed to rapid tool wear formed on the inserts along with increasing speed from 175 m/min to 350 m/min. It is well-known that the cutting speed is more effective on tool wear than feed and depth of cut. Maximum speed value recommended by tool manufacturers for CBN inserts in hard turning process is generally 250 m/min. In case of 350 m/min, the rapid formation of tool wear is normal due to extreme temperatures in the cutting zone. Figure 3.7 confirms this claim.

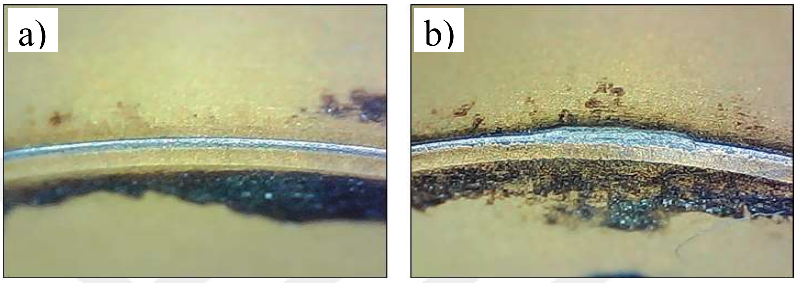

Figure 3.7 Tool wear images of O-20 inserts at a) 175 m/min and b) 350 m/min

3.1.3 Roundness Error

Roundness error of bearing rings is an issue that needs to be carefully investigated. As known, their roundness error should be kept at a minimum level since a rotational motion takes place on raceways of outer and inner rings in ball bearings. In conventional bearing manufacturing processes, it is expected that the raceway roundness error of a soft ring after the turning operations will be averagely 50 µm. After the grinding processes of hardened rings, it reduces to 1.5 µm. Therefore, Re can have an important issue in HT processes employed instead of GR process. The rings with higher roundness error (>1.5 µm) can cause higher noise levels in which they are operated in a ball bearing assembly. Moreover, service life of bearings may end prematurely due to this situation.

Figure 3.8 shows the variation of Re values with tool geometry, cutting speed and feed. As shown in Figure 3.8, The lowest values of the Re are measured in the cutting process using V-15 inserts corresponding to the lowest cutting forces, whereas the highest one is obtained in cutting process using O-20 inserts corresponding to the highest forces. This case can be considered as evidence showing the effect of cutting forces on Re.

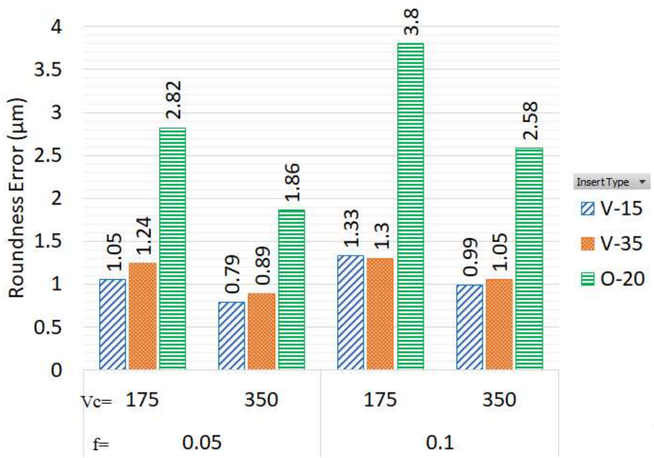

Figure 3.8 The variation of roundness error values with tool geometry, cutting speed and feed

There is a noticeable relationship between passive force and Re (Figure 3.9). As shown in Figure 3.9, as passive force increases, roundness error increases. It is determined that there also is a similar relationship between other force components and Re.

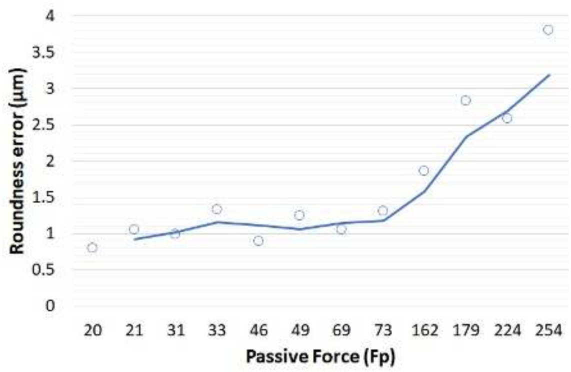

Figure 3.9 Relationship between passive force and roundness error

It is observed in Figure 3.8 that roundness error increases with increasing feed (from 0.05 mm/rev to 0.1 mm/rev) while it also decreases with increasing cutting speed (from 175 m/min to 350 m/min). This case can be explained with the decreases and increases in the cutting forces depending on increasing cutting speed and feed respectively. The best result (0.79 µm) was obtained under the cutting condition at which the lowest force value was measured (V-15 insert, cutting speed of 175 m/min and feed of 0.05 rev/min).

3.1.4 Noise Level

Noise level is one of significant quality indicators in deep groove ball bearings. The surface roughness, waviness, and roundness error of raceway of a ball bearing affect its noise level. In addition, many additional factors such as unproper lubrication, bearing inaccuracies and contamination can lead to higher noise levels during an operation. After hard turning process within the scope of this work, the raceway of the rings was superfinished and then assembled into ball bearings. The noise levels of all bearings were checked with a vibration tester. The test results are given in Table 3.1.

Table 3.1 Test results of noise level

No	Cutting speed (m/min)	Feed (mm/rev)	Depth of cut (mm)	Insert type	L-band (%)	M-band (%)	H-band (%)	Re (µm)	Ra (µm)
1	175	0.05	0.06	V-15	35	25	20	1.05	0.14
2	350	0.05	0.06	V-15	20	25	30	0.79	0.175
3	175	0.1	0.06	V-15	50	25	30	1.33	0.482
4	350	0.1	0.06	V-15	25	20	20	0.99	0.484
5	175	0.05	0.06	V-35	35	20	35	1.24	0.137
6	350	0.05	0.06	V-35	20	25	20	0.89	0.158
7	175	0.1	0.06	V-35	55	20	25	1.30	0.457
8	350	0.1	0.06	V-35	30	20	25	1.05	0.443
9	175	0.05	0.06	O-20	110	25	25	2.82	0.217
10	350	0.05	0.06	O-20	110	20	20	1.86	0.246
11	175	0.1	0.06	O-20	120	25	20	3.80	0.255
12	350	0.1	0.06	O-20	120	50	75	2.58	0.303

QQ6 (very quiet) Q6 (quiet) N (standard quality) G (noisy)

Noise level tests of ball bearings are carried out in accordance with ISO 15242 standard. Their vibration measurement methods and evaluation strategies are clearly defined in this standard. According to the standard, the rotational speed of deep groove ball bearings is determined as either 900 or 1800 rpm for vibration analysis In noise level tests in this study, the rotational speed was selected as 1800 rpm in accordance with Ref. [94]. FFT (Fast Fourier Transform) vibration spectrum is mostly preferred for vibration analysis of bearings. In FFT spectrum, the horizontal axis represents the frequency (hertz) while the vertical axis is the amplitude. While making an evaluation, disagreeable anomalies in the low band (50-300 Hz), medium band (300-1800 Hz) and high band frequencies (1800-10000 Hz) are considered [94–96]. The low band is associated with the effects of raceway defects created by bad chucking, grinding spindle runout, raceway roundness error etc. while medium band is closely related to the surface waviness produced during the various machining operations. Finally, the high band is directly related to results of the surface finishing operations such as honing, superfinishing and lapping of raceways and balls [97].

The vibration tester employed in determination of noise levels during tests reflects the noise anomalies occurring at these frequencies to an operator as a percentage value. There are four noise levels (NL) for bearings. These are QQ6 (NL<50%), Q6 (51%<NL<66%), N (67%<NL<100%), G (101%<NL<30%). According to Table 3.1, the bearings with inner rings machined by O-20 inserts are noisier. Higher noise level of the bearings is closely related to higher Re and Ra values of the raceways of inner rings. Although superfinishing process was applied to raceways of inner rings after HT process, this case shows it is not enough in reducing of noise level of ball bearings with inner rings machined by O-20 inserts. Since the depth of cut is very small (only 3 μm), it is considered that the Re of the raceway was not able to be tolerated with the superfinishing process. All other results (the noise levels of V-15 and V-35 inserts) are in Q6 and QQ6 classes. The better results were obtained at lower feed value (0.05 rev/min). All of them are in QQ6 class.

3.1.5 White and Dark Layer Formations

During hard turning operations, some microstructural changes (phase transformations) in surface and subsurface of work material may take place due to large amount of heat generated in the cutting zone. As a result of these transformations, two structures defined as white (untempered martensite) and dark layers (overtempered martensite) generally form. In this study, both optical microscopy and SEM were used to examine phase transformations on all test samples. Microstructural pictures of work materials machined by V-15, V-35 and O-20 inserts are given in Figure 3.10.

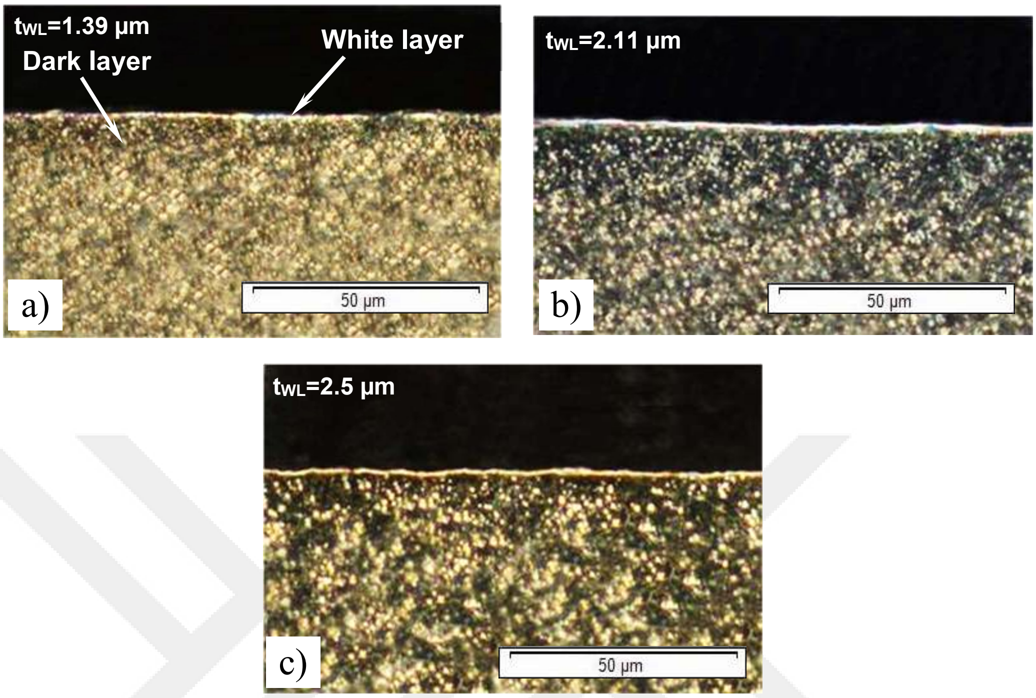

Figure 3.10 White layer formations on samples machined by a) V-15, b) V-35 and c) O-20 inserts

As shown in Figure 3.10, the white layer formations are observed in microstructures of all machined samples at cutting speed of 350 m/min and feed of 0.05 rev/min. The thicknesses of the white layers (t_{wl}) of samples machined by V-15, V-35 and O-20 inserts were measured as 1.39 µm, 2.11 µm and 2.5 µm, respectively. The thickest one was measured on the sample machined by O-20 insert. As mentioned earlier, after 3D turning simulations, it was found that tool-workpiece contact areas of V-15, V-35 and O-20 inserts are 11.131x10^{-3} mm^2, 16.460x10^{-3} mm^2 and 47.531x10^{-3} mm^2 respectively. O-20 insert with largest tool-workpiece contact area (47.531x10^{-3} mm^2) form thicker white layer owing to larger nose radius. Larger tool-workpiece contact area leads to higher frictions and thus, cutting temperatures significantly increases in cutting zone. Excessive heat in the cutting zone also causes to form thicker white layer. Similar case is valid for V-35 insert with thicker white layer (2.11 µm) than that of V-15 insert (1.39 µm). Temperature rises in cutting process in which V-35 insert is employed are because of increasing tool-workpiece contact area with an increase in negative effective rake angle (from 15° to 35°). Force results confirm this claim.

Cutting speed is the one of the most important factors that increase the temperatures in the cutting zone. In Figure 3.11, both optical microscope (left side) and SEM pictures (right side) of microstructures of the samples machined V-35 at different cutting speeds are given. When the cutting speed is increased from 175 m/min to 350 m/min, white layer thickness increases from 1.26 to 2.11 μm. This case is an important indicator for temperature rises in cutting zone with increasing cutting speed. In addition, dark layer formation was observed in different thicknesses in the workpiece where high temperatures occurred.

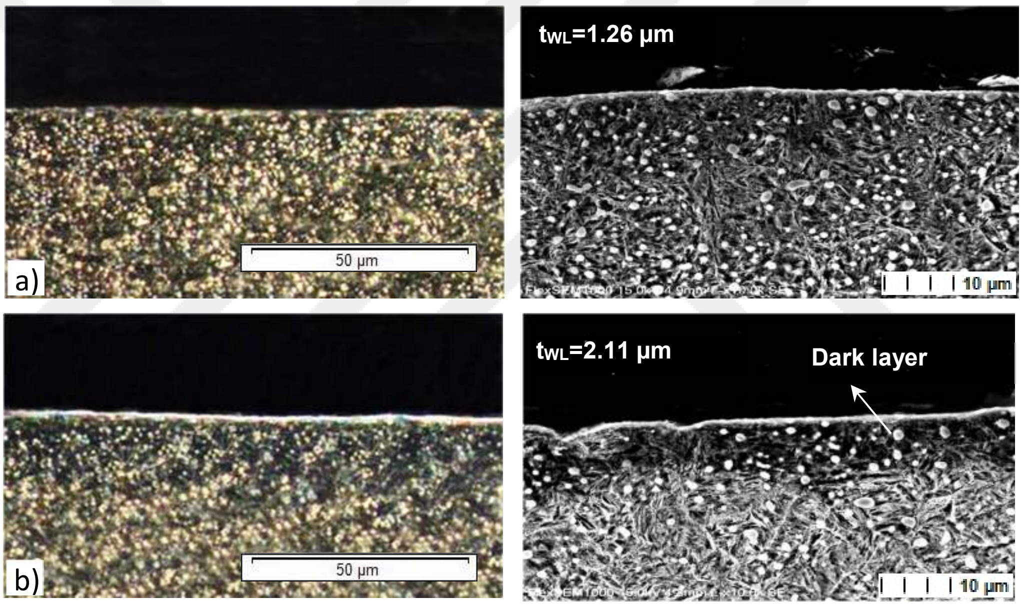

Figure 3.11 White layer formations at a) 175 m/min and b) 350 m/min

3.1.6 Residual Stresses

During hard turning operations, residual stresses occur on work surface and subsurface due to thermo-mechanical effects. These stresses have a direct effect on fatigue life of the machinery components. The residual stresses in both axial and hoop (circumferential) directions at the surface of the machined samples at all cutting conditions are shown in Figure 3.12.

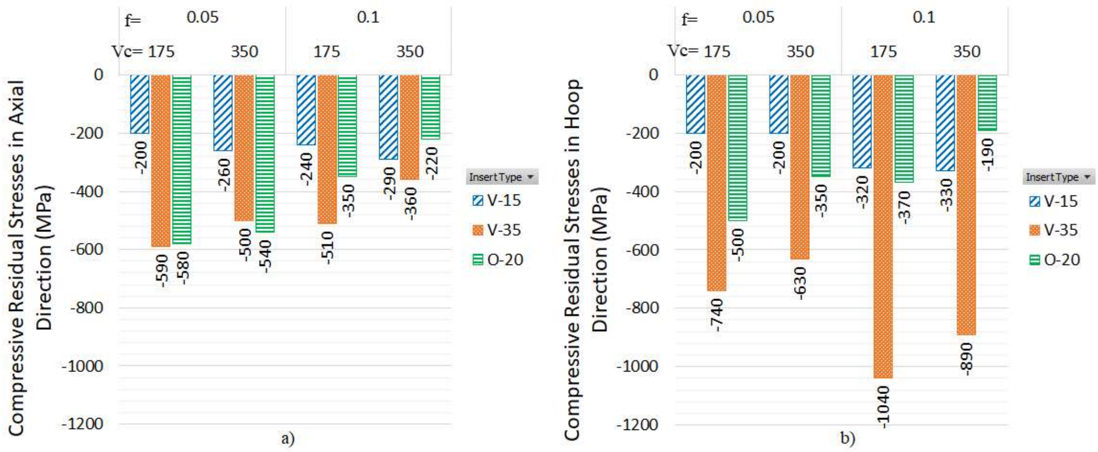

Figure 3.12 Surface residual stresses in a) axial and b) hoop directions

As shown in Figure 3.12, all residual stresses are in compressive direction (negative). Since hard turning is carried out by cutting inserts with negative effective rake angles, formation of compressive stresses on work surface and subsurface are an expected result. In general, it is possible to say that compressive stresses in the hoop direction (cutting speed direction) are higher than those in axial direction (feed direction) [32]. This is because tangential force values are higher than feed force values. In the axial direction, the greatest compressive stress is measured on surface machined by V-35 insert at 175 m/min and 0.05 mm/rev, while in the hoop direction, it is produced on surface cut by V-35 insert at 175 m/min and 0.1 mm/rev. That is, it can be said that V-35 inserts induce the higher compressive stresses on the work surface due to their larger effective rake angle (35°) in comparison to those of V-15 and O-20 inserts.

It is well-known that there is also a close relationship between cutting speed and residual stresses. Accordingly, it can be observed in Figure 3.12 that compressive stresses of V-15 inserts increase while those of V-35 and O-20 inserts decrease in both axial and hoop directions with increasing the cutting speed from 175 m/min to 350 m/min. The decreases in compressive stresses with the use of V-35 and O-20 inserts can be explained by dramatic increases in heat amount generated at the tool-workpiece interface with increasing cutting speed due to their larger tool-workpiece contact areas. As the temperatures increase in the cutting zone, the stresses on the work surface tend to turn from compression to tensile. V-15 inserts produce lower temperatures with increasing cutting speed during hard machining due to their less tool-workpiece contact areas. Lower temperatures increase the effect of plastic deformation on compressive stresses [86]. This case also leads to the increases in compressive stresses on the work surface. The measured force values (Figure 3.3) and tool-workpiece contact areas (Figure 3.4) confirm this claim.

It is clear that feed has an important impact on cutting forces (Figure 3.3) and thus, residual stresses (Figure 3.12). According to Figure 3.12, compressive stresses of V-15 inserts increase while ones of O-20 inserts generally decrease in both axial and hoop directions with an increase feed from 0.05 mm/rev to 0.1 mm/rev. This case can be attributed to higher heat generation owing to higher cutting forces and larger tool-workpiece contact areas during machining with O-20 inserts and to higher plastic deformation impact due to lower heat generation during machining using V-15 inserts. It is a known fact that higher tensile stresses are induced by higher thermal loads on the work surface during hard machining [98]. However, a remarkable point in Figure 3.12 is that while compressive stresses of V-35 inserts decrease in axial direction, they increase in hoop direciton wtih increasing feed.

Tool geometry affects direction and magnitude of residual stresses greatly at the work surface and subsurface. To increase the cutting-edge strength of the inserts, the cutting edge is either chamfered or honed. As mentioned earlier, cutting inserts with chamfer angles of 15° (V-15), 35° (V-35), 20° (O-20) were employed during tests in scope of this study. Since V-15 and V-35 inserts are fitted to toolholder with a normal rake angle of 0°, their chamfer angles are considered as effective rake (Figure 3.13.a and Figure 3.13.b). On the other hand, there is a normal rake angle of -8.5° in the toolholder where the O-20 insert is attached. For this reason, the effective rake angle of O-20 insert is evaluated as -28.5° (Figure 3.13.c). As shown in Figure 3.13, as the negative rake angle increases, the compressive zone (CZ) widens and the tensile zone (TZ) becomes narrower and thus, compressive stresses are induced at work surface and subsurface. In case of a reduction in the negative rake angle, the residual stresses shift to the tensile direction due to larger tensile zone. In brief, the rake angle directly affects the residual stresses.

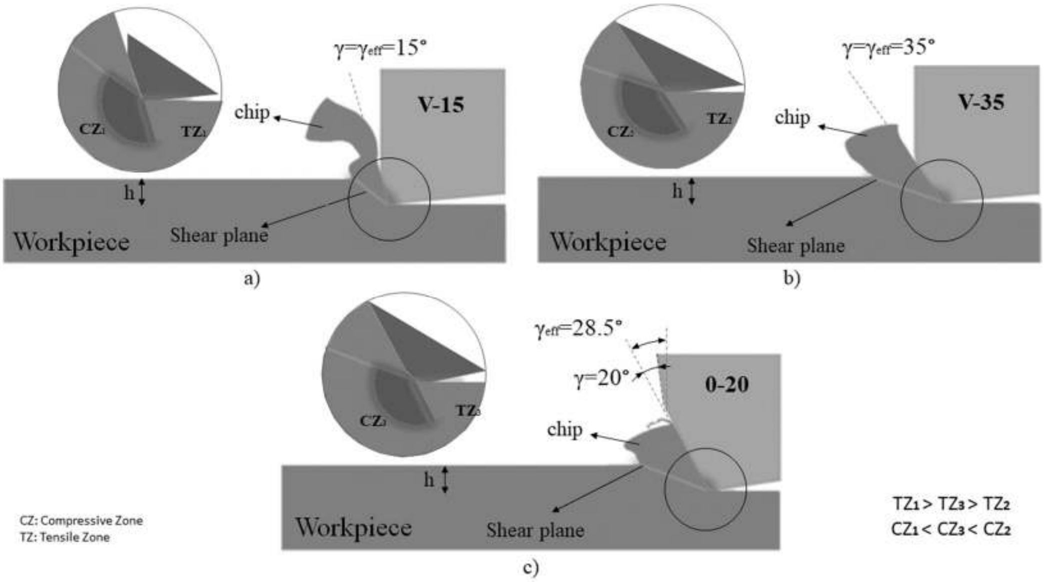

Figure 3.13 The effects of effective rake angle on compressive and tensile zones in orthogonal plane of a) V-15 insert b) V-35 insert c) O-20 insert

Figure 3.14 presents the stress depth profile of the specimens machined by cutting inserts with three different geometries at 175 m/min and 0.05 mm/rev. As shown in Figure 3.14, the maximum compressive stresses were measured on the sample machined by the V-35 insert. The highest compressive stresses become -770 MPa at a depth of 5 μm in both axial and hoop directions. The compressive stresses measured on the samples machined with V-15 insert are lower when compared to those of V-35 insert. Although they have same tool geometry (rhombus) as one another, the most obvious reason for lower stress values is smaller negative effective rake angle of V-15 insert. As mentioned earlier, an increase in negative rake angle increases the cutting forces (especially passive force in hard turning). Higher passive forces also induce larger compressive stresses. Namely, it is possible to say that there is a close relation between passive force and compressive stresses. On the other hand, it is not possible to establish a similar correlation between compressive stresses of V-35 and O-20 inserts. Although the passive forces become maximal during hard turning with the O-20 insert due to its larger nose radius, their compressive stresses are lower in comparison to those of V-35 insert. The main reason for lower compressive stresses with the O-20 insert is that its tool-workpiece contact area is approximately four times larger than the rhombus inserts (V-15 and V-35) and thus, this case results in excessive heat generation in cutting zone. As mentioned earlier, increasing temperatures in the cutting zone, lead to the residual stresses to shift from compressive direction to tensile direction. Another remarkable point in Figure 3.14 is that higher compressive stresses were measured up to depth of 20 µm in both axial and hoop directions on samples machined by the V-35 inserts.

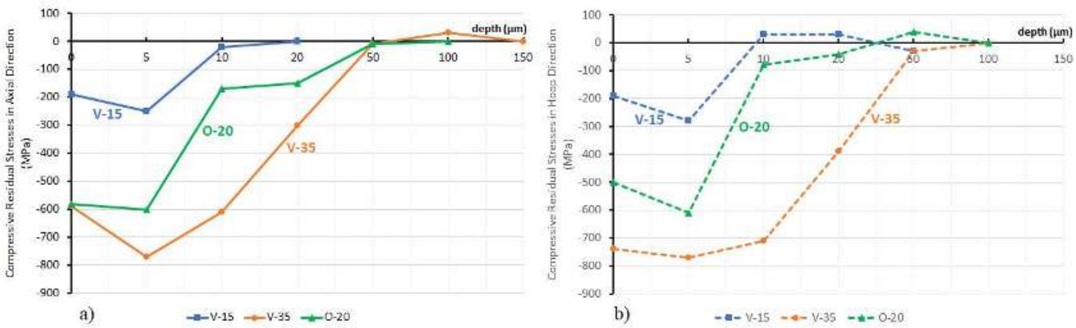

Figure 3.14 The effects of tool geometry on stress depth profile in a) axial and b) hoop directions

3.2 Second Section of Test Results

In the second step of the study, GR, HT, DR operations applied to inner rings are compared in terms of surface roughness, residual stresses, roundness error, noise level and fatigue life. For each manufacturing method, four inner rings were prepared, and total twelve inner rings were assembled along with outer rings and sufficient number of balls into bearings. In the previous step, it was assessed that the samples hard-turned by the V-35 inserts at 175 m/min and 0.05 mm/rev generally outperform in comparison to those of other cutting conditions and insert types. For this reason, eight samples for HT and DR were machined by the V-35 inserts. The test results of the bearing samples are presented in this section.

3.2.1 Surface Roughness

It is well-known that different manufacturing methods form different surface textures on a work material. Therefore, selection of proper manufacturing methods is very important to better surface quality. In this section, the effects of GR, HT, DR methods on surface roughness are discussed. It is a known fact that grinding is a method widely used in machining of hardened steels. Similarly, HT and DR methods are still employed in the bearing industry to improve surface quality, fatigue life and so on of ball bearings. For this reason, the effects of three methods on surface quality are investigated and after the measurements, surface roughness results are given in Figure 3.15. As shown in Figure 3.15, HT produces smoother surfaces than standard GR process applied to inner rings of the ball bearings. This is because larger insert nose radius (0.8 mm) and lower feed value (0.05 mm/rev) in HT process, and larger abrasive grit size of the grinding wheel (120) in GR process. The lowest roughness values are measured on work surface formed by DR process. An improvement of 46% was observed in Ra and Rz values. There is a considerable reduction (~46% in comparison to HT) in roughness parameters (Ra and Rz) after DR process). It is well-known that DR eliminates the micro notches and burrs, and feed marks on the work surfaces occurring during machining operations such as GR and HT. This also is a reason for smoother surfaces after DR process.

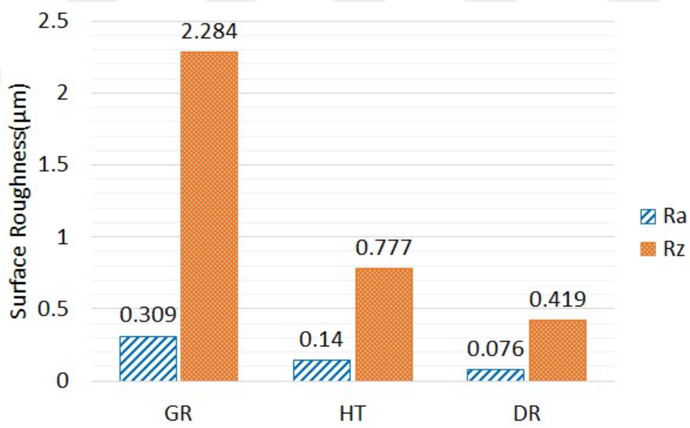

Figure 3.15 Surface roughness results for three manufacturing methods

3.2.2 Roundness Error

Roundness error is one of the most important factors affecting the fatigue life of the bearings. The mean Re values measured on raceways of inner rings produced by three different methods (GR, HT and DR) are given in Figure 3.18. As shown in Figure 3.18, GR process produced the lowest Re value (0.6 µm). During preparation of the specimens, GR process was carried out in the form of plunge cutting. Therefore, there is no axial movement of the grinding wheel, namely, inner rings are not subjected to axial forces during cutting. In addition, since grinding wheels are precisely shaped in accordance with the raceway of the inner ring prior to grinding process, in such grinding processes, form errors can be rarely observed on inner rings except the use of worn wheel and non-rigid machine tool. Under these conditions, obtaining the lowest Re value with grinding process is an expected result. During HT, inner rings are subjected to axial (thrust) forces as well as tangential and passive forces due to feed (axial) motion of the cutting tool. In addition, as explained in Section 3.1.1, the inserts with larger negative rake angle produce higher cutting forces. It can be said that third additional force component and higher force values are two of the most important reasons for medium level Re values in HT process. The highest Re value was produced by HT followed by DR. In DR process conducted in the scope of this study, the rolling tool applied a quite high pressure (300 bars) to raceway of the inner rings in radial and axial directions. The raceway profile of the inner rings is substantially deteriorated with the effect of high pressures in DR and higher forces in HT.

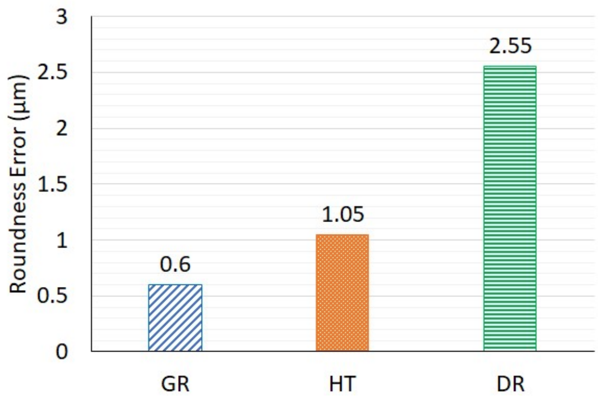

Figure 3.16 Mean Re values for three manufacturing methods

3.2.3 Residual Stresses

Residual stresses formed in the raceway of inner rings directly affect the fatigue life of ball bearings. Tensile residual stresses have a reducing effect on the fatigue life. Therefore, compressive stresses are desired instead of tensile stresses on the raceway which is the running surface of the balls to improve fatigue life of the ball bearings. In this context, GR, HT, DR methods were applied to the inner rings of the bearings and then to observe their effects on the residual stresses, their stress depth profiles were determined in the XRD measuring device. Residual stress depth profiles for three manufacturing methods are shown in Figure 3.17.

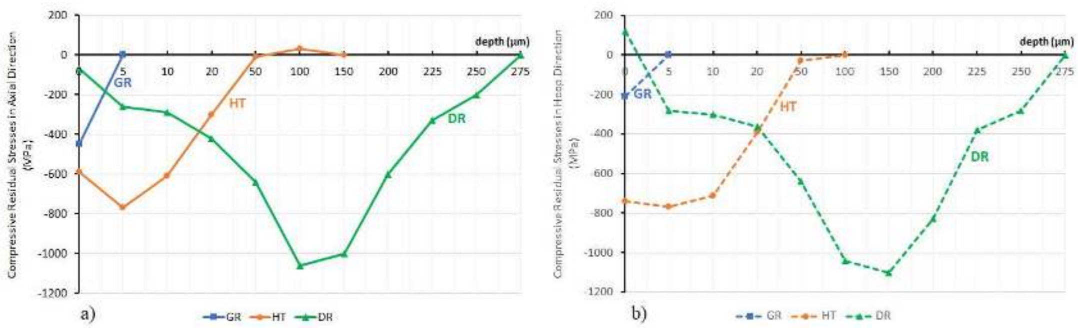

Figure 3.17 Stress depth profiles in a) axial and b) hoop directions

As shown in Figure 3.17, the maximal compressive stress was observed on the specimen manufactured by DR process. The highest compressive stress was measured as -1100 MPa at a depth of 150 µm in hoop direction. Another remarkable point in Figure 3.17 is that compressive stresses are observed in deeper zones in comparison to GR and HT processes. As mentioned earlier, DR is not a material removal process and only a mechanical surface and subsurface treatment method applied to increase fatigue strength of work materials under extreme pressures up to 400 bars. This process can produce much higher compressive stresses when compared to GR and HT processes and push them away into deeper zones of work surface (Figure 3.17). However, as shown in Figure 3.17, DR produced smaller compressive stresses in axial direction and tensile stresses in hoop direction on the work surface. This is because higher temperatures generated due to a larger friction zone between ball and work surface shift the stresses to tensile direction. The higher temperatures and rapid cooling during the DR process lead to the local thermal expansion and contraction of the work surface. This is reason for smaller compressive stresses in axial direction and tensile stresses in hoop direction on the work surface. Also, maximum compressive stress was measured as -770 MPa in HT process. In this process, the compressive residual stresses tend to decrease after a depth of 5 µm. Compressive stresses were observed up to a depth of 50 µm in the HT samples. Lower percent cold work (%CW- the degree of plastic deformation) during HT process than that of DR is a reason for lower and shallower compressive stresses. In the manufacturing of bearing rings, GR process is used as the conventional method of machining the raceway. The maximum compressive stress was measured as -450 MPa in axial direction in the samples produced by GR method. This stress value is the residual stress measured on the surface of the raceway. Residual stresses become zero at depth of 5 µm. It is well-known that higher temperatures are generated during GR process. Higher thermo-mechanical loads during grinding process shifted compressive stresses to tensile stresses at depth of 5 µm.

3.2.4 Noise Level

As mentioned earlier, the surface roughness, waviness, and roundness error of the raceway of ball bearings dramatically affect the noise level. After the GR, HT, DR processes, the raceway of the inner rings was superfinished and then assembled into ball bearings. The noise levels of all assembled bearings were checked using a vibration tester. The test results are given in Table 3.2.

Table 3.2 Test results of noise level

No	Operation	L-band (%)	M-band (%)	H-band (%)	Mean Re (µm)	Ra (µm)
1	GR	25	20	20	0.60	0.309
2	HT	35	25	20	1.05	0.14
3	DR	120	25	20	2.55	0.255

QQ6 (very quiet) Q6 (quiet) N (standard quality) G (noisy)

The vibration tester employed in determination of noise levels during tests reflects the noise anomalies occurring at these frequencies to an operator as a percentage value. There are four noise levels (NL) for bearings. These are QQ6 (NL<50%), Q6 (51%<NL<66%), N (67%<NL<100%), G (101%<NL<30%). As shown in Table 3.2, the bearing with the inner ring produced by DR method is noisy (G) in L-band. As mentioned earlier, L-band is closely related to roundness error of the raceway of the ball bearing. Although superfinishing process was applied to the inner ring raceway after DR process, this case shows that it is not enough in reducing of noise level of the bearing with inner ring produced by DR process. Since the depth of cut is very small (only 3 µm), it is considered that the roundness error of the raceway was not able to be tolerated with the superfinishing process. All other results (the noise levels of GR and HT) are in QQ6 classes. The best results were obtained with GR process.

3.2.5 Fatigue Life

Deep groove ball bearings are load-bearing machine elements. Therefore, their ability to withstand cyclic loads under harsh operating conditions has importance to longer fatigue life. It is a known fact that a possible plastic deformation that can occur on the balls and raceways of rings due to static and dynamic loads significantly affects the bearing service life. Under high-stressed working conditions, flaking and spalling on the surfaces of their raceways and the balls start to form. In addition, the tensile residual stresses are main reason for work surface cracks that lead to premature failure and shorter fatigue life of machinery elements [99]. The compressive residual stresses provide an additional protection against surface-initiated spalling [100]. Therefore, the compressive stresses are desired to form instead of tensile stresses on raceways of bearing rings since they improve the fatigue life [101, 102].

In fatigue tests, the bearings were operated at a rotational speed of 3000 rpm. Meanwhile, loads of 10000 N and 4000 N were applied in the radial and axial directions, respectively. During fatigue tests of bearings lubricated with G183 grease (ORS code), the temperatures of the outer and the inner rings were measured as 90°C and 115°C, respectively. After the specimens were assembled to the test apparatus, they were operated until they failed under test conditions. L50 theoretical life value (average life) determined using MESYS Rolling Bearing Calculation program under above-mentioned test conditions and lubrication parameters was found to be 431 hours. The life data of the bearings after the tests were analyzed on Weibull distribution. They were also interpreted statistically using MINITAB program. Firstly, a probability graph was used to determine how well the selected distribution fits test data. This graph is a probability plot formed according to the lifetime using the Weibull distribution in the MiniTab software. In the Figure 3.18, life probability graph of 6208-type bearings with the ground inner ring raceway are given.

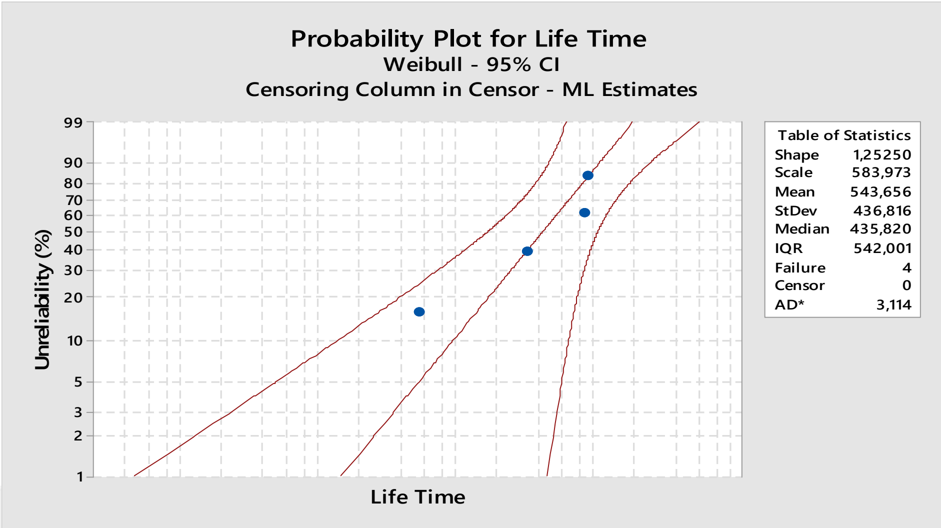

Figure 3.18 The lifetime probability graph of the bearings with the ground inner rings

Total four GR bearings were tested. This distribution (Figure 3.18) was plotted at confidence interval of 95%. If fatigue life data are within this confidence interval, it is significant to model it in the selected confidence interval. The Shape (β) parameter is called the slope of the Weibull distribution. This value is considered to be greater than 1. The shape parameter value also determines failure rates of tested samples. For example, if $\beta > 1$, the failure rate of tested sample increases with time (The distribution models wear-out failures, which tend to occur after some time passes) and if $\beta < 1$, the failure rate decreases with time (The process has many premature failures and fewer failures as time passes). The parameter value is calculated as 1.2525 according to this distribution. Also, the shape parameter varies depending on stress distribution in the tested samples. It increases with increasing stresses. The distribution of the parameter represents the confidence intervals of the statistical analysis and the dependence on the stress level. Parameter β value varies with respect to the planned number of tests to be performed. The parameter β value increases with decreasing number of test samples, however, the test reliability decreases as the number of test samples decreases. The scale (η) parameter is called the characteristic life. The characteristic life value is known as L36.8 (reliability of 36.8%) in the literature [103, 104]. An increase in characteristic life causes overall fault behavior to shift to higher fault times. Namely, it increases with low stress intensity in the tested samples. In this case, it causes an increase in error times. After analyses conducted according to the Weibull distribution, the experimental fatigue life values at confidence of 90% (10% unreliable) and confidence of 50% (50% unreliable) were coded as B10 and B50, respectively. The experimental fatigue life of the bearings with GR inner rings (standard bearings) obtained at B10 and B50 levels were compared to the fatigue life of HT and DR bearings in the scope of this thesis study. In the Figure 3.21, life probability graph of the 6208-type bearings with the hard turned inner ring raceways is given.

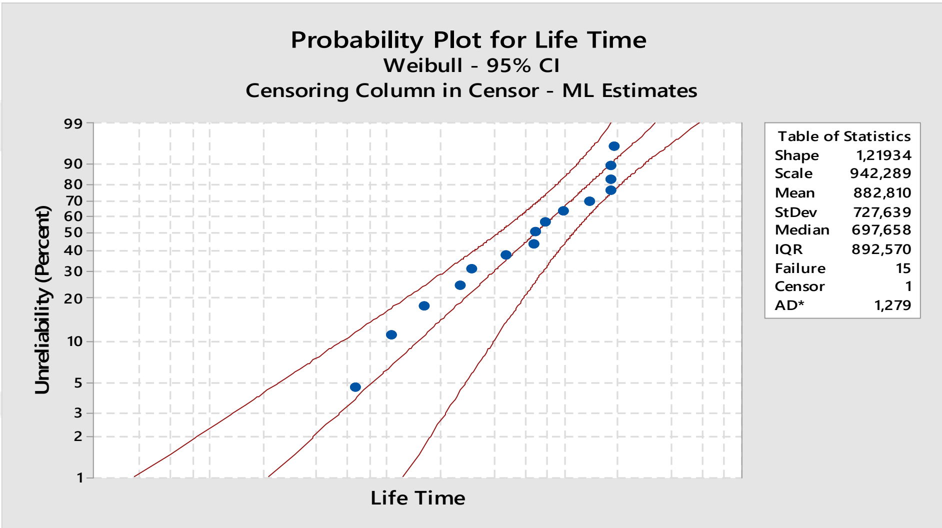

Figure 3.19 The lifetime probability graph of the bearings with the hard turned inner rings

Total sixteen HT bearings were tested. This distribution (Figure 3.19) was plotted at 95% confidence interval and its shape (β) parameter is calculated as 1.219. The experimental fatigue life of HT bearings at B10 and B50 levels improves by 42% and 62%, respectively when compared to standard bearings. “Right Censored Data” method was used while this distribution was plotted. The reason for using "Right Censored Data" is that when a bearing doesn't fail in much longer periods than its maximum lifetime or there are some errors originated from lubrication conditions and test apparatus, the bearing must be censored. Total sixteen bearings were tested in fatigue life tester. However, only test data for a bearing (a bearing with experimental life of seven teen hours) was censored due to a shaft error in test apparatus. Therefore, test data for fifteen bearings is represented in Figure 3.19. In the Figure 3.20, the life probability graph of the 6208-type bearing with hard turned and deep rolled inner rings is illustrated.

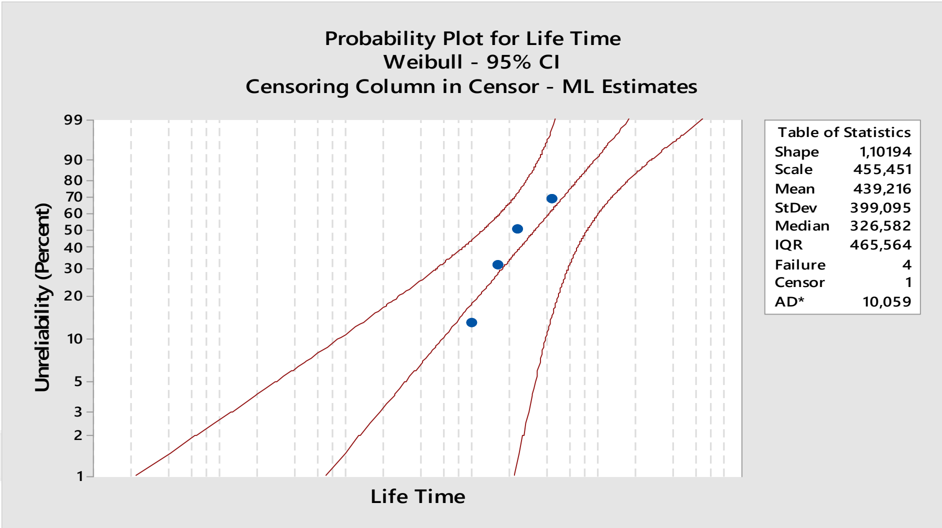

Figure 3.20 The lifetime probability graph of bearings with had turned and deep rolled inner rings

Total five DR bearings were tested. The distribution (Figure 3.20) was plotted at 95% confidence interval and its shape (β) parameter is calculated as 1.101. The experimental fatigue life of the DR bearings at B10 and B50 levels decreases by 38% and 25%, respectively in comparison to standard GR bearings. During fatigue life tests, only a test data was censored owing to chemical degradation of the grease employed in a bearing. Although total five bearings were tested, test data for four bearings is illustrated in Figure 3.20 due to a censored data.

Experimental fatigue life results at B10 and B50 levels are widely used in the literature [105–107]. For this reason, while comparing the fatigue lives of the bearings produced by three different methods, fatigue life results at B50 level (at confidence of %50) are considered. It is found that at B50 level in comparison to GR ones, the fatigue life of HT bearings is longer by 61% while that of DR bearings is shorter by 25%. Accordingly, HT bearings exhibit the longer life than those of GR and DR bearings. In addition, it is determined that DR bearings have shorter life than those of GR bearings.

The fatigue life of the bearings can also be evaluated according to the distribution plots. Figure 3.21 shows the distribution plots of GR, HT, and DR bearings. As shown in Figure 3.21, all bearings have completed their useful fatigue lives.

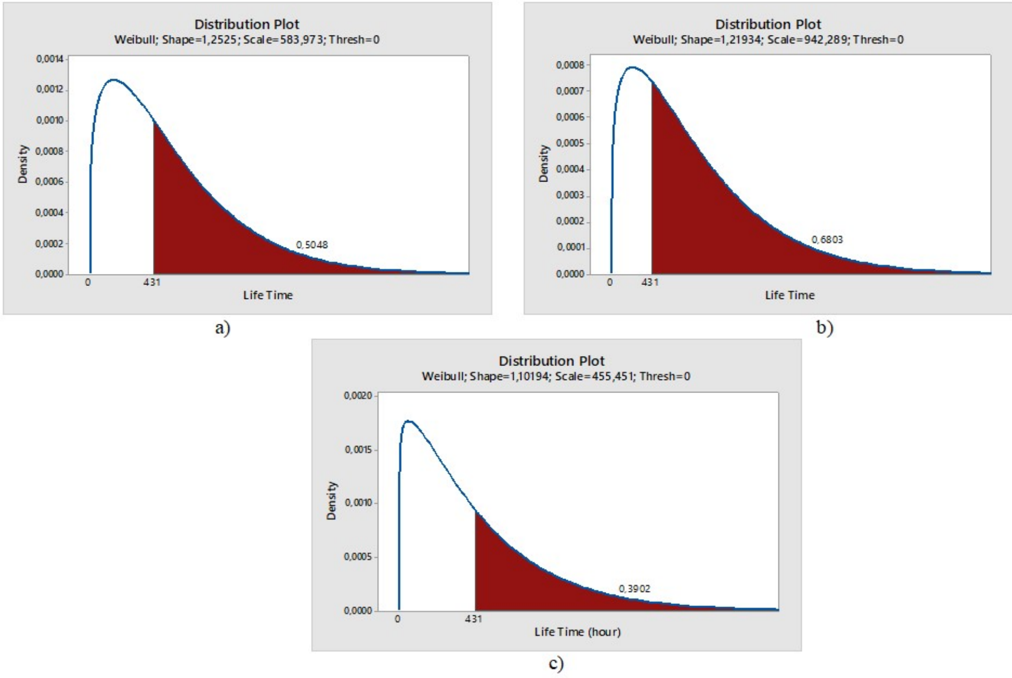

Figure 3.21 Distribution plots of a) GR, b) HT and c) DR bearings

As a result of the statistical analyses conducted using test data of GR bearings, the completion probability of their L50 theoretical life (431 hours) is 50%. In other words, the reliability of the bearings tested at 431 hours is R(t) 50%. The probability values for HT and DR bearings are approximately 68% and 40%, respectively. This case is another indicator that fatigue life of HT bearings are longer than those of GR and DR bearings.

Another evaluation strategy is the hazard plot for lifetime. This strategy illustrates the variation of failure rates of ball bearings with the test time. Figure 3.22 shows that the failure rates of the ball bearings increase with time. In other words, their failure rates increase with an increase in life span. This is an indicator for the wear-out failures. That is, the bearing begins to wear out with time and suddenly fails at a critical wear level. Some surface defects such as pitting (Figure 3.23.a) and spalling (Figure 3.23.b) are two of main reasons for the wear-out failures. It can be observed in Figure 3.22 that the failure rate of HT bearings is lower than those of GR and DR bearings.

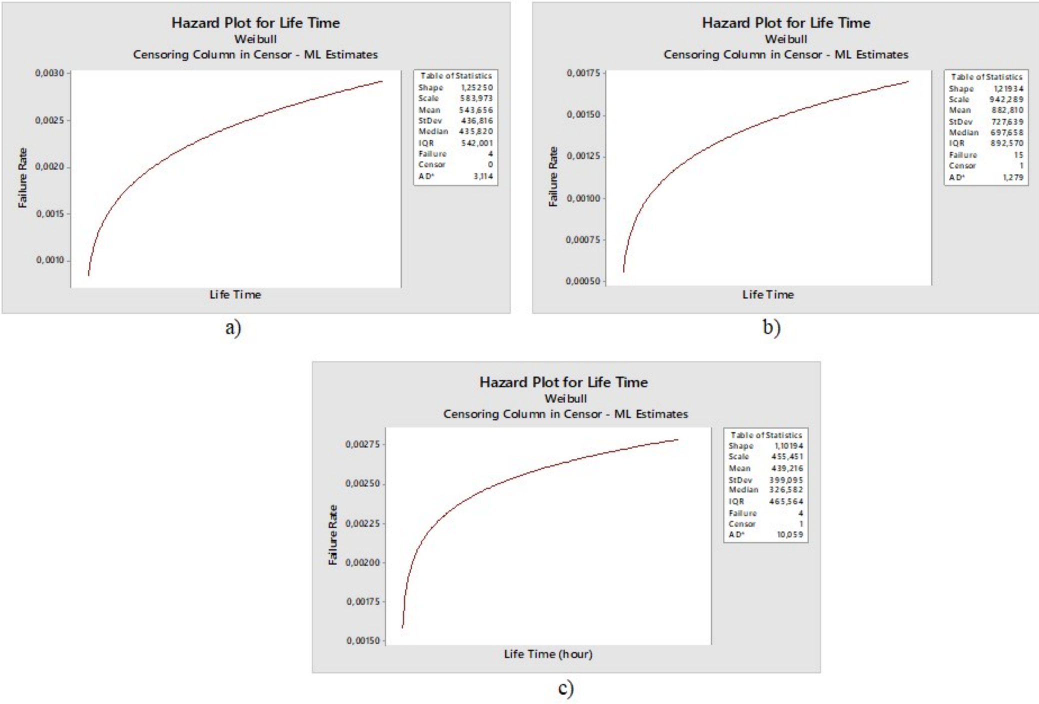

Figure 3.22 Hazard plots of a) GR, b) HT and c) DR bearings

As mentioned earlier, fatigue life of ball bearings depends on the magnitude and direction of the loads during operation, raceway geometry and roughness, material type, operating temperature, lubricant applied, lubrication conditions, rolling speed, and many other factors and variables [108, 109]. Due to small contact area, stresses accumulate in a small subsurface volume. Therefore, subsurface stresses result in some types of fatigue damages. Their initiation may be at surface defects or below contact surface [110–112].Two main damage types formed in the bearing raceways after fatigue life tests are shown in Figure 3.25. These are pitting and spalling. Pitting is a damage type formed on raceway surface due to foreign small parts such as dirt or metal particles and atmospheric impacts (oxidation). Spalling is a result of surface and/or subsurface fatigue causing fractures in running surfaces such as raceways of ball bearings. Both of them substantially affect the fatigue life of the ball bearings. They lead to the wear-out failures in operation conditions.

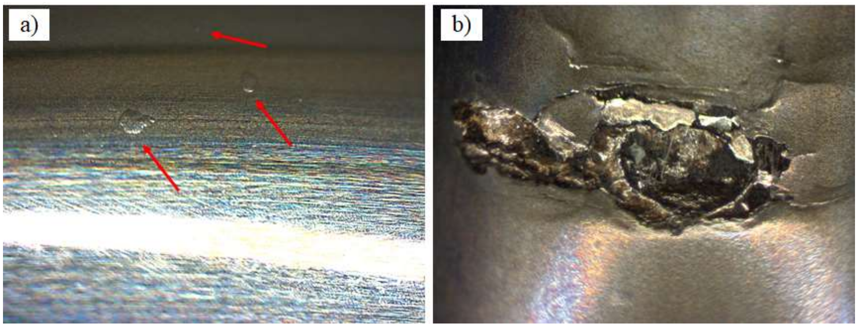

Figure 3.23 Some surface defects on raceways of ball bearings; a) pitting and b) spalling

Considering life tests, HT bearings ensure the longest bearing life while DR bearings have shorter bearing life than HT and GR bearings. Higher life performance of HT bearings can be explained with the combination of high compressive stresses, low roundness error and surface roughness values of raceways of inner rings. On the other hand, although DR process performed under excessive pressures up to 300 bars produces higher compressive residual stresses at deeper layers of work surface, the raceway Re of the inner rings is not within the desired tolerances. As mentioned earlier, form error of inner ring raceway drastically affects the fatigue life of bearings.

CHAPTER 4

CONCLUSION AND FUTURE WORK

4.1 Summary of The Present Study

In this study, the effects of hard turning and deep rolling process on surface integrity and fatigue life of raceway of deep groove ball bearings were investigated. The inner rings of the 6208-type deep groove ball bearings were employed as a work material during the tests. This study consists of two important steps. In the first step, the effects of cutting conditions and tool geometry on cutting forces, raceway roundness error and surface integrity (surface roughness, residual stresses, subsurface phase transformations) were studied in hard turning of the bearing steel (62 HRC). In the second step, the performances of grinding, hard turning, hard turning+deep rolling operations applied to raceway of inner rings are compared to each other in terms of surface integrity, noise level and fatigue life. The findings of the thesis study are as follows:

- O-20 inserts produced much higher force values under all cutting conditions than V-15 and V-35 inserts. This can be mainly attributed to larger tool nose radius of O-20 inserts (4.7625 mm) than that of V-15 and V-35 inserts (0.8 mm). Larger nose radii ensure larger tool-workpiece contact area and thus, the forces increase due to increasing frictions at the tool-workpiece interface.
- It was observed that Ra and Rz values of O-20 inserts are lower than those of V-15 and V-35 inserts at higher feed value (0.1 mm/rev) while they are higher at lower feed value (0.05 mm/rev). It is well-known that larger nose radius positively affects surface roughness at higher feed values. At lower feed values, BUE formation is a reason for higher roughness values.
- It was found that there is a noticeable relationship between cutting forces and roundness error. As the force values increase, the roundness error increases. Therefore, O-20 inserts lead to maximal roundness error values.

- The bearings with inner rings hard turned by O-20 inserts reached to higher noise levels than ones machined by V-15 and V-35 inserts under all cutting conditions. The noise level of the bearings is closely related to the roundness error and surface quality of the raceways of the inner rings.
- White layer formations were observed in microstructures of all machined samples at cutting speed of 350 m/min and feed of 0.05 rev/min. The thickest one was measured on the sample machined by O-20 insert. O-20 insert with largest tool-workpiece contact area form thicker white layer owing to larger nose radius and excessive heat in the cutting zone.
- Highest compressive stresses were measured on the sample machined by the V-35 insert. This can be mainly attributed to the increases in cutting forces due to its larger effective negative rake angle. Higher passive forces induce larger compressive stresses.
- Compressive residual stresses of V-15 inserts increase while those of V-35 and O-20 inserts decrease in both axial and hoop directions with increasing the cutting speed from 175 m/min to 350 m/min. The decreases in compressive stresses with the use of V-35 and O-20 inserts can be explained by dramatic increases in heat amount generated at the tool-workpiece interface with increasing cutting speed due to their larger tool-workpiece contact areas. As the temperatures increase in the cutting zone, the stresses on the work surface tend to turn from compression to tensile.
- Hard turning produces smoother surfaces than standard grinding process applied to inner rings of the ball bearings. This is because larger insert nose radius (0.8 mm) and lower feed value (0.05 mm/rev) in HT process, and larger abrasive grit size of the grinding wheel (120 µm) in GR process. The lowest roughness values are measured on work surface formed by DR process. This is explained by the fact that it removes micro notches and burrs and feed marks from deep rolling work surfaces.
- GR process produced the lowest roundness error value due to perfectly shaped grinding wheels and lower force values. The highest Re value was produced by HT followed by DR process. Re of inner ring raceway is substantially

deteriorated with the effect of high pressures in the deep rolling and higher forces in hard turning.

- Highest compressive stress was observed on the specimen manufactured by DR process. The compressive stresses are reached to deeper layers of work surface in comparison to GR and HT processes. DR process is a mechanical surface and subsurface manufacturing method without material removal applied to increase fatigue strength under high pressures. As a result, it can produce much higher compressive stresses than the GR and HT processes and push them deeper into the work surface.
- DR produced smaller compressive stresses in axial direction and tensile stresses in hoop direction on the work surface. This is because higher temperatures generated due to a larger friction zone between ball and work surface shift the stresses to tensile direction.
- DR bearings reached much higher noise levels than HT and GR bearings. The noise level of the bearings is closely related to the roundness error and surface quality of the raceways of the rings.
- HT bearings ensure the longest bearing life while DR bearings have shorter bearing life than HT and GR bearings. Higher life performance of HT bearings can be explained with the combination of high compressive stresses, low roundness error and surface roughness values of raceways of inner rings.
- Although DR operation under excessive pressures produces higher compressive residual stresses in the deeper layers of the work surface, DR bearings have a lower fatigue life than HT and GR bearings. This can be mainly attributed to the raceway roundness error of the inner rings is not within the desired tolerances during DR process. The roundness error of the inner ring raceway greatly affects the fatigue life of the bearings.

4.2 Future Work

Experimental study results showed that it is possible to obtain better fatigue life with hard turning process. In the deep rolling process, although higher compressive residual stresses are produced in the deeper layers of the work surface, the fatigue life was lower compared to other methods. The main reason for this is the roundness error of the inner ring raceway caused by the excessive loads and pressures during deep rolling. Thus, there is a need to improve deep rolling performance. For this reason, following suggestions can be used for future works in machining of raceway bearings to obtain better fatigue life performance:

- Different ball diameter can be tried in order to obtain lower thrust force values during deep rolling process.
- Effects of various spindle speed and feed can be studied in deep rolling.
- The deep rolling thrust pressure creates higher compressive residual stresses in deeper layers of the work surface. Some studies can be conducted on minimization of the roundness error by reducing the hydraulic oil pressure in deep rolling process.
- Different cooling/lubrication conditions such as cryogenic cooling, MQL and cryo-MQL can be investigated in hard turning process to provide better surface integrity.

REFERENCES

[1] Liu, C.R., & Mittal, S. Single-step superfinish hard machining: Feasibility and feasible cutting conditions. Robotics and Computer-Integrated Manufacturing, *12*, 15–27, 1996

[2] Umbrello, D., Jayal, A.D., Caruso, S., Dillon, O.W., & Jawahir, I.S. Modeling of white and dark layer formation in hard machining of AISI 52100 bearing steel. Machining Science and Technology, *14*, 128–147, 2010

[3] Thiele, J.D., & N. Melkote, S. Effect of cutting edge geometry and workpiece hardness on surface generation in the finish hard turning of AISI 52100 steel. Journal of Materials Processing Technology, *94*, 216–226, 1999

[4] Vomacka, P., & Walburger, H. Residual stresses due to hard-machining-industrial experiences. Materials Science Forum, *347*, 592–597, 2000

[5] Parrish, G. *Carburizing:Microstructures and Properties* (1st ed.). Portland:ASM Internatıonal. 1999

[6] Notoya, H., Yonetani, S., & Takatsuji, Y. Influence of Grinding Conditions on Residual Stress and Distortion in the Ground Layer. Transactions of the Japan Institute of Metals, *27*, 534–545, 1986

[7] Hua, J., Umbrello, D., & Shivpuri, R. Investigation of cutting conditions and cutting edge preparations for enhanced compressive subsurface residual stress in the hard turning of bearing steel. Journal of Materials Processing Technology, *171*, 180–187, 2006

[8] D'Addona, D.M., & Raykar, S.J. Analysis of Surface Roughness in Hard Turning Using Wiper Insert Geometry. Procedia CIRP, *41*, 841–846, 2016

[9] Richt, C. A Hard Turn Toward Efficiency. Gear Solutions, *7*, 22–31, 2009

[10] Luminoso, L. *Hard-part turning strategies*. Retrieved 28 Dec 2021, from

https://www.canadianmetalworking.com/canadianmetalworking/article/cutting tools/hard-part-turning-strategies. 12 July 2019

[11] Klocke, F., Brinksmeier, E., & Weinert, K. Capability Profile of Hard Cutting and Grinding Processes. CIRP Annals, *54*, 22–45, 2005

[12] Guo, Y.B., & Liu, C.R. Mechanical properties of hardened AISI 52100 steel in hard machining processes. Journal of Manufacturing Science and Engineering, *124*, 1–9, 2002

[13] Tonshoff, H.K., Arendt, C., & Ben Amor, R. Cutting of hardened steel. CIRP Annals - Manufacturing Technology, *49*, 547–566, 2000

[14] Bartarya, G., & Choudhury, S.K. State of the art in hard turning. International Journal of Machine Tools and Manufacture, *53*, 1–14, 2012

[15] Grzesik, W., Żak, K., & Kiszka, P. Comparison of surface textures generated in hard turning and grinding operations. Procedia CIRP, *13*, 84–89, 2014

[16] Ramesh, A., Melkote, S.N., Allard, L.F., Riester, L., & Watkins, T.R. Analysis of white layers formed in hard turning of AISI 52100 steel. Materials Science and Engineering, 2005

[17] Dhar, N.R., & Kamruzzaman, M. Cutting temperature, tool wear, surface roughness and dimensional deviation in turning AISI-4037 steel under cryogenic condition. International Journal of Machine Tools and Manufacture, *47*, 754–759, 2007

[18] Grzesik, W. Cutting Tool Materials. *In Advanced Machining Processes of Metallic Materials* (2nd ed.) (35-64). Netherlands: Elsevier Science. 2016

[19]. Cubic Boron Nitride (cBN). Retrieved 12 May 2020, from http://www.tomeidiamond.co.jp/en/tec/tec-10.html.

[20] Panda, A., Sahoo, A.K., Rout, A.K., Kumar, R., & Das, R.K. Investigation of Flank Wear in Hard Turning of AISI 52100 Grade Steel Using Multilayer

Coated Carbide and Mixed Ceramic Inserts. Procedia Manufacturing, *20*, 365–371, 2018

[21] Liu, X.L., Wen, D.H., Li, Z.J., Xiao, L., & Yan, F.G. Cutting temperature and tool wear of hard turning hardened bearing steel. Journal of Materials Processing Technology, *129*, 200–206, 2002

[22] Grzesik, W. *Advanced Machining Processes of Metallic Materials: Theory, Modelling and Applications* (1nd ed.). UK: Elsevier Science. 2008

[23] Sandvik Coromant. *Hard part turning with CBN*. Retrieved 02 Feb 2021, from https://www.sandvik.coromant.com/sitecollectiondocuments/downloads/global/catalogues/en-gb/c-2940-137.pdf. Nov 2012

[24] Groover, M. *Fundementals of Modern Manufacturing Materials,Processes and Systems* (4th ed.). United States of America: John Wiley & Sons . 2010

[25] Sandvik Coromant. *Catalogues & Handbooks*. Retrieved 29 May 2021, from https://www.sandvik.coromant.com/en-gb/downloads/pages/default.aspx

[26] Dahlman, P., Gunnberg, F., & Jacobson, M. The influence of rake angle, cutting feed and cutting depth on residual stresses in hard turning. Journal of Materials Processing Technology, *147*, 181–184, 2004

[27] Davim, J.P. *Machining of hard materials* (1st ed.). NY : Springer. 2011

[28] Mıtsubishi. *Function of tool features for turning*. Retrieved 29 Dec 2021, from http://www.mitsubishicarbide.com/en/technical_information/tec_turning_tools/tec_hsk-t/tec_hsk-t_technical/tec_turning_honing_land

[29] Davoudinejad, A., & Noordin, M.Y. Effect of cutting edge preparation on tool performance in hard-turning of DF-3 tool steel with ceramic tools. Journal of Mechanical Science and Technology, *28*, 4727–4736, 2014

[30] Thiele, J.D., & Melkote, S.N. Effect of tool edge geometry on workpiece subsurface deformation and through-thickness residual stresses for hard turning

of AISI 52100 steel. Journal of Manufacturing Processes, *2*, 270–276, 2000

[31] Umbrello, D., Micari, F., & Jawahir, I.S. The effects of cryogenic cooling on surface integrity in hard machining: A comparison with dry machining. CIRP Annals - Manufacturing Technology, *61*, 103–106, 2012

[32] Çetindağ, H.A., Çiçek, A., & Uçak, N. The effects of CryoMQL conditions on tool wear and surface integrity in hard turning of AISI 52100 bearing steel. Journal of Manufacturing Processes, *56*, 463–473, 2020

[33] Nazir, A. Influence of Wiper and Conventional Inserts at Profile Geometry During Turning of D2 Tool Steel. Engineering Technology Open Access Journal, *1*, 156–162, 2018

[34] Monroy Vazquez, K.P., Giardini, C., & Ceretti, E. Cutting Force Modeling. In *CIRP Encyclopedia of Production Engineering* (315-329). Portland:Springer Berlin Heidelberg. 2014

[35] Grzesik, W. *Machining of Hard materials. In Machining: Fundamentals and Recent Advances* Davim JP (ed) (97-124). London: Springer. 2008

[36] Matsumoto, Y., Barash, M.M., & Liu, C.R. Cutting mechanism during machining of hardened steel. Materials Science and Technology (United Kingdom), *3*, 299–305, 1987

[37] Thiele, J.D., & N. Melkote, S. Effect of cutting edge geometry and workpiece hardness on surface generation in the finish hard turning of AISI 52100 steel. Journal of Materials Processing Technology, *94*, 216–226, 1999

[38] Yi, J., Jiao, L., Wang, X., Xiang, J., Yuan, M., & Gao, S. Surface roughness models and their experimental validation in micro milling of 6061-T6 al alloy by response surface methodology. Mathematical Problems in Engineering, *2015*, 2015

[39] Adapa mould. *The definition of surface roughness*. Retrieved 29 Dec 2021, from https://adapa.dk/the-definition-of-surface-roughness/

[40] Bouacha, K., Yallese, M.A., Mabrouki, T., & Rigal, J.F. Statistical analysis of surface roughness and cutting forces using response surface methodology in hard turning of AISI 52100 bearing steel with CBN tool. International Journal of Refractory Metals and Hard Materials, *28*, 349–361, 2010

[41] Zurita, O., Di-Graci, V., Capace, M., Zurita -Verónica, O., & Capace, D.-G.-M. Effect of cutting parameters on surface roughness in turning of annealed AISI-1020 steel. Revista Facultad de Ingeniería, *27*, 111–118, 2018

[42] Umbrello, D., Yang, S., Dillon, O.W., & Jawahir, I.S. Effects of cryogenic cooling on surface layer alterations in machining of AISI 52100 steels. Materials Science and Technology (United Kingdom), *28*, 1320–1331, 2012

[43] Perenda, J., Trajkovski, J., Žerovnik, A., & Prebil, I. Residual stresses after deep rolling of a torsion bar made from high strength steel. Journal of Materials Processing Technology, *218*, 89–98, 2015

[44] Islam, M.N. Effect of additional factors on dimensional accuracy and surface finish of turned parts. Machining Science and Technology, *17*, 145–162, 2013

[45] Boy, M., Ciftci, I., Gunay, M., & Ozhan, F. Application of the taguchi method to optimize the cutting conditions in hard turning of a ring bore. Materiali in Tehnologije, *49*, 765–772, 2015

[46] Çiçek, A., Kıvak, T., & Ekici, E. Optimization of drilling parameters using Taguchi technique and response surface methodology (RSM) in drilling of AISI 304 steel with cryogenically treated HSS drills. Journal of Intelligent Manufacturing, *26*, 295–305, 2013

[47] Sui, W., & Zhang, D. Four Methods for Roundness Evaluation. Physics Procedia, *24*, 2159–2164, 2012

[48] Mills, M. *Introduction to the measurement of roundness*. Retrieved Jun 2021, from https://www.taylor-hobson.com/pressreleases/news/2010/april/news-tutorial-introduction-to-the-measurement-of-roundness. 16 Apr 2010

[49] Umbrello, D., & Filice, L. Improving surface integrity in orthogonal machining of hardened AISI 52100 steel by modeling white and dark layers formation. CIRP Annals - Manufacturing Technology, *58*, 73–76, 2009

[50] Ramesh, A., & Melkote, S.N. Modeling of white layer formation under thermally dominant conditions in orthogonal machining of hardened AISI 52100 steel. International Journal of Machine Tools and Manufacture, *48*, 402–414, 2008

[51] Zhang, F., Duan, C., Sun, W., & Ju, K. Effects of cutting conditions on the microstructure and residual stress of white and dark layers in cutting hardened steel. Journal of Materials Processing Technology, *266*, 599–611, 2019

[52] Chou, Y.K., & Song, H. Thermal modeling for white layer predictions in finish hard turning. International Journal of Machine Tools and Manufacture, *45*, 481–495, 2005

[53] Ordás, N., Penalva, M.L., Fernández, J., & García-Rosales, C. Residual stresses in tool steel due to hard-turning. Journal of Applied Crystallography, *36*, 1135–1143, 2003

[54] Noyan, I.C., & Cohen, J.B. *Residual Stress* (1st ed.). NY: Springer. 1987

[55] Revel, P., Jouini, N., Thoquenne, G., & Lefebvre, F. High precision hard turning of AISI 52100 bearing steel. Precision Engineering, *43*, 24–33, 2016

[56] Hua, J., Shivpuri, R., Cheng, X., Bedekar, V., Matsumoto, Y., Hashimoto, F., & Watkins, T.R. Effect of feed rate, workpiece hardness and cutting edge on subsurface residual stress in the hard turning of bearing steel using chamfer + hone cutting edge geometry. Materials Science and Engineering A, *394*, 238–248, 2005

[57] Matsumoto, Y., Hashimoto, F., & Lahoti, G. Surface integrity generated by precision hard turning. CIRP Annals - Manufacturing Technology, *48*, 59–62, 1999

[58] Altenberger, I. Deep rolling - The past, the present and the future. Proceedings of the 9th International Conference on Shot Peening, 144–155, 2005

[59] Delgado, P., Cuesta, I.I., Alegre, J.M., & Díaz, A. State of the art of Deep Rolling. Precision Engineering, *46*, 1–10, 2016

[60] Wong, C.C., Hartawan, A., & Teo, W.K. Deep cold rolling of features on aero-engine components. Procedia CIRP, *13*, 350–354, 2014

[61] Abrão, A.M., Denkena, B., Köhler, J., Breidenstein, B., & Mörke, T. The inducement of residual stress through deep rolling of AISI 1060 steel and its subsequent relaxation under cyclic loading. International Journal of Advanced Manufacturing Technology, *79*, 1939–1947, 2015

[62] Klocke, F., & Mader, S. Fundamentals of the Deep Rolling of Compressor Blades for Turbo Aircraft Engines. Steel Research International, *76*, 229–235, 2005

[63] Groche, P., Engels, M., Steitz, M., Müller, C., Scheil, J., & Heilmaier, M. Potential of mechanical surface treatment for mould and die production. International Journal of Materials Research, *103*, 783–789, 2012

[64] Abrão, A.M., Denkena, B., Breidenstein, B., & Mörke, T. Surface and subsurface alterations induced by deep rolling of hardened AISI 1060 steel. Production Engineering, *8*, 551–558, 2014

[65] Grzesik, W., & Zak, K. Modification of surface finish produced by hard turning using superfinishing and burnishing operations. Journal of Materials Processing Technology, *212*, 315–322, 2012

[66] Hosseini, S.B., Klement, U., Yao, Y., & Ryttberg, K. Formation mechanisms of white layers induced by hard turning of AISI 52100 steel. Acta Materialia, *89*, 258–267, 2015

[67] Vomacka, P., & Walburger, H. Residual stresses due to hard-machining-industrial experiences. Materials Science Forum, *347*, 592–597, 2000

[68] Caruso, S., Umbrello, D., Outeiro, J.C., Filice, L., & Micari, F. An experimental investigation of residual stresses in hard machining of AISI 52100 steel. Procedia Engineering, *19*, 67–72, 2011

[69] Zhou, J.M., Walter, H., Andersson, M., & Stahl, J.E. Effect of chamfer angle on wear of PCBN cutting tool. International Journal of Machine Tools and Manufacture, *43*, 301–305, 2003

[70] Groover, M. *Fundementals of Modern Manufacturing Materials,Processes and Systems* (4th ed.). USA:John Wiley & Sons. Inc. 2010

[71] Yallese, M.A., Chaoui, K., Zeghib, N., Boulanouar, L., & Rigal, J.F. Hard machining of hardened bearing steel using cubic boron nitride tool. Journal of Materials Processing Technology, *209*, 1092–1104, 2009

[72] Özel, T., Hsu, T.K., & Zeren, E. Effects of cutting edge geometry, workpiece hardness, feed rate and cutting speed on surface roughness and forces in finish turning of hardened AISI H13 steel. International Journal of Advanced Manufacturing Technology, *25*, 262–269, 2005

[73] Singh, D., & Rao, P.V. A surface roughness prediction model for hard turning process. International Journal of Advanced Manufacturing Technology, *32*, 1115–1124, 2007

[74] Liu, M., Takagi, J.I., & Tsukuda, A. Effect of tool nose radius and tool wear on residual stress distribution in hard turning of bearing steel. Journal of Materials Processing Technology, *150*, 234–241, 2004

[75] Javidi, A., Rieger, U., & Eichlseder, W. The effect of machining on the surface integrity and fatigue life. International Journal of Fatigue, *30*, 2050–2055, 2008

[76] Jouini, N., Revel, P., Mazeran, P.E., & Bigerelle, M. The ability of precision hard turning to increase rolling contact fatigue life. Tribology International, *59*, 141–146, 2013

[77] Maiß, O., Denkena, B., & Grove, T. Hybrid machining of roller bearing inner

rings by hard turning and deep rolling. Journal of Materials Processing Technology, *230*, 211–216, 2016

[78] Pape, F., Neubauer, T., Maiß, O., Denkena, B., & Poll, G. Influence of Residual Stresses Introduced by Manufacturing Processes on Bearing Endurance Time. Tribology Letters, *65*, 1–8, 2017

[79] Pape, F., Maiss, O., Denkena, B., & Poll, G. Enhancement of roller bearing fatigue life by innovative production processes. Industrial Lubrication and Tribology, *71*, 1003–1006, 2019

[80] Azo Materials. *AISI 52100 Alloy Steel*. Retrieved 23 Sept 2021, from https://www.azom.com/article.aspx?ArticleID=6704. 26 Sept 2012

[81] Askeland, D.R., Fulay, P.P., & Bhattacharya, D.K. *Essentials of Materials Science and Engineering* (2nd ed.). Cengage India. 2013

[82] Guo, Y.B., & Liu, C.R. Mechanical Properties of Hardened AISI 52100 Steel in Hard Machining Processes. Article in Journal of Manufacturing Science and Engineering, *124*, 1–9, 2002

[83] J. Paulo Davim. *Machining of Hard Materials* (1st ed.). London: Springer-Verlag London. 2011

[84] Ecoroll Company. *Hydrostatic Tools HG2 – HG25*. Retrieved 20 Sept 2020, from https://www.ecoroll.de/en/products/hydrostatic-tools.html

[85] Denkena, B., & Köhler, J. Consideration of the form of the undeformed section of cut in the calculation of machining forces. Machining Science and Technology, *14*, 455–470, 2010

[86] Sharman, A.R.C., Hughes, J.I., & Ridgway, K. The effect of tool nose radius on surface integrity and residual stresses when turning Inconel 718^{TM}. Journal of Materials Processing Technology, *216*, 123–132, 2015

[87] Sood, R., Guo, C., & Malkin, S. Turning of Hardened Steels. Journal of

Manufacturing Processes, *2*, 187–193, 2000

[88] Tang, L., Gao, C., Huang, J., Lin, X., & Zhang, J. Experimental investigation of the three-component forces in finish dry hard turning of hardened tool steel at different hardness levels. International Journal of Advanced Manufacturing Technology, *70*, 1721–1729, 2014

[89] Aslan, E., Camuşcu, N., & Birgören, B. Design optimization of cutting parameters when turning hardened AISI 4140 steel (63 HRC) with Al2O3 + TiCN mixed ceramic tool. Materials and Design, *28*, 1618–1622, 2007

[90] Lin, H.M., Liao, Y.S., & Wei, C.C. Wear behavior in turning high hardness alloy steel by CBN tool. Wear, *264*, 679–684, 2008

[91] Ebrahimi, A., & Moshksar, M.M. Evaluation of machinability in turning of microalloyed and quenched-tempered steels: Tool wear, statistical analysis, chip morphology. Journal of Materials Processing Technology, *209*, 910–921, 2009

[92] Chou, Y.K., & Song, H. Tool nose radius effects on finish hard turning. Journal of Materials Processing Technology, *148*, 259–268, 2004

[93] Brown, I., & Schoop, J. The effect of cutting edge geometry, nose radius and feed on surface integrity in finish turning of Ti-6Al4V. Procedia CIRP, *87*, 142–147, 2020

[94] International Standart Organization. Rolling Bearings - Measuring methods for vibration (ISO 15242-4:2017 (E)). Switzerland:ISO. 2017

[95] Mais, J. Spectrum Analysis-The key features of analyzing spectra. SKF USA Inc., 1–32, 2002

[96] International Standart Organization. Rolling Bearings - Measuring methods for vibration (ISO 15242-1:2015 (en)). Switzerland:ISO. 2015

[97] Sayles, R.S., & Poon, S.Y. Surface topography and rolling element vibration.

Precision Engineering, *3*, 137–144, 1981

[98] Pawar, S., Salve, A., Chinchanikar, S., Kulkarni, A., & Lamdhade, G. Residual Stresses during Hard Turning of AISI 52100 Steel: Numerical Modelling with Experimental Validation. Materials Today: Proceedings, *4*, 2350–2359, 2017

[99] Lorösch, H.-K. Influence of Load on the Magnitude of the Life Exponent for Rolling Bearings. ASTM International, 275–292, 1982

[100] Voskamp, A.P. Microstructural changes during rolling contract fatigue: Metal fatigue in the subsurface region of deep groove ball bearing inner rings. Published Doctoral thesis, Bibliotheek Tecnische Universiteit, Delft. 1997

[101] Güley, V., Tekkaya, A.E., Savaş, T., & Özhan, F. Experimental Investigation of Residual Stresses after Heat Treatment and Grinding Processes in the Production of Ball Bearing Rings. Materials Science Forum, *571–572*, 27–32, 2008

[102] Alfredsson, B. A Study on Contact Fatigue Mechanisms. Published Doctaral Thesis, Department of Solid Mechanics Royal Institute of Technology Stockholm, Sweden. 2000

[103] Vlcek, B.L., Hendricks, R.C., & Zaretsky, E. V. Monte Carlo Simulation of Sudden Death Bearing Testing. Tribology Transactions, *47*, 188–199, 2004

[104] Shuaib Khan, M., Pasha, G.R., & Hesham, A. Theoretical Analysis of Inverse Weibull Distribution. WSEAS Transactions on Mathematics, *7*, 30–38, 2008

[105] Erdemir, A. Rolling-contact fatigue and wear resistance of hard coatings on bearing-steel substrates. Surface and Coatings Technology, *54–55*, 482–489, 1992

[106] Stickels, C.A. Rolling contact fatigue tests of 52100 bearing steel using a modified NASA ball test rig. Wear, *98*, 199–210, 1984

[107] Farrahi, G.H., Ahmadi, A., & Reza Kasyzadeh, K. Simulation of vehicle body

spot weld failures due to fatigue by considering road roughness and vehicle velocity. Simulation Modelling Practice and Theory, *105*, 102168, 2020

[108] Vlcek, B.L., & Zaretsky, E. V. Rolling-Element Fatigue Testing and Data Analysis—A Tutorial. Tribology Transactions, *54*, 523–541, 2011

[109] Romanowicz, P.J., & Szybiński, B. Fatigue Life Assessment of Rolling Bearings Made from AISI 52100 Bearing Steel. Materials, *12*, 371, 2019

[110] Ebert, F.J. Fundamentals of Design and Technology of Rolling Element Bearings. Chinese Journal of Aeronautics, *23*, 123–136, 2010

[111] Evans, M.H., Walker, J.C., Ma, C., Wang, L., & Wood, R.J.K. A FIB/TEM study of butterfly crack formation and white etching area (WEA) microstructural changes under rolling contact fatigue in 100Cr6 bearing steel. Materials Science and Engineering: A, *570*, 127–134, 2013

[112] Rycerz, P., Olver, A., & Kadiric, A. Propagation of surface initiated rolling contact fatigue cracks in bearing steel. International Journal of Fatigue, *97*, 29–38, 2017

CURRICULUM VITAE

PERSONAL INFORMATION

Name Surname : Gökhan SAĞIR

EDUCATION

Bachelor : Balıkesir University / (2008-2012)

Master Degree : Ankara Yıldırım Beyazıt University / (2014-continued)

WORK EXPERIENCE

Site Chief : TÜPRAŞ/Alser Soğutma LLC. (2012 - 2013)

Manufacturing Engineer: Ortadoğu Rulman Sanayi Co. Inc. (ORS AŞ.) / (2017 - continued)

TOPICS OF INTEREST

- Manufacturing, Machinability, Material Science, CAD, CAM, Macro NC Programming

December 2021

ANKARA

Department of Mechanical Engineering

Gökhan SAĞIR